



Universiteit  
Leiden  
The Netherlands

## Tailoring x-ray tomography techniques for cultural heritage research

Bossema, F.G.

### Citation

Bossema, F. G. (2024, May 23). *Tailoring x-ray tomography techniques for cultural heritage research*. Retrieved from <https://hdl.handle.net/1887/3754491>

Version: Publisher's Version

License: [Licence agreement concerning inclusion of doctoral thesis in the Institutional Repository of the University of Leiden](#)

Downloaded from: <https://hdl.handle.net/1887/3754491>

**Note:** To cite this publication please use the final published version (if applicable).

# **Tailoring X-ray tomography techniques for cultural heritage research**

Proefschrift

ter verkrijging van  
de graad van doctor aan de Universiteit Leiden,  
op gezag van rector magnificus prof. dr. ir. H. Bijl,  
volgens besluit van het college voor promoties  
te verdedigen op donderdag 23 mei 2024  
klokke 11.15 uur

door

Francien Gerda Bossema

geboren te Amsterdam, Nederland  
in 1994

**Promotores:**

Prof. dr. K.J. Batenburg

Prof. dr. E. Hermens

**Promotiecommissie:**

Prof. dr. I. Smeets

Prof. dr. A. Plaat

Prof. dr. C.-B. Schönlieb (University of Cambridge)

Prof. dr. V. Cnudde (Universiteit Utrecht)

Dr. M. Domínguez Delmás (Naturalis Biodiversity Center)

The research presented in this dissertation was carried out at the Centrum Wiskunde & Informatica (CWI) in Amsterdam, in collaboration with the Rijksmuseum Amsterdam; the British Museum, London (chapters 4 and 5); and The J. Paul Getty museum, Los Angeles (chapter 4).

Financial support was provided by the Dutch Research Council (NWO), programme project number 628.007.033, and Netherlands Institute for Conservation Art and Science (NICAS). The FleX-ray Laboratory is supported by the Dutch Research Council, project number 639.073.356. The project that is presented in chapter 5 was supported by a Small Project grant for the IntACT project from the Netherlands Institute for Conservation, Art and Science (NICAS). Francien G. Bossema was supported by Prins Bernhard Cultuurfonds, Jo Kolk Studiefonds, Catherina van Tussenbroekfonds and European Women in Mathematics Association (EWM) to take up a research placement at the British Museum in London.



# Contents

<b>1</b>	<b>Introduction</b>	<b>1</b>
1.1	2D and 3D imaging . . . . .	2
1.2	Computed tomography workflow . . . . .	5
1.3	Computed tomography in cultural heritage . . . . .	12
1.4	Research questions . . . . .	18
<b>2</b>	<b>Integrating expert feedback in an explorative CT scanning workflow</b>	<b>23</b>
2.1	Material and methods . . . . .	26
2.2	Results: case study of a wooden cornett . . . . .	33
2.3	Discussion and conclusions . . . . .	38
<b>3</b>	<b>Line trajectory X-ray tomography for dendrochronology of large historical wooden objects</b>	<b>41</b>
3.1	Methods . . . . .	43
3.2	Experiments and results . . . . .	48
3.3	Discussion and conclusions . . . . .	53
<b>4</b>	<b>Marker-based 3D CT imaging using only basic 2D X-ray equipment</b>	<b>59</b>
4.1	Results . . . . .	61
4.2	Discussion . . . . .	68
4.3	Methods . . . . .	71
<b>5</b>	<b>Interactive visualisation of the interior and exterior of cultural heritage objects</b>	<b>77</b>
5.1	Related work and common practice . . . . .	78
5.2	Contributions and data availability . . . . .	80
5.3	Material and methods . . . . .	80
5.4	Results . . . . .	84
5.5	Discussion and conclusions . . . . .	94
<b>6</b>	<b>Conclusion and outlook</b>	<b>97</b>
6.1	Contributions and limitations . . . . .	97
6.2	Continued research . . . . .	100
6.3	Outlook . . . . .	100

<b>Bibliography</b>	<b>103</b>
<b>A Appendix A:</b>	
<b>Supplementary information</b>	<b>121</b>
A.1 Supplementary methods . . . . .	121
A.2 Supplementary figures and tables . . . . .	129
<b>B Appendix B:</b>	
<b>Intact user guidelines</b>	<b>133</b>
B.1 Installation . . . . .	133
B.2 The INTACT plugin . . . . .	136
B.3 Basic Blender controls . . . . .	143
B.4 Using vertex selections for registration . . . . .	146
<b>List of publications</b>	<b>149</b>
<b>Samenvatting</b>	<b>153</b>
<b>Curriculum Vitae</b>	<b>157</b>



# 1

## Introduction

Visualizing the internal structure is a crucial step in acquiring knowledge about the origin, state, and composition of cultural heritage artifacts. Among the most powerful techniques for exposing the interior of cultural heritage objects is computed tomography (CT), a technique that computationally forms a 3D image using hundreds of radiographs acquired in a full circular range. The diversity in materials, shapes and sizes of cultural heritage objects poses a challenge for the broad application of this technique, since each scan needs to be tailored to the object. Moreover, the lack of affordable and versatile CT equipment in museums, combined with the challenge of transporting precious collection objects, currently keeps this technique out of reach for most cultural heritage applications. In this thesis, we explore how CT imaging can be further integrated in cultural heritage applications by 1) integrating expert feedback into the data acquisition process, 2) tailoring acquisition methods to obtain specific information, 3) developing a low-cost method to use in-house X-ray facilities for 3D CT imaging and 4) providing tools to interactively visualise and inspect the CT data.

In this introductory chapter, we will first discuss the difference between 2D and 3D imaging (section 1.1). We then present the concepts underlying each of the steps of the CT research process (section 1.2). Next, we will outline the possibilities and challenges of the application of CT imaging to cultural heritage objects (section 1.3). We close with the research questions underlying the chapters in this thesis (section 1.4).

## 1.1 2D and 3D imaging

### 1.1.1 2D radiography

In 2D X-ray imaging or *radiography*, X-rays travel through an object and a detector measures the intensity of the X-rays after they leave the object. Based on the length of the object and the density of the materials the X-rays are absorbed. Thus, a ‘shadow-like’ image of the interior is formed on the detector. On a single X-ray image, all features along a line from the source to the detector are superimposed on the image and depth information is lost. This makes it difficult to distinguish between features when they are behind higher density materials, because these occlude lower density features. Inspection of individual features within the object can therefore be challenging. 2D X-ray imaging is used in museums for the live radiographic inspection of objects to investigate possible internal damage or to obtain information about how it was made. In figure 1.1 radiographs of a wooden sculpture from the Rijksmuseum are shown, which was scanned for the purpose of dating the wood by inspecting the tree rings.



**Figure 1.1:** a) *Woman with lantern*, Rijksmuseum collection [159], b) five radiographs that together show the entire object.

### 1.1.2 3D computed tomography

A 3D CT dataset is obtained from collecting radiographs in a full angular range around the object. These radiographs are then combined into a 3D reconstruction image. This digital representation of the object can be sliced open to obtain cross-sections in any direction. A CT reconstruction provides depth information and pulls apart the different features, which greatly enhances the knowledge that can be gained from the scan compared to the individual radiographs. An example of 3D CT imaging is shown in figure 1.2 for the same wooden statue as presented in figure 1.1. This shows the increased information gain of the 3D CT image compared to the 2D radiographs. The radiograph does not contain sufficient information to extract a horizontal cross-section of the tree rings, which would be needed for dating the wood. A horizontal slice from the 3D CT reconstruction, however, provides a sharp image of the tree rings, enabling dating of the object [63].

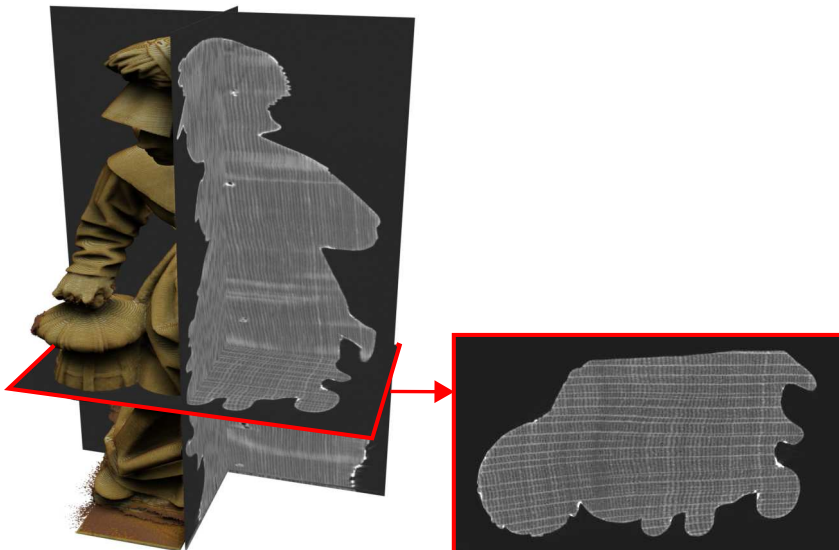


**Figure 1.2:** CT reconstruction of the *Woman with lantern*: 3D visualisation and orthogonal slices, horizontal slice showing the tree ring pattern.

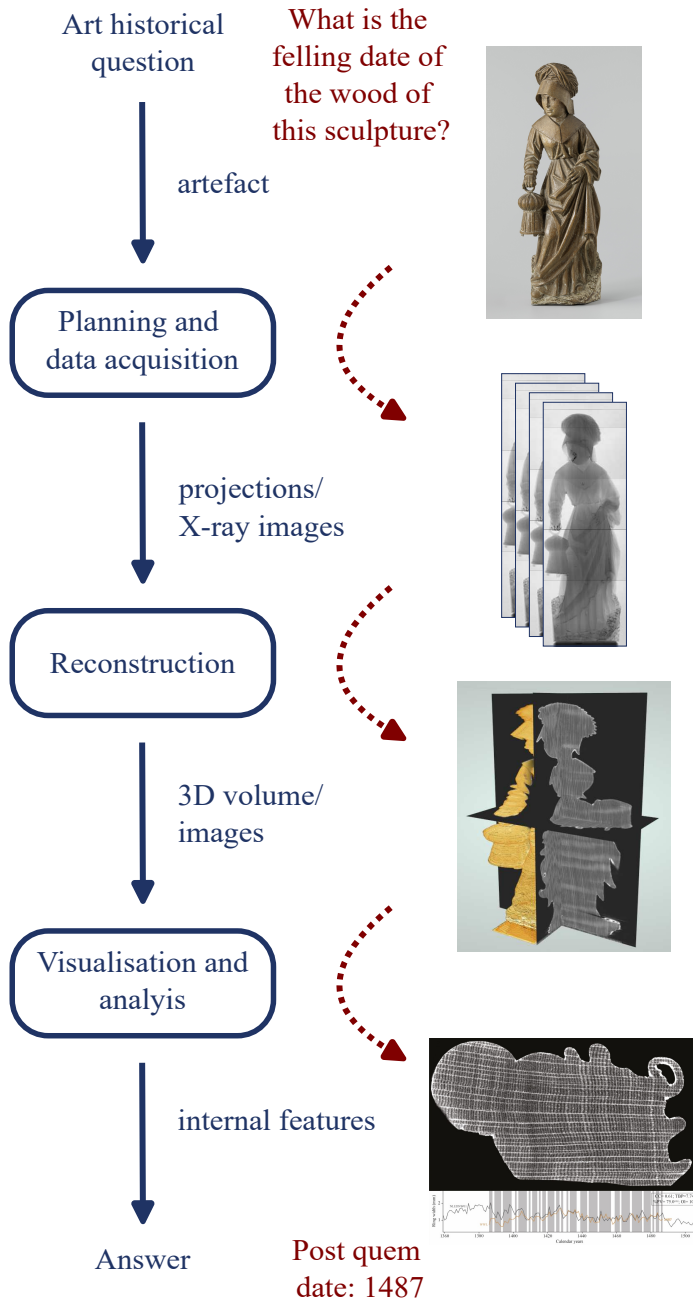


**Figure 1.3:** CT scanning research process from question to answer (in blue), with an example detailing the process of scanning the *Woman with lantern* (in red). A *post quem date* is an earliest date for the felling of the tree, such that the object must have been made after that date.

## 1.2 Computed tomography workflow

Since the invention of CT by Sir Godfrey Hounsfield in 1967 [151], this technique has been applied to many applications outside the original application in the medical domain [102]. Over the last decades, it has also been increasingly applied to the investigation of art objects. An important challenge for the general implementation of CT scanning for cultural heritage objects is that there is a wide variety of art objects, with different sizes, shapes and materials. Therefore, there is not one standard way to CT scan an art object. In contrast, for medical CT scans the position and general shape of the interior is known beforehand and the densities of the subjects are similar [16, 95]. The state-of-the-art medical scanners have been optimized with respect to these characteristics and standard acquisition protocols have been developed, which are repeatable for different patients. In the case of cultural heritage studies, it is unknown beforehand which features are present in the object and what scan specifications are needed to image them.

When CT scanning cultural heritage objects, the scanning process needs to be adapted to the object and the questions that are related to it. The research process is shown in figure 1.3. It starts from an object based question (or questions) by an object expert (e.g. ‘what is the felling date of the wood of this sculpture?’). During the data acquisition phase X-ray images are collected from a range of angles, possibly in multiple scans if the object is larger than the detector. This series of X-ray images is then the input for a reconstruction algorithm, which produces a 3D image of the interior of the object. This reconstruction is visualised and inspected to extract features (e.g. tree rings) that can answer the original research question.

The main phases in the CT research process for cultural heritage objects are shown in figure 1.3: planning and data acquisition, reconstruction, and visualisation and analysis. On the right side these phases are illustrated by the steps in the scanning process of the *Woman with lantern*, from the Rijksmuseum collection [159]. Below we will discuss each of the research process phases in detail and outline the limitations, specifically as they apply to the scanning of cultural heritage objects.

### 1.2.1 Planning and data acquisition

The first step towards resolving questions using CT imaging is the data acquisition. Below we discuss the components of the CT system and how X-ray images are formed.

#### The CT scanner

X-ray imaging setups for scanning static objects typically consist of an X-ray source, a detector and a rotation stage in between, on which the object is mounted (see figure 1.4). For our workflow, we use a cone-beam X-ray source and a digital flat-panel detector. In dedicated CT systems, the location of each of these components are accurately known and the rotation stage can be controlled to obtain radiographs at precise angular steps. The distance from the source to the rotation axis is called the *source object distance* (SOD) and the distance from rotation axis to the detector

*object detector distance* (ODD). In order to be able to CT scan an object, the object needs to fit within the confines of the CT scanner and fully rotate. It also needs to be stable and not move in between X-ray images. When the object is wider or taller than the field of view of the detector, it is necessary to make *tiled* scans: multiple CT scans with the source and detector at different locations. The choice for the number of vertical and horizontal tiles and the tiling method, either moving detector only or both source and detector, depends mostly on the shape of the object. Additionally, the tiling method influences the reconstruction step, which is further described in section 1.2.2.

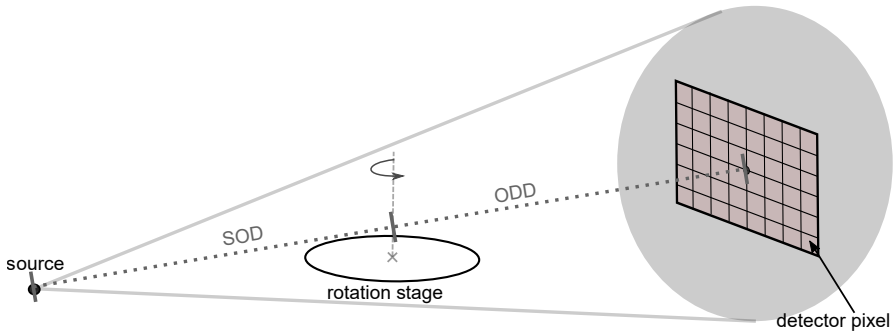


**Figure 1.4:** Schematic representation of a standard CT setup consisting of an X-ray source, a detector and a rotation stage in between.

## X-ray absorption and projections

X-ray images are also called *radiographs* or *projections* and are formed by taking measurements of the intensity of the X-rays after they are attenuated by the object. This results in a projection of the object's internal structure. The X-ray absorption is material dependent [48, 50, 95]. The intensity  $I(l)$  measured at a point on the detector depends on the length and material of the object, following Lambert-Beer's Law:

$$I(l) = I_0 e^{-\int_l \mu(x) dx}, \quad (1.1)$$

where  $\mu(x)$  is the absorption coefficient of the material,  $l$  the line from the source to that point on the detector and  $I_0$  the intensity of the X-rays when they leave the source.

Equation 1.1 can be rewritten to obtain the linearized photon count along  $l$ :

$$p(l) = -\log\left(\frac{I(l)}{I_0}\right) = \int_l \mu(x) dx. \quad (1.2)$$

For a schematic illustration, see figure 1.5.

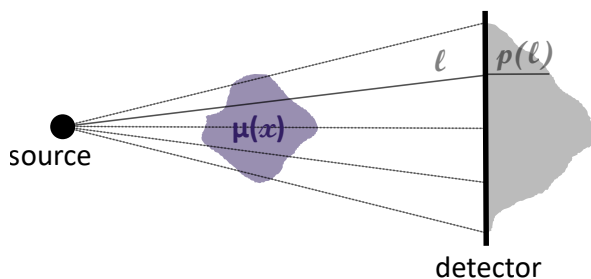


**Figure 1.5:** Schematic representation of X-ray absorption along a line  $l$ .

The values of the projection measurement depend on a number of parameters: source intensity, exposure time and the material composition and location of internal features within the object. What is seen on the projection image further depends on the precise location of the source, object and detector, as well as the orientation of the object and the acquisition angles. In figure 1.6 this is illustrated with two radiographs of a 17th century cutlery case taken at two different angles. Due to the cone shape of the beam, the object is moreover magnified on the projection. The magnification factor  $m$  is determined by  $m = \frac{SOD+ODD}{SOD}$ . The higher the magnification, the smaller the features that can be seen in the reconstruction. In order to obtain sufficiently high contrast in the features, the source settings (energy and power) need to be tailored to the object [106].

### Planning and data collection

When it has been decided to perform a CT scan of an object, the first consideration is how to mount it on the rotation stage. Mounting the object in a fixed and stable manner is important to obtain accurate results and ensuring the safety of the object. This is often done by designing a foam holder specific for the object. The foam is almost transparent on the X-ray image, while it allows to stabilise the object and keep it in a position that is easiest for the scanning process. With the object in the scanner, the CT scans are designed. First, it is determined how many scans are necessary to obtain data of the entire object. Second, the source settings (energy, power) and exposure time that give the highest contrast in the X-ray image are investigated [106]. A CT dataset is then recorded, which consists of a set of projections, typically hundreds to thousands acquired across a full rotational range. Additionally, a darkfield (a projection with the source turned off) and a flatfield (a projection with the source on and no object in between) are collected to compensate for defects in the detector and background radiation that produces noise. In a metadata file the source settings, exposure time and the locations of the source, detector and rotation stage are recorded, as well as the rotation angles. Depending on the settings, the time for a single scan varies from minutes to hours. This needs to be taken into account when planning the scans of objects that have to return to the museum within a certain amount of time, usually the same day.



**Figure 1.6:** a) Cutlery case from the Rijksmuseum collection [158], b) and c) two radiographs of the lid of the cutlery case, with c) rotated ninety degrees with respect to b). Image adapted from [106].

### 1.2.2 Reconstruction

After data acquisition, a CT reconstruction algorithm computes a 3D volumetric image of the scanned object based on the acquired radiographs and the metadata. In this section we will first introduce the underlying inverse problem and then discuss reconstruction algorithms and tiled reconstructions.

#### The inverse problem

Tomographic reconstruction is an inverse problem, in which an image of the original object is obtained from a series of projections of that object. When scanning an object, we obtain a finite number of measurements, namely one intensity measurement per detector pixel per projection. This is the projection data  $\mathbf{b} \in \mathbb{R}^{N_\alpha \times N_p}$  with  $N_\alpha$  the number of projections and  $N_p$  the number of detector pixels. The vector  $\mathbf{x} \in \mathbb{R}^{N_v}$  defines the cubic reconstruction volume, with  $N_v$  the number of voxels in each direction. In most cases, the object is assumed to be contained in this reconstruction volume. The resolution or *voxel size* of the reconstruction depends on the magnification  $m$  and the detector pixel size  $\delta$ , and is given by  $\frac{\delta}{m}$ .

Due to the fact that we have a finite number of measurements, the forward projection can be formulated as a system of linear equations. The forward operator  $\mathbf{A}$  depends on the acquisition trajectory and thus on the locations of the source, detector and object and the rotation angles. Each component of the matrix  $\mathbf{A}_{ij}$  corresponds to the absorption of object voxel  $j$  of the ray that leads to measurement  $i$ . The vector  $\mathbf{x}$  is the digital representation of the object that leads to the acquired projection data  $\mathbf{b}$ :

$$\mathbf{Ax} = \mathbf{b}. \quad (1.3)$$

#### Reconstruction algorithms

The goal of reconstruction algorithms is to find a vector  $\mathbf{x}$  which leads to the acquired projection data  $\mathbf{b}$ . We distinguish between two types of reconstruction algorithms: filtered backprojection methods and iterative methods.

Filtered backprojection type algorithms have been developed to obtain fast reconstructions for specific acquisitions geometries. The reconstruction is obtained by first

applying a well-chosen filter  $\mathbf{h}$  to the acquired data and then backprojecting it into the reconstruction volume:

$$\mathbf{x} = \mathbf{A}^T(\mathbf{h} * \mathbf{b}). \quad (1.4)$$

A standard method for reconstruction of a circular cone beam geometry is the Feldkamp-Davis-Kress (FDK) algorithm [72]. Within the reconstruction algorithm, the acquisition trajectory is required to be circular and the angles equidistant. The flexibility of these methods is therefore limited.

Another approach to finding a solution to the inverse problem, are iterative reconstruction methods. These methods aim to minimize the difference between the forward projected image representation and the data, for example:

$$\min_{\mathbf{x}} |\mathbf{A}\mathbf{x} - \mathbf{b}|^2. \quad (1.5)$$

One widely used iterative reconstruction method is the Simultaneous Iterative Reconstruction Technique (SIRT) [87]. The SIRT algorithm operates by performing a gradient descent to minimize the residual, which is determined by forward-projecting the current estimate of the object representation and comparing it to the data. In each iteration, the current estimate  $\mathbf{x}^i$  is updated to obtain the next estimate  $\mathbf{x}^{i+1}$  as follows:

$$\mathbf{x}^{i+1} = \mathbf{x}^i + \mathbf{C}\mathbf{A}^T\mathbf{R}(\mathbf{b} - \mathbf{A}\mathbf{x})^i, \quad (1.6)$$

where  $\mathbf{C}$  is a diagonal matrix containing the inverse of the sum of the columns:  $c_{jj} = \frac{1}{\sum_i a_{ij}}$  and  $\mathbf{R}$  for the rows:  $r_{ii} = \frac{1}{\sum_j a_{ij}}$ , compensating for the number of rays that hit each pixel and the number of pixels that are hit by each ray.

The SIRT method is more flexible than the before mentioned FDK algorithm, since it can be used with different acquisition geometries. A drawback is that it is relatively slow and computationally intensive.

### Tiled scan reconstructions

There are a few methods to obtain tiled scans and reconstructions for objects that do not fit within the detector frame. Below we address the different methods and outline the advantages and challenges of the reconstruction. For each of these methods it is important to have sufficient overlap between neighboring radiographs. Which of these methods are possible depends on flexibility of the hardware and software that controls the scanner components.

- **Vertical tiling: moving detector only**

If only the detector is moved, the images are sampled from the same cone beam. Therefore, the radiographs can be stitched together for each projection angle to form one large radiograph, from which the reconstruction can be computed as if it were a single scan. This makes it possible to use any reconstruction algorithm. For this method, the height is however limited to the height of the cone beam at the detector distance, since if we move the detector too far up or down, the beam will no longer fall on it and part of the detector will be in

shadow. Moreover, on the edge of the beam, it may be possible that cone angle artefacts appear. These artefacts are distortions in the reconstructed image that are caused by the larger angle between the source and detector.

- **Vertical tiling: moving detector and source**

When moving the detector and source together vertically, the images are sampled from different cones. Because the rotation axis is projected onto the center of the detector, the region of interest (ROI) section of the object is captured in all the projections and therefore the different scans can be reconstructed independently and merged afterwards.

- **Horizontal tiling: moving detector only**

In general horizontal tiling is more challenging than vertical tiling, because the rotation axis is no longer projected onto the detector for all tiles. Similar to vertical tiling, if only the detector is moved, the radiographs can be merged before reconstruction and any reconstruction algorithm can be employed. Again, a drawback is the limited movement range due to the size of the cone beam.

- **Horizontal tiling: moving detector and source**

By moving detector and source together, the drawback of the previous method is avoided. Now, it is however not possible to merge the radiographs before reconstruction, because they are sampled from different cones. A reconstruction can be obtained by using an interactive algorithm, such as the SIRT algorithm described above, providing the different datasets and metadata to the algorithm all at once.

Which of the tiling methods is chosen is highly object and question dependent. The size and shape and how the object is positioned can influence the tiling method and number of tiles. The tiling method moreover influences the image quality and obtained resolution. For a CT scan of a painting from the Rijksmuseum collection *Cadmus sowing dragons' teeth*, we tested two options for mounting the object and tiling the scans on a mockup plank (see figure 1.7). Since the aim of the scan was to obtain a cross section of the tree rings, only a ROI along the width of the painting was needed. The horizontal tiling needed significantly fewer tiles. The vertical tiling needed more tiles and material outside the ROI moved through the field of view, but the final image quality was higher than the horizontal tiling. The vertical tiling could also be reconstructed faster and more easily. Due to the very small width of the tree rings, a high resolution and image quality were needed and thus the vertical tiling mode was used for the final scan of the panel painting.

Another example is the *Woman with lantern*, which was scanned with five vertical scans moving both source and detector, see figure 1.1. The FDK reconstruction method was applied to each of the scans, with were afterwards merged using the Flexbox toolbox [108].

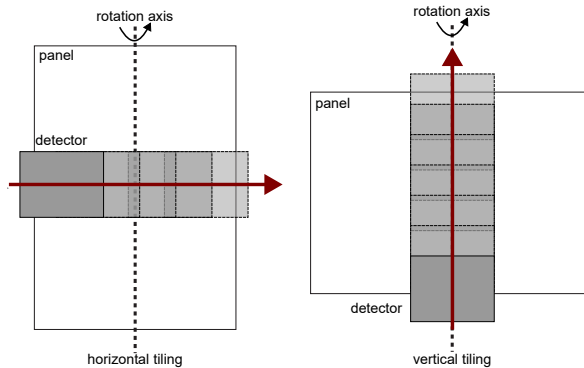


**Figure 1.7:** Schematic indicating the two tiling modes that were investigated for the scan of a panel painting, the panel is outlined in white and the detector in grey, with lighter grey indicating subsequent detector positions. Image adapted from [60].

### 1.2.3 Visualisation and analysis

When the reconstructions have been obtained, these need to be inspected to obtain the answer to the original question. Below we first discuss the visualisation options and then the search for internal features that answer the questions about the object.

#### 2D slices and 3D representation

There are multiple options for investigating and visualising CT reconstruction data. Within the medical world, specialised software tailored to the scanner and purpose, is regularly supplied by the manufacturer of the hardware. Within laboratory settings, the use of free and open source software ImageJ [166] is widespread. While it is easy to view the data as a sequence of slices in ImageJ, its 3D capabilities are limited. It can be challenging to look at 2D cross sections of a 3D object as the relationship between what can be seen on the outside and the internal features is not always clear. A 3D visualisation can assist in making these connections clear.

For 3D visualisations of CT data there are several options, amongst which Slicer3D [71] is an open source solution that is used for both medical and academic purposes. There are also commercial options available, such as the versatile 3D visualisation programs VGStudio [201] and Avizo/Amira [192] but their cost limits their availability and suitability in cultural heritage institutions lacking sufficient funding. Another non-commercial option for volume rendering is Dragonfly [66], which offers a non-commercial licence for academic research.

#### Internal features

The last step in the CT research workflow is to look for the internal features that can answer the art historical question that started the workflow. These features are very diverse and specific to the object and the question. They can for example be glue

lines, cracks, tree rings or layers and patches of different materials.

In the case of the *Woman with lantern* for example the features of interest were the tree rings. The radiographs in figure 1.1 do not give sufficient information, since for tree ring measurements a cross section through the wood is needed. The CT reconstruction does provide this cross section. The horizontal slice shown in figure 1.2 can be used for tree ring measurements to obtain a date for the when the tree was cut (see figure 1.8).

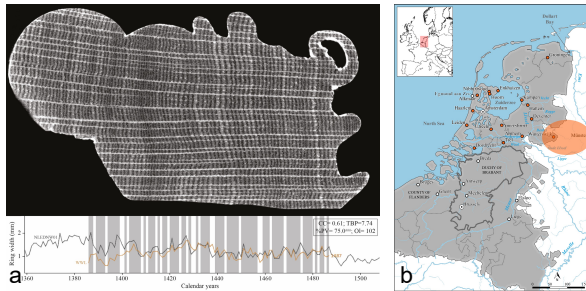


**Figure 1.8:** A slice from the CT scan from which the tree ring series could be measured (a) to obtain a *post quem* date (an earliest date for the felling of the tree) of 1487 and a provenance region (b). Image adapted from [63].

## 1.3 Computed tomography in cultural heritage

### 1.3.1 Applications in cultural heritage

Although CT imaging was originally developed for medical purposes, it has been applied to cultural heritage as well over the past decades. The investigation of interior features of an art object can give valuable information about the date and provenance of the object, the current conservation state and the making process.

#### Dating and provenancing objects

CT can be used for the dating and provenancing of objects. In particular it is well suited for the investigation of tree ring patterns for dendrochronological measurements, as it provides access to the inner structure of the wood when the tree-ring patterns cannot be retrieved by direct inspection on the surface [19, 58, 135, 182].

The *Woman with lantern* is an example of successful dating and provenancing based on CT imaging. A horizontal cross section from the CT scan such as the one shown in figure 1.2c, could be used for tree ring measurements (see figure 1.8a) which led to a *post quem* date (an earliest date for the felling of the tree) and moreover a provenance for the wood (see figure 1.8b). This provenance could be used to draw conclusions about historical Dutch timber trade.

### Assessing the current conservation state

CT imaging can yield additional insights into the conservation state of an object and previous restoration interventions [47, 134, 149, 150]. It can be used to assess the current condition of the object for restoration and conservation purposes, revealing information on internal damage such as cracks, gaps and filler material [140, 178].

In the case of a 17th century cornett (figure 1.9a), a single X-ray image shows that the upper half is much less dense than the lower half, indicating that the top half is more damaged by woodworm (figure 1.9b). In the ROI CT scan (figure 1.9c and d), however, the exact structure and severity of the tunneling could be investigated.

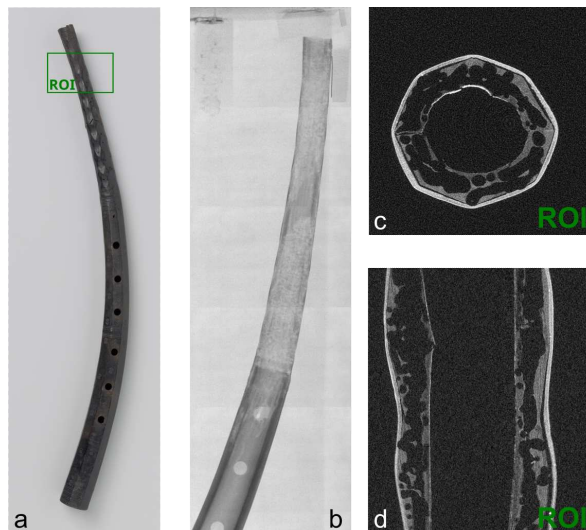


**Figure 1.9:** a) Cornett [157] with ROI region indicated, b) X-ray image of the top half of the cornett, c) horizontal and d) vertical slices through the CT reconstruction of the ROI.

### Determining the making process

An important application of CT imaging for cultural heritage is the determination of the making process, since this can shed light on the creative process of the artist. For example, searching for lines in a terracotta statue can shed light on whether the clay was press molded or freely worked by hand [81] and scanning glass beads led to a better understanding of the production process and tools used to create them [132].

The example shown in figure 1.10 is the plaster sculpture *Python killing a Gnu* from the J. Paul Getty museum collection. The original object was smaller and more condensed. Later, the object was reconfigured to its current shape. In the horizontal slice through the base, clear evidence of the reconfiguration can be seen (figure 1.10c) as the original square base is enveloped in the current, more rocky base.

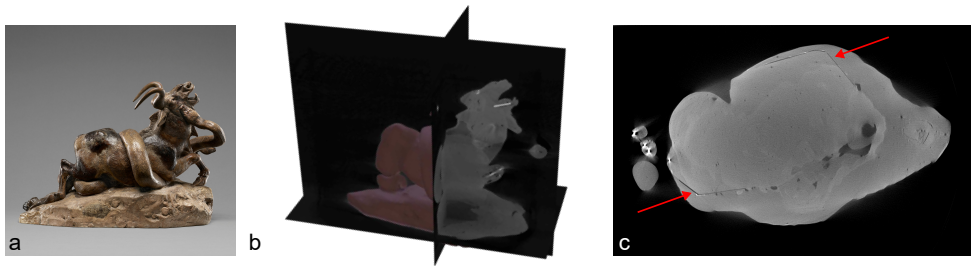


**Figure 1.10:** a) *Python killing a Gnu* [190], b) 3D CT reconstruction volume representation with orthogonal slices and c) horizontal slice showing the original square base enclosed in the current base.

### 1.3.2 Challenges for the application of CT to cultural heritage

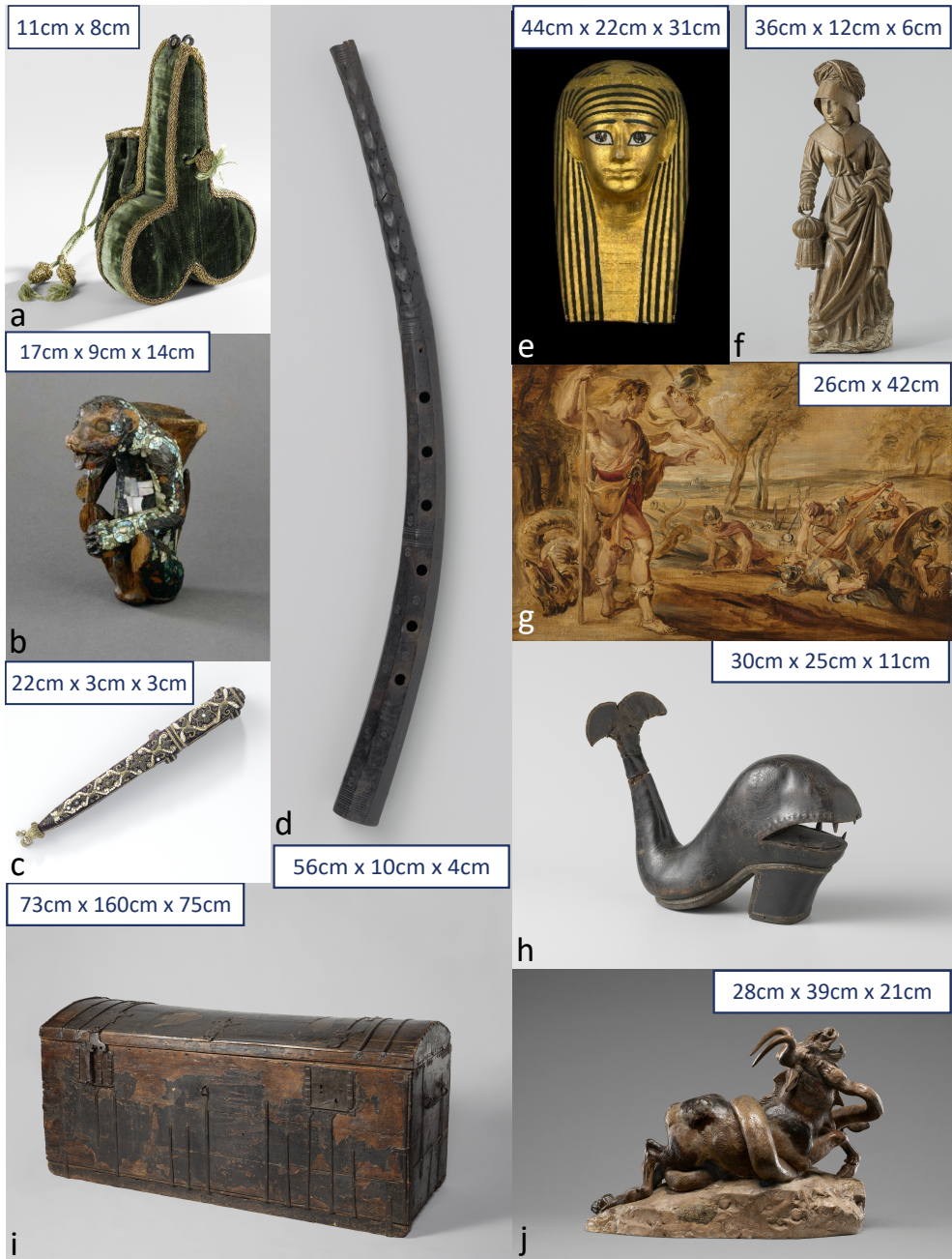
Despite the known advantages of CT as a technique to obtain information about the interior of objects, it has not been widely implemented in museum research facilities. There are a couple of reasons why this technique has been difficult to apply to museum collection objects at large, which we will discuss in this section.

#### Shapes and sizes of objects

The variety in shapes and sizes of cultural heritage objects poses a challenge due to the often confined space in the scanner. First, they need to fit and be able to fully rotate within the scanner. Second, when the object is longer in one direction than another, it is difficult to find source settings to have sufficient contrast over the full rotational range. This is for example the case for paintings, which are long in one direction and thin in the other. In figure 1.11 the wide range of shapes, sizes and materials of objects that were investigated in the course of the research for this thesis is shown.

**Figure 1.11:** Overview of the objects scanned in the course of the research for this thesis and their sizes:

- a) Green velvet purse with gold thread, after 1580, Rijksmuseum collection nr. BK-KOG-29 [153],
- b) Jaguar figure, wood covered with mosaic, 1400-1521, British Museum, collection nr. Am,+ .165,[187], ©The Trustees of the British Museum.
- c) Cutlery case, purple velvet embroidered with pearls and gold thread, c. 1600-1625, Rijksmuseum collection nr. BK-NM-3086, [158],
- d) Cornett, boxwood and leather, c. 1600-1650, Rijksmuseum collection nr. BK-AM-62-B [157],
- e) Mummy mask, cartonnage, 1stC BC-1stC, British Museum, collection nr. EA 29472 [188], ©The Trustees of the British Museum,
- f) Woman with lantern, oakwood, c. 1500-1550, Rijksmuseum collection nr. BK-NM-9253 [159],
- g) Cadmus, Guided by Minerva, Observes the Spartoi Fighting, Peter Paul Rubens (after), oil on paper laid down on panel, before 1747, Rijksmuseum collection nr. SK-A-4051 [156],
- h) Bottle in the shape of a shoe, leather, brass and wood, c. 1675-1700, Rijksmuseum collection nr. BK-KOG-1382 [155],
- i) Book chest of Hugo de Groot, wood, leather and metal, c. 1600-1615, Rijksmuseum collection nr. NG-KOG-1208 [154],
- j) Python Killing a Gnu, Antoine-Louis Barye, plaster, wax and metal, c. 1840-1860, The J. Paul Getty collection nr. 85.SE.48 [190].



### Variety of materials

Cultural heritage objects are made of a large variety of different materials, making the choice of acquisition settings a challenge, especially when the object contains both high and low density materials. This is most pronounced when one of the materials is a metal. This is for example the case for the cutlery case (figure 1.12a). See figure 1.12b for an example, where the gold thread surrounding the cutlery case causes streaking artefacts in the reconstruction. By carefully choosing the source settings and beam filtration, these artefacts can be reduced (figure 1.12c).

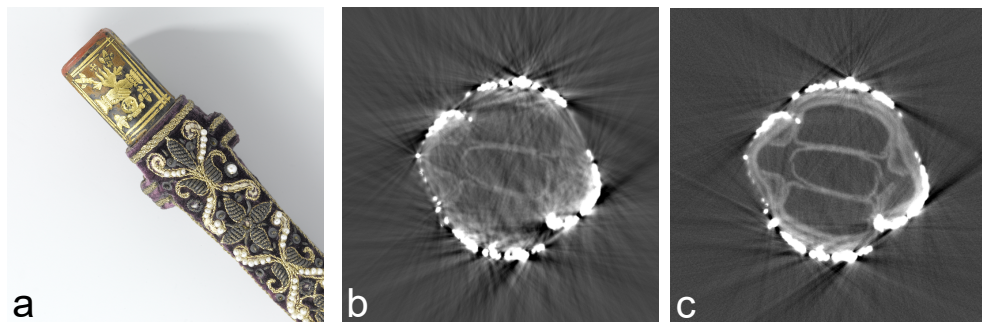


**Figure 1.12:** a) Detail of the cutlery case [158], b) and c) horizontal reconstruction slice of the widest section of the cutlery case with b) an untailored acquisition scheme, c) an acquisition scheme for which the source settings and beam filtration have been carefully chosen. Image adapted from [106].

### Accessibility of scanning facilities

Most museums do not have CT scanning facilities in-house, making it necessary to move precious collection items to external scanning facilities. CT scans carried out at commercial scanning facilities can moreover be expensive. In this thesis, multiple facilities have been used, each with their own specific characteristics with regard to hardware and software. The most-often used facilities are the FleX-ray lab, a laboratory micro-CT scanner situated at the Centrum Wiskunde & Informatica in Amsterdam (figure 1.13a), and the in-house X-ray facility of the Rijksmuseum (figure 1.13b). In this thesis, we also use datasets recorded at the X-ray facilities in the British Museum (London) and the J. Paul Getty Museum (Los Angeles).



Figure 1.13: a) The Flex-ray lab at CWI, b) the in-house X-ray facility at the Rijksmuseum.

### Data interpretation

The usual way of displaying the 3D reconstruction as 2D slices hampers the interpretability of the scans, because it can be a challenge to relate the features in a 2D cross-section to the three dimensional object. A 3D visualisation can assist in overcoming this issue, but a challenge for the interpretation of such 3D visualisations is that these do not reflect the actual colors and textures of the object. This is especially challenging for cultural heritage experts, who are trained to look at the original objects closely and move around and handle them to inspect the exterior details and not at a greyscale digital representation.

## 1.4 Research questions

In this thesis, we address the challenges outlined above by answering the research questions outlined in this section. Below, we indicate how the chapters in this thesis deal with the research questions and how the newly developed methods were applied to case studies from the cultural heritage domain.

### Research question 1.

How can expert knowledge be integrated in the CT acquisition process to facilitate efficient answering of heritage questions?

In chapter 2 we discuss how active involvement of object experts can guide the acquisition process to efficiently answer questions about the objects. In many CT scanning facilities a CT scan is performed and the data is given to the object expert after the object has left the scanning facility. This means that the process needs to be repeated if the answer cannot be found by analysing the dataset. We argue that it is important to actively involve the object expert in the scanning process and adapt the scanning approach based on intermediate feedback. Not only can we collect information to answer the original question, but the collaborative inspection of intermediate results can lead to additional information because new features of interest can be identified and captured.

In chapter 2 we demonstrate the process by detailing the approach taken to scan a 17th century cornett (see figure 1.9) from the Rijksmuseum collection with active participation of the object experts and imaging experts. The scanning process was steered to obtain ROI scans answering questions that were inspired by intermediate results (see figure 1.14).

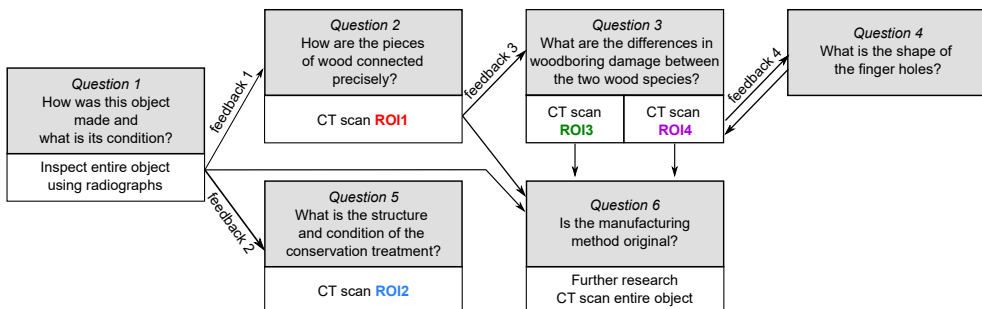


**Figure 1.14:** Example schematic of the workflow employed during the investigation of a 17th century cornett, indicating the steering of the scanning process by expert feedback.

**Research question 2.**

When a full CT is not feasible due to the size or shape of the object, can we design object tailored acquisition schemes to obtain the specific information that answers the art historical research question?

In chapter 3 we explore the possibility of obtaining specific information from a series of radiographs, when a full CT acquisition is not possible due to the large size of the object. When the object fits in the confines of the CT scanner, usually a full CT acquisition by taking images while rotating the object 360° is obtained. Using reconstruction algorithms, this data is then combined into a 3D reconstruction of the object. This approach however excludes objects that are too large to fit in the CT scanner. However, to answer some questions, no full 3D reconstruction is required. One of these cases is dendrochronological research, in which tree ring series are measured and compared to reference chronologies to determine the age and provenance of the wood. For this purpose a cross-section of the tree rings is needed. We developed an acquisition and reconstruction approach that uses X-ray data by moving an object on a linear trajectory between the source and detector to obtain clear images of the tree rings (see figure 1.15).

The approach for obtaining images of tree rings is first demonstrated on test planks in chapter 3. For these, the tree rings were visible on the outside and therefore the obtained tree ring measurements from the reconstructed X-ray images could be compared to the traditional method of measuring on photographs. Consequently, this approach is applied to the Hugo de Groot bookchest from the Rijksmuseum collection [154].

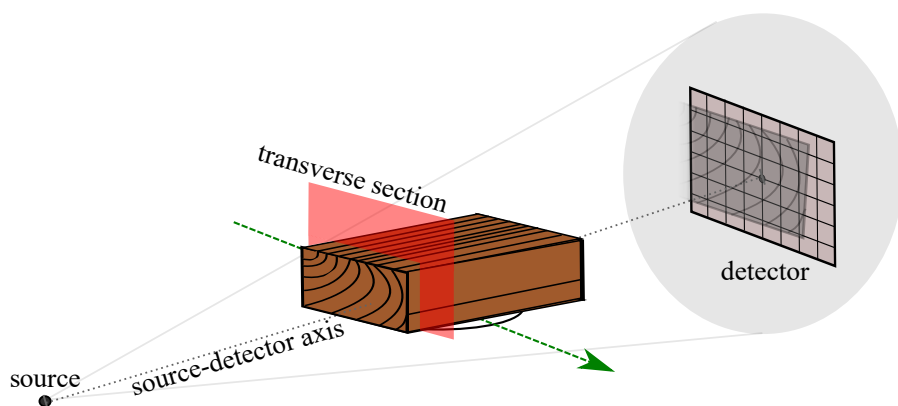


Figure 1.15: Line trajectory scanning.

**Research question 3.**

How can we optimise the use of the in-house X-ray facilities for live radiography by developing methods to use these setups for 3D imaging of museum collection objects?

In chapter 4, we propose a novel approach for creating accurate CT reconstructions using only standard radiography equipment already available in most larger museums. Specifically, we demonstrate that a combination of basic X-ray imaging equipment, tailored marker-based image acquisition protocols, and tailored data-processing algorithms can achieve 3D imaging of collection objects without the need for a costly CT imaging system. Our work paves the way for adoption of CT technology across museums worldwide.

We implemented our marker-based approach in the British Museum (London), the J. Paul Getty Museum (Los Angeles), and the Rijksmuseum (Amsterdam). In chapter 4, we demonstrate the method by scanning a small wooden test object in all three scanning facilities to compare the resulting 3D reconstructions. We moreover applied the method to a case study from the J. Paul Getty museum: *Python killing a Gnu* by Antoine-Louis Barye (French, 1796 - 1875), see figure 1.16. The CT reconstruction provided considerably more insight into the making process of this interesting sculpture than previously acquired radiographs. It showed the different layers of plaster and the parts where the object had been remodelled, as well as where metal rods are keeping the different pieces together.

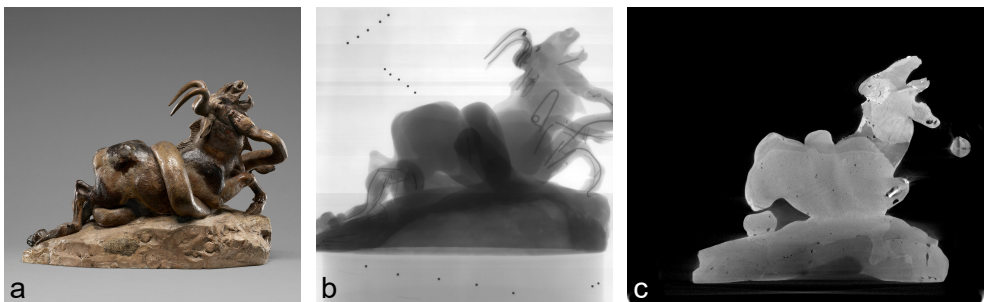


**Figure 1.16:** a) *Python killing a Gnu* [190], b) radiograph containing markers, c) cross section of the CT reconstruction.

**Research question 4.**

How can the data be visualised to improve the interpretability of CT scan data for conservators, restorers and art historians?

One of the challenges for the broad implementation and adoption CT imaging for cultural heritage research is the interpretation of the data. The 3D data is usually inspected as 2D slices or cross-sections through the object. It can be difficult to relate what is seen on the outside of the object to the features shown by the 2D cross-sections, especially for museum professionals, who are trained to look closely at the objects and handle them. 3D surface scans have been employed for the visualisation and digitization of the exterior of 3D objects. These scans give the colours and textures of the object and the information gained is thus complementary to CT scans, which give a greyscale density-based image of the interior. Therefore, in chapter 5, we provide an interactive visualisation plugin for the open-source software Blender, to combine and inspect two complementary 3D imaging modalities: CT images, which capture the interior; and surface scans, which capture the exterior (see figure 1.17).

The plugin workflow was applied to four case studies from the collections of the Rijksmuseum, Amsterdam, and the British Museum, London. Each of the objects presented their own challenges for data analysis and visualisation. The simultaneous visualisation of the exterior and interior led to new insights into the making process of these objects.

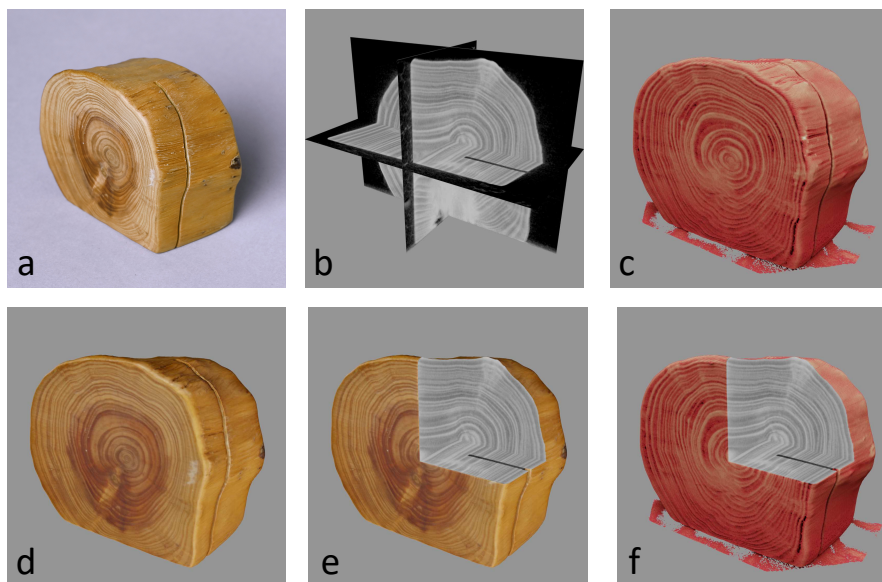


**Figure 1.17:** Combining CT scans and surface scans of a small wooden block: a) photograph of a small wooden block (h 5cm x w 6cm x d 3cm), b) X-ray CT scan represented as orthogonal slices, c) CT 3D volume render, d) surface scan, e) combined image modalities showing surface scan and slices, f) CT 3D volume render and slices.



# 2

## Integrating expert feedback in an explorative CT scanning workflow

Imaging science and computational methods have increasingly been applied to cultural heritage objects over the past decades [55, 56, 100, 141, 146], including optical coherence tomography [185], non-destructive X-ray imaging modalities such as radiography [206], phase contrast [120] and macroscopic X-ray fluorescence [177] and investigations combining multiple techniques [112, 197]. The focus in this chapter is on absorption X-ray tomographic imaging. The application of imaging with radiographs is well established in cultural heritage research, and used to investigate many different types of objects [82, 110, 137]. Radiographs provide a 2D representation of a 3D object, hence it is a challenge to extract data about features at different depths [137, 162]. CT imaging allows for a 3D representation of the object, thus providing information on the exact locations of features within and distinguishing layers [129, 150, 163]. Since the invention of Computed Tomography (CT) by Sir Godfrey Hounsfield in 1967 [151], it has been applied to several applications outside medicine [102]. In particular, CT scans have been used successfully for visualising and studying the interior of cultural heritage objects [5, 63, 113, 123, 125, 126, 149, 150, 163, 209] as well as for digitization of 3D objects [77].

---

This chapter is based on:

F. G. Bossema, S. B. Coban, A. Kostenko, P. van Duin, J. Dorscheid, I. Garachon, E. Hermens, R. van Liere, and K. J. Batenburg. “Integrating expert feedback on the spot in a time-efficient explorative CT scanning workflow for cultural heritage objects”. *Journal of Cultural Heritage* 49 (2021), pp. 38–47.

In CT-based research in the fields of technical art history and conservation, the research questions are linked to internal structures and features that are difficult to access, such as toolmarks or fingerprints inside the object, or separation lines between different materials. The governing questions can be related to the manufacturing process and structure, requiring information on the material composition of the object and the artist's techniques. For example, imaging the tree rings in wooden objects can assist in dating the object [19] and searching for lines in a terracotta statue can shed light on whether the clay was press molded or freely worked by hand [81]. Investigation by CT scanning can also be used to assess the current condition of the object for restoration and conservation purposes, revealing information on internal damage such as cracks, gaps and filler material [140, 178]. This will reveal any structural modifications that have an impact on the original state of the object.

The exploration process for studying art objects differs from medical applications, for which CT was originally developed [48, 103, 151]. For medical CT scans the position and general shape of the interior is known beforehand; the densities of the subjects are similar [16, 95]. The state-of-the-art medical scanners have been optimized pertaining to these characteristics. In the case of cultural heritage studies, it is unknown beforehand which features are present in the object and what scan specifications are needed to image them. Currently, the investigation process for each project involving CT scans starts by selecting a scanner. Which scanner is appropriate for a given purpose is closely linked to the size of the object and the required resolution of the reconstructed 3D image, as these lead to specific hardware requirements [50, 129, 180]. Published research often concerns a single object or multiple with similar characteristics, as these can be scanned at the same facility. Depending on the requirements of the CT scan, one selects either a medical scanner (resolution in the range of 1 mm [5, 19, 113, 121, 143]), industrial scanner (resolution in the range of 100 micron [19, 58, 82, 167, 182]), a lab-based scanner (resolution below 100 micron [47, 123, 181, 195, 198]), a synchrotron facility (resolution in the range of 10 micron or smaller [119, 180]) or specialised small-scale CT scanners (sub-micron to nanoscale resolution [74]).

In case there are no suitable in-house CT facilities, the process of CT scanning a cultural heritage object requires extensive planning with respect to transport of the object and the setup of the experiment, often taking a few weeks or even months for synchrotron facilities to arrange [180]. Once at the facility, the focus is to acquire as much data as the allocated time allows. The reconstructions are examined by the art expert at a later time. CT scans offer a wealth of information about the interior, which often stimulates new investigations. This exploration aspect clashes with the static nature of CT imaging, in which we collect data, reconstruct images and analyse results in a sequential order. Explorative investigation implies the repetition of these steps, greatly increasing the time needed to complete the research and raising challenges such as logistics, additional experiments and increased cost.

The long-term goal of the CT scanning approach presented in this chapter is an efficient implementation of an exploratory CT imaging process within museum research facilities. The key objectives of this chapter are i) detailing the requirements for a single scanner to perform explorative imaging; ii) describing the link between the

scanner design, algorithm development and expert (technical and heritage) involvement in the process, to carry out the exploration efficiently; iii) demonstrating that the timespan of the investigation is essential: carrying out the investigation, with the object and experts jointly present, in a single scanning session enables to expose details that might otherwise go unseen.

To our knowledge, we describe for the first time how the combination of a flexible scanning setup and direct expert feedback enables immediate follow-up actions, influencing the CT scanning process by insights gathered on the spot. This leads to an interactive workflow for explorative CT scanning, which potentially reduces the work that can span over a couple of weeks at different scanners (or even facilities) down to a single day, increasing both time- and cost-efficiency and research throughput.

## Research aim

We present the insights and experiences gained from two interdisciplinary research projects: the See-Through Museum [191] and Impact4Art [54]. It presents the collaborative work of the CT imaging scientists from the Centrum Wiskunde & Informatica (CWI), and conservators, curators and researchers from the Rijksmuseum, Amsterdam. We aim to establish explorative CT imaging as a way to enable efficient collaborative CT-based research of art objects, driven by developments and expertise in both these fields. As we want the exposition to be accessible to a broad audience (possibly with less detailed knowledge in CT imaging), we include detailed explanations of technical concepts using diagrams and case studies.

We describe the key characteristics of cultural heritage objects that are significant for CT scanning (object shape, feature resolution, object materials) and outline which degrees of freedom are required to accommodate a broad range of investigations in a single scanner design (zooming, tiling and object orientation). For each individual degree of flexibility, the implementation is illustrated on a small example. As a proof-of-concept, the complete explorative workflow is then illustrated with a case study of scanning a wooden cornett, in which the experts' feedback was essential to steer the scanning process in response to the observations, answering a chain of questions within a one day timespan.

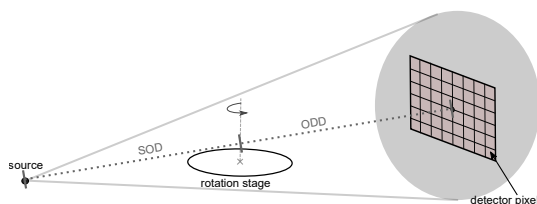


**Figure 2.1:** Schematic representation of a CT setup.

## 2.1 Material and methods

In this section, we first address the key characteristics of 3D cultural heritage objects that may be investigated by CT scanning. We then introduce the basics of CT imaging as well as the technical requirements to carry out the explorative workflow.

### 2.1.1 Key characteristics and technical requirements

The study of cultural heritage objects by CT scanning is substantially different from other CT-based investigations, such as in the fields of (bio)medical imaging and industrial quality control. In particular, the following key characteristics apply to the broad set of cultural heritage objects we encountered in the See-Through Museum and Impact4art projects:

- **Multi-scale features**

The internal features vary in scale independently of the size of the object. Toolmarks, for example, range from coarse to finely detailed. In order to image them at the required resolution one needs to be able to zoom into the object.

- **Sizes and shapes of objects**

Cultural heritage objects have hugely varying sizes, from small ivory beads to large wooden cabinets. The shapes can also differ from one another: from a simple, spherical object to more complex shapes, such as the elongated shape of a statue with outstretched arms. To accommodate the range of sizes and shapes, at the desired resolution, tiled CT scans are required and have, for example, been applied to large musical instruments [47].

- **Multi-material objects**

The objects in cultural heritage research can consist of multiple materials. The density of each material may vary. Cultural heritage objects often contain metal parts [82, 193] or might be entirely made of metal [18], causing artefacts in the reconstructed image such as streaks of cupping effects which are due to the beam hardening, photon starvation or scattering of the X-rays [21, 98, 116, 168, 181]. The barrier imposed by dense materials should therefore be avoided as much as possible, creating a need for flexibility in object orientation and positioning.

### 2.1.2 Principles of CT imaging

A CT setup consists of the following components: an X-ray source, a rotation stage and a detector. The diagram in figure 2.1 illustrates a point source that emits X-rays in a conical shape onto a flat panel detector. These X-rays travel through the object, which is mounted on the rotation stage. The absorption is material dependent [48, 50, 95]. The energy of the X-rays and the exposure time influence the quality of the data and determine the effective radiation dose the object receives. The potential effect of the radiation exposure depends on the settings of the scan and the characteristics of the object [17, 83].

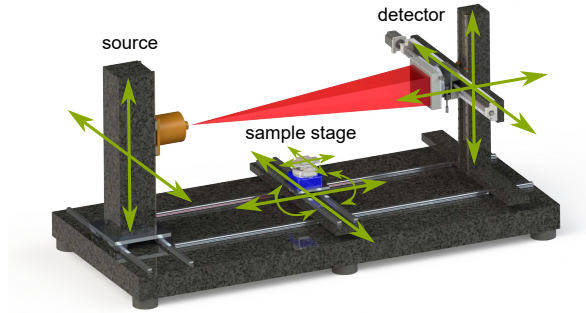


**Figure 2.2:** Schematic representation of the freedom of movement of components, indicated by arrows, in the FleX-ray laboratory CT setup. Image made after figure 2b in [53], with permission from the authors.

A single 2D detector image is called a radiograph or a projection. For a CT scan, the object is rotated and projections are taken from different angles. Typically, a full 360 degrees rotation is performed, with a constant rotation step size between the projection images in the order of 0.1 degree. The inner features are thus captured from many viewpoints. Mounting the object in a fixed and stable manner is particularly important in obtaining accurate results and ensuring the safety of the object.

### 2.1.3 Flexible setup

The concepts discussed in the following subsection, namely zooming, tiling and object orientation, are imposed by the variety of characteristics of the objects. Although there exist systems that facilitate one or more of these concepts [4, 115], it is rare to encounter a single scanner that has the degrees of freedom in each of the system components (source, detector, rotation stage) needed to facilitate them in a single apparatus. The FleX-ray laboratory at CWI [53] is an example of such a system. The setup consists of a cone-beam X-ray source with spot size 17 micron and energy range 20kV-90kV and a flat-panel detector of 1536x1944 pixels with pixel size  $0.0748mm^2$ . The freedom of movement of the components is outlined in figure 2.2. The laboratory combines a highly flexible CT scanner with newly developed algorithms and software for on-the-fly image analysis, enabling the prototyping of a wide range of X-ray based scanning methodologies.

### 2.1.4 Tailored reconstruction algorithms

The data from a CT scan consists of a large number of projections. Next to the hardware requirements that these large datasets (in the order of several GB) pose, the computing infrastructure needs to be available on the spot to process the data for inspection. A fast network connection that directly interfaces the data collection by the CT scanner with the accompanying reconstruction software is therefore a key

requirement of an explorative workflow. At the FleX-ray laboratory, the acquired data can be processed using the provided software, Acquila (TESCAN-XRE), within minutes of a scan being completed. In order to take the flexible movement of components into account for a full object reconstruction, tailored algorithms have been developed that are immediately available while operating the CT scanner. For example, if there is no single orientation that gives accurate results, it is possible to scan in multiple orientations and combine the data to improve the image quality [109]. For the reconstructions in the next sections we use the FleXbox software that was developed at CWI for this purpose [108]. The resulting 3D reconstruction, which is saved as a stack of slices through the object, can be visualised for inspection in any direction, using for example the freely available Fiji/ImageJ software [160].

### 2.1.5 Degrees of freedom for adapting the scanning process

We now illustrate how the various degrees of freedom in the settings and positioning of source, stage, and detector are linked to the characteristics of cultural heritage objects outlined in section 2.1.1.

#### Zooming

Zooming can be achieved by increasing the magnification of the object, for example by moving it closer to the source. This is shown in figure 2.3. In figure 2.4 an example of zooming is shown on a CT scan of a fragment of fabric [36], a mock object resembling a type of object we may encounter in cultural heritage studies.

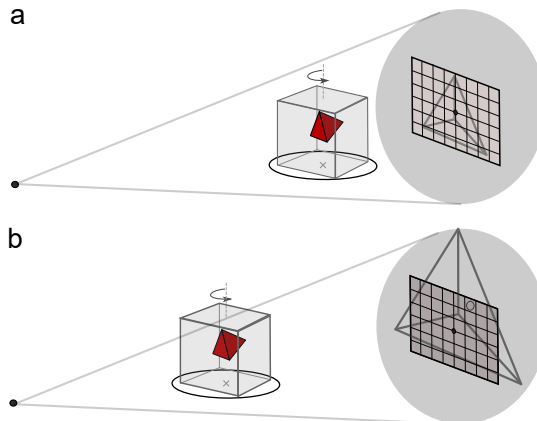


**Figure 2.3:** Schematic of the zooming in on an object in a CT setup. a) Imaging a pyramid in a box: at this magnification, the entire pyramid is visible on the detector. b) Zooming in to achieve higher resolution, by moving the rotation stage with the object closer to the source. More details can now be seen, such as the tiny void within the pyramid.

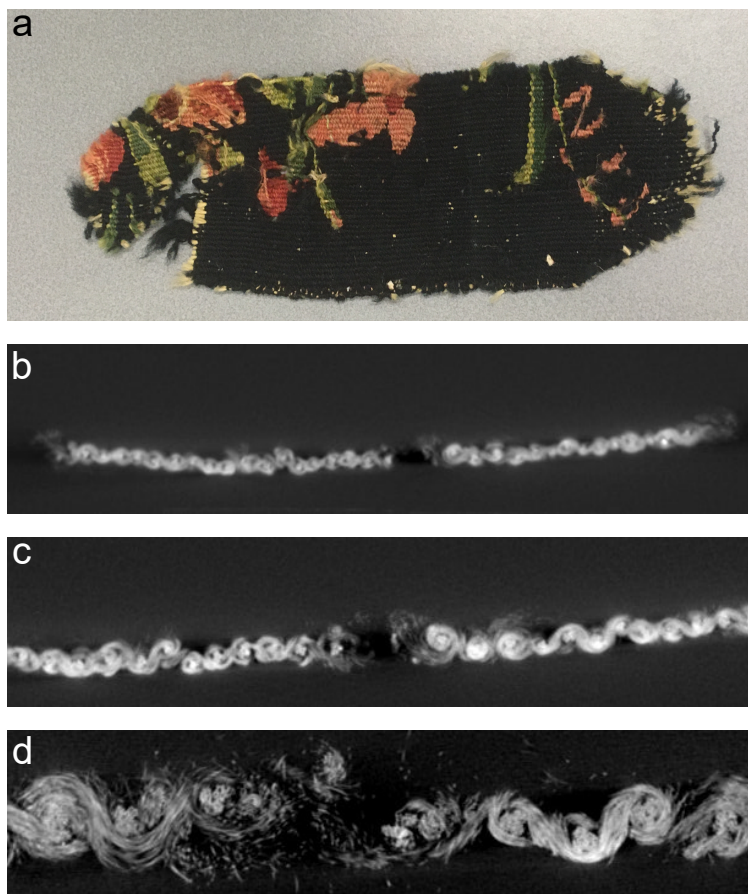


**Figure 2.4:** Example CT scans of a fragment of fabric to illustrate zooming. a) The piece of woven fabric that was scanned. b) Reconstruction slice from a low resolution CT scan (voxel size: 131 micron). The hole in the middle of the fabric can be perceived. c) Reconstruction slice from a higher resolution region of interest CT scan (voxel size: 82 micron). This higher resolution shows the knots in the weaving pattern of the fabric. d) Reconstruction slice from a high resolution region of interest CT scan (voxel size: 33 micron). At this resolution the individual yarns and, where the fabric is frayed, the individual threads that make up the yarn can be seen.

## Tiling

Tiled scans can be performed by moving the source and detector around between CT scans, a full rotation of the object is recorded for each location. Examples of tiling modes are given in figure 2.5. In figure 2.6 we present an example of a vertically tiled CT scan [40, 41] of an oak sculpture of *Woman with lantern*, 35.8 cm high, c. 1500-1525 (Rijksmuseum, Amsterdam) [159]. It was scanned for the purpose of dating by tree ring measurement [63].

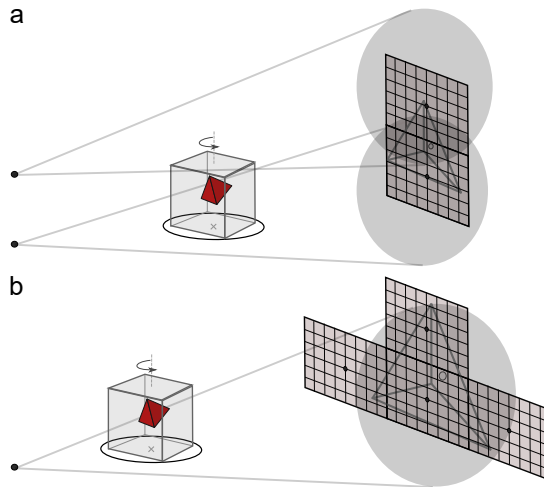


**Figure 2.5:** Schematic of how tiling is achieved in a CT setup. a) Vertical tiling: changing both source and detector positions between the CT scans. b) Tiling to capture the entire object at a higher magnification, example given here is performed by changing the detector position while keeping the source fixed.



**Figure 2.6:** Example CT scan of a wooden sculpture to illustrate tiled scanning. a) *Woman with lantern* [159]. b) The sculpture mounted on the rotation stage in the FleX-ray scanner. c) Radiographs showing the five tiles needed to image the entire object. d) The radiographs in (c) combined to obtain a single radiograph of the entire sculpture.

## Object orientation

Object orientation can be adjusted either by manually changing the positioning of the object on the stage (possibly changing the mount of the object) or by adjusting the trajectory of the source and detector to achieve a similar change of viewpoint. In figure 2.7 the effect of object orientation on the radiograph of an object with a metal support is shown. As an example object, we CT scanned an ivory bead with a metal bar through the middle to show the effect of object orientation on the reconstructed image, shown in figure 2.8.

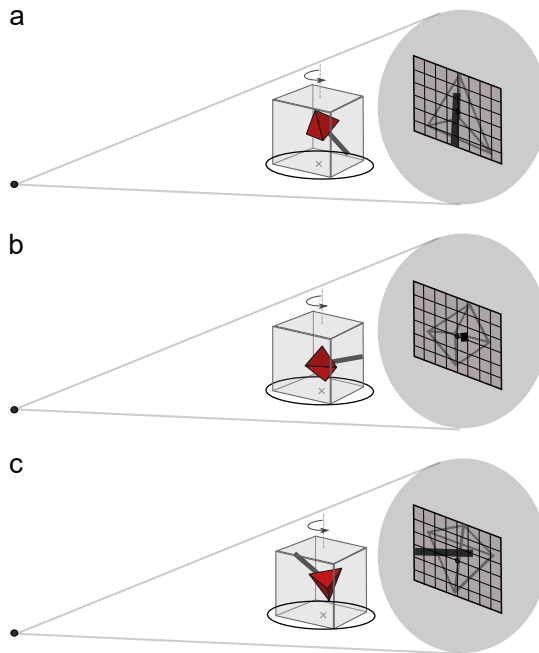


**Figure 2.7:** Schematic of changing object orientation in a CT setup. a) Here, the scanned object contains a metal stick. When rotated, the shape of the shadow on the detector remains approximately the same, forming a barrier over different parts of the object in the radiographs. b) Changing the orientation with respect to (a), with the metal stick now parallel to the rotation stage. The shadow of the stick ranges from only a dot to a horizontal bar (see (c)). The difference in shadowing during the scan will affect some parts of the object more than the others. c) The object in the same orientation as in (b), rotated by 90 degrees.

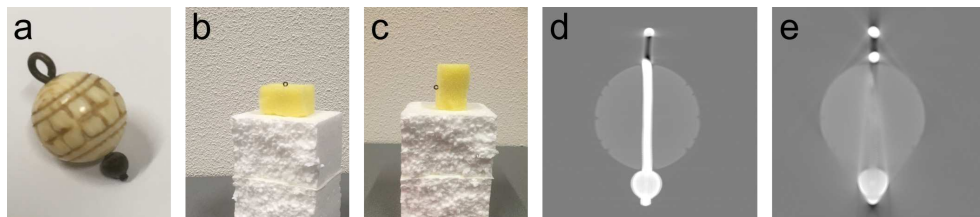


**Figure 2.8:** Example CT scans of an ivory bead on a metal bar to illustrate the use of object orientation to avoid shadowing by dense materials. a) Ivory bead on a metal bar. The bead is contained in a piece of sponge for scanning in two orientations: b) vertical (left) and c) horizontal (right). d) Slice of the 3D reconstruction of the bead with the bar vertical during CT scanning. e) Slice of the 3D reconstruction of the bead with the bar horizontal during CT scanning. The reconstructed volume was aligned with the volume in d) using manual landmark registration to show an equivalent slice through the object.

## 2.2 Results: case study of a wooden cornett

The examples in the previous section were chosen to illustrate each of the three technical requirements. In this section, we present a proof-of-concept study that brings together the flexible scanner design and the software to rapidly inspect the object after the CT scan using both radiographs and 3D reconstructions. New questions, based on the observations of the art expert, guide the settings of the next CT scan to perform. The demonstration was carried out in the FleX-ray laboratory at CWI.

The object under investigation is a cornett (see figure 2.10a), a curved woodwind musical instrument made in Italy between 1600-1650 (Rijksmuseum, Amsterdam) [157]. The cornett is made of wood, entirely lined with leather and is 56cm long. A recent study [93], performed during the conservation treatment on a fracture in the upper part of the cornett, has shown that it consists of different wood species: the upper section containing the mouthpiece, identified as cherry wood, being severely damaged by insect infestation, while the lower part containing the finger holes, probably made of boxwood, was left almost untouched. The initial question concerned the manufacturing method and conservation status of the cornett (*Question 1* in figure 2.9). As the leather lining does not allow a visual inspection of the wooden parts of the cornett, CT scanning was employed to visualise the interior.

To ensure that the object was securely mounted on the rotation stage, a mount was specifically designed for the cornett (see figure 2.10b). It was made from a rectangular piece of Ethafoam® [69], attached with polyethylene hotmelt adhesive within a groove in an octagonal foam base to create a vertical stand. One end of the object rested in a cut-out in the foam base, and the object was secured upright with a cotton tape through a hole in the vertical stand. This made it possible to safely modify the object position and to flip it vertically on the stand. Ethafoam® is often used for mounting as it is cheap and widely available, easy to mould into an appropriate shape, and lightly absorbs the travelling X-rays.

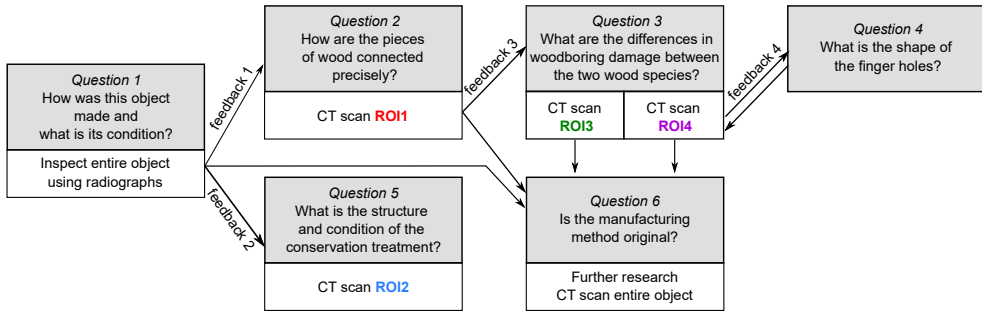


Figure 2.9: Schematic of the workflow employed during the investigation of the cornett.

## 2.2.1 Tiled inspection with radiographs

### Question 1: “How was this object made and what is its condition?”

The conservators questioned the current condition of the object and the manufacturing process, e.g. the damage by the insect infestation and how the curved object was hollowed out. An inspection with radiographs of the entire object was carried out in a dynamic process in which the scanner components were moved around at the request of the conservator and the resulting radiographs were shown directly on the screen next to the scanner. Due to the height constraint of the scanner, first the lower half of the object was inspected, and then the object was flipped within the mount to inspect the remaining half. The vertical and horizontal range of motion needed to provide a full view of the object while rotating it over  $360^\circ$  is illustrated by the radiographs in figure 2.10c. Both object orientation and tiling were thus necessary to obtain a full view of the object. The values for the voltage and power were investigated and chosen to be 70kV and 42W, respectively, and were kept the same throughout the scanning process. The radiographs confirmed that there were two different species of wood as the densities of the two sections were different. Based on the inspection, the conservators raised *Question 2* in figure 2.9: How are the pieces connected precisely? This required a higher resolution CT scan of the region containing the joint (ROI1). The total time needed for the preparation and inspection was approximately 1.15h (mounting: 15min, parameter investigation: 15min, inspection and discussion: 45min).

## 2.2.2 CT scanning the joint

### Question 2: “How are the pieces of wood connected precisely?”

Following the inspection by the conservators (*Feedback 1*), we performed a CT scan of the region containing the joint (ROI1) at image resolution 50 micron. Each of the ROI scans consisted of 1200 projections. The data was used for a reconstruction on the spot and shown on the screen next to the scanner for analysis by the conservators. They asked if it was possible to perform a CT scan of the region in higher resolution. The total time for this investigation was 40 minutes (preparation: 5min, scan: 15min, reconstruction: 10min, discussion: 10min).

We zoomed in by moving the object closer to the source to focus on the region of interest with image resolution 25 micron (ROI 1, see figure 2.10e,i). Analysis of the reconstruction of this CT scan confirmed that the pieces of wood were connected with a lap-joint with different layers of material (leather and wood) clearly identified. It also became apparent that both the lower and upper sections consist of two longitudinal pieces of wood, as a thin glue joint was visible on the horizontal slices (figure 2.10e). The conservators then wanted to investigate the difference in woodboring damage between the two species (*Question 3*). Total time needed was 35 minutes (preparation: 5min, scan:15min, reconstruction: 10min, discussion: 5min).

### 2.2.3 CT scanning the infested section

#### **Question 3: “What are the differences in woodboring damage between the two species?”**

In the CT scan of the joint, it became apparent that both parts had been damaged by the insects. The conservators expected only the upper part to be damaged, as there were no holes on the outside on the lower part. The ROI1 reconstructions showed that the lower wood had been infested to some degree close to the joint but was otherwise nearly untouched. The conservators were interested in visualising the damage in both parts further from the joint (*Feedback 2*). Keeping the same object position and moving the source and detector up and down to image different sections and slightly changing the object orientation to make sure the region of interest stayed in the field of view, two more ROI CT scans at image resolution 25 micron were performed to investigate these questions (ROI 3,4). ROI3 revealed the devastating effect of the insect infestation in the upper half of the cornett and the tunnelling structure. The conservators remarked how porous the wood had become, and how little wood was left to support the instrument (see Figures 2.10g,k). This new information clearly documents the condition, illustrating how fragile the substrate has become and why the damage occurred precisely in this area. The ROI4 reconstruction revealed that the lower part was indeed almost untouched by the insects (see Figures 2.10h,l). The thin glue joint of the two longitudinal pieces of wood was again visible on the horizontal slices (figure 2.10g,h). The time needed for each ROI CT scan was 40 min (preparation: 5min, scan: 15min, reconstruction: 10min, discussion: 10min).

### 2.2.4 CT scanning a section containing finger holes

#### **Question 4: “What is the shape of the finger holes?”**

The location for the ROI4 CT scan was chosen to include a finger hole, which could provide a possible insight into the manufacturing process: the shape of the finger and thumb holes (*Feedback 4*). Based on the analysis, the conservators identified the finger hole to be undercut to account for intonation corrections by the maker.

In addition, the CT scan showed in more detail the longitudinal joint. From this the conservators concluded that to construct the hollow interior of the cornett, the makers used a single piece of wood, split and carved out each half to create the curved bore before putting the halves back together. The tree ring patterns were visible on

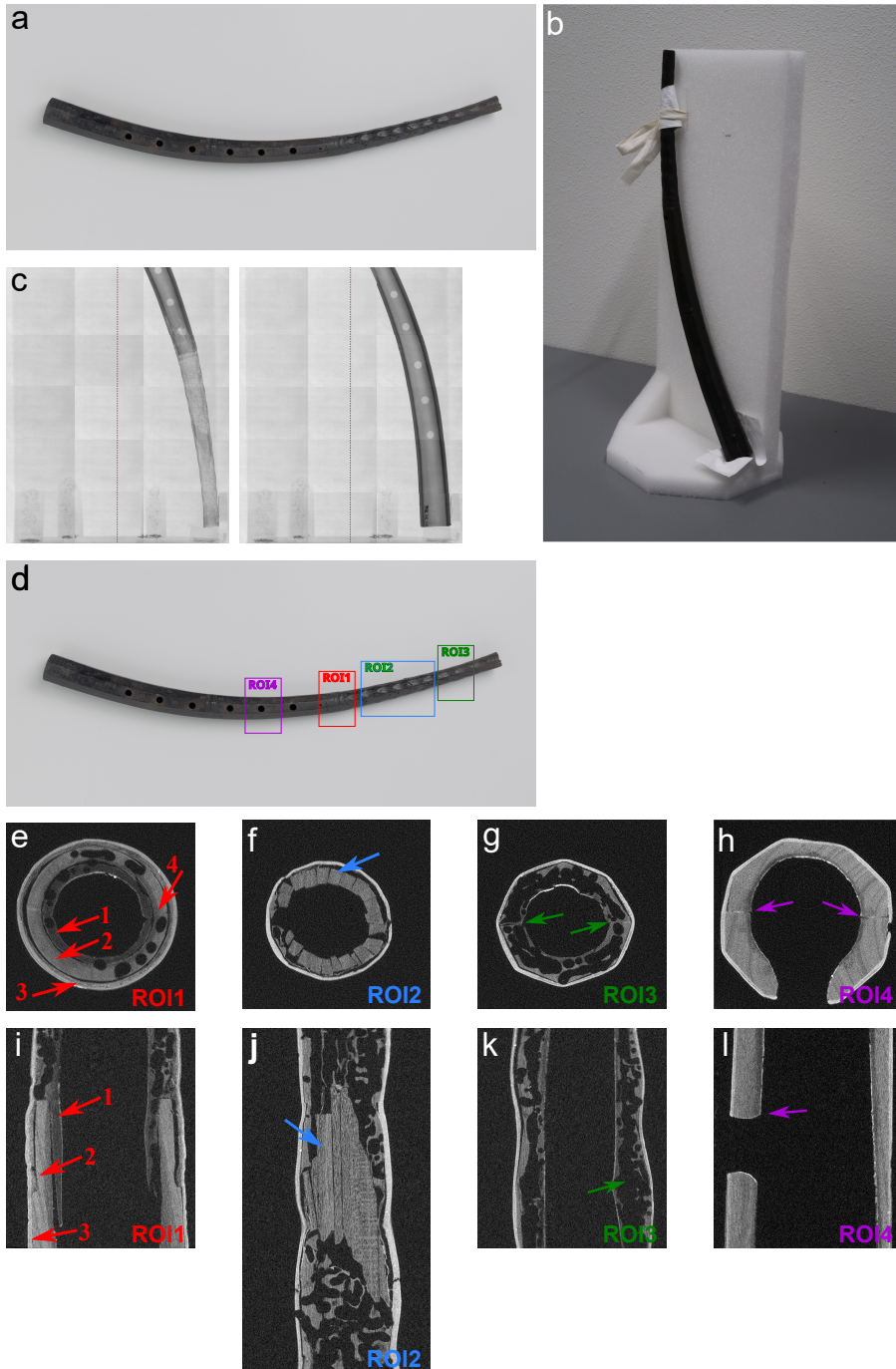
the reconstruction, and indicated that the halves were indeed from the same piece of wood. A new question arose based on this CT scan, namely whether the size of the curvature and thus the diameter of the tree section could be estimated from these images. Fitting the curvature lines to a circle, we estimated that the section used to make the instrument can be placed at approximately 10-20 cm from the pith in the transversal section of the tree trunk. The curvature excludes the possibility that the cornett was made from a branch or a section including the pith.

## 2.2.5 CT scanning the restoration

### Question 5: “What is the structure and condition of the restoration?”

Following the inspection by radiographs of the full object, the conservators were also interested in the location where the cornett had been broken and later restored in 2018 [93]. In order to investigate and monitor the structure and long term effect of the restoration, ROI2 was scanned at 25 micron image resolution. According to the conservation report, small custom-shaped sticks were inserted to replace missing wood. The inserts were covered with Japanese paper and retouched so that the intervention is practically invisible from the outside. The region of interest was larger than the previous ones, meaning a 2-tile CT scan was necessary to capture the details at the same resolution. The reconstruction showed the conservation method clearly (Figures 2.10f,j), providing an excellent documentation for future reference and for the monitoring of long term effects. The total time needed for this investigation was 1 hour (preparation: 10min, scan: 30min, reconstruction: 10min, discussion: 10min).

**Figure 2.10:** The case study concerning the CT scanning a 17th century cornett. a) Cornett. [157]. b) The cornett and its Ethafoam® mount. c) Left: 15 tiles to inspect the upper part of the cornett with radiographs. The 15 tiles show the necessary range of motion to rotate the object over 360° during inspection. Right: 15 tiles to inspect the lower part of the cornett with radiographs after rotating it vertically on the mount. The red dashed line indicates the centre of rotation mapped onto the merged radiographs. d) The cornett with the regions of interest (ROI) indicated in rectangles. e) Horizontal reconstruction slice of ROI1 (voxel size 25 micron), showing the wood of the upper part (1) and lower part (2) within each other, the leather lining (3) on the outside and the thin glue joint separating the two longitudinal wood pieces (4). f) Horizontal reconstruction slice of ROI2 (voxel size 25 micron), showing the wooden sticks inserted during the conservation treatment (marked by the arrow). g) Horizontal reconstruction slice of ROI3 (voxel size 25 micron), showing the damage by insect infestation in the upper section of the cornett and the joint (marked by the arrow). h) Horizontal reconstruction slice of ROI4 (voxel size 25 micron), showing the tree rings, joint (marked by the arrows) and a finger hole. i) Vertical reconstruction slice of ROI1, showing the lap-joint between the upper wood (1), and lower wood (2) and the leather lining (3). j) Vertical reconstruction slice of ROI2, showing the wooden sticks inserted during the conservation treatment (marked by the arrow). k) Vertical reconstruction slice of ROI3, showing the damage by insect infestation in the upper section of the cornett (marked by the arrow). l) Vertical reconstruction slice of ROI4, showing the shape of the finger hole (marked by the arrow).



## 2.2.6 Further research

### Question 6: “Is the manufacturing method original?”

As it would not be practical to bring the object to the scanner again, we decided to use one more day to CT the entire object to facilitate further research and have a complete digital representation of the object for future reference. We performed a 30-tile CT scan at the resolution of 50 micron to image the entire object. As during the inspection it was necessary to first scan the lower half in 15 tiles, then flip the object in the mount and scan the other half. For each tile 1201 projections were taken. The tiling was automated by writing a script with exact locations for source and detector positions during the CT scan (locations corresponding to the radiographs in figure 2.10c). The scanning took in total 7.5 hours (preparation: 1 hour, first tiled scan: 3 hours, repositioning: 30 minutes, second tiled scan: 3 hours).

The investigation of this cornett using CT imaging illustrates how an explorative workflow facilitated by one scanner increases both time-efficiency and research throughput. The inspection and consequent refinement of scans by the experts was performed on a single day (taking in total approximately 5 hours), and led to more questions and analysis. It stimulated further research outside the CT facility mainly regarding the originality of the manufacturing method with two wood species. Investigations were carried out to determine whether other cornetts have comparable structures with multiple wood species, and to further analyse the CT scans for art historical and conservation purposes [64].

## 2.3 Discussion and conclusions

The wide range of objects investigated by CT in cultural heritage is imposing challenges for applying an explorative workflow, where new questions are continuously asked based on the outcome of imaging observations. In this chapter we have discussed the key requirements for enabling a time-efficient workflow for CT scanning of cultural heritage objects and presented our implementation of such a workflow in the FleX-ray laboratory at CWI, where a CT scanner with several degrees of freedom is combined with a fast computational imaging solution that allows to inspect results while the object is in the scanner, asking new questions and planning new scans that can be carried out immediately.

A flexible imaging workflow with support for a wide range of magnification factors and detector tiling can effectively address the key characteristics of CT scanning for cultural heritage research: multi-scale features, sizes and shapes of objects and multi-material objects. Through fast user feedback, this allows for the adjustment of scanning parameters on the spot, giving a wide range of possibilities to investigate features in detail that are discovered during the scanning process. The case study shows how the time-efficient explorative workflow can benefit research, as for example *Question 5* was inspired by the initial inspection with radiographs of the entire object. The scans of ROI2, ROI3, and ROI4 are direct consequences of expert feedback, in which the experts enquired about specific sections of the object interior based on

the analysis of the radiographic inspection. This was only made possible via the explorative workflow, where we modified the scanning parameters to investigate on the indication of the experts.

Our approach requires a highly flexible CT scanner and the presence of both the CT imaging scientist and the curator or conservator. The FleX-ray scanner at CWI (Amsterdam) provides the required scanning flexibility for relatively small objects. Many cultural heritage objects do not conform to this size constraint, or are difficult to move outside the museum. The technical requirements for implementing such a workflow on-site should therefore be taken into account in the design of X-ray facilities in museums. Although our approach does not replace the investigations with different X-ray imaging modalities such as phase contrast, or very high resolution scanning at synchrotrons, it offers a broad range of applications where absorption imaging is the main investigation. Follow-up research, such as the development of a more automated scanning and feature extraction process, is required to turn it into a methodology that can be applied at large. With the approach described in this chapter, we hope to contribute to the establishment of a more time- and cost-efficient workflow to optimise the knowledge gain from CT scanning cultural heritage objects.



# 3

## Line trajectory X-ray tomography for dendrochronology of large historical wooden objects

Scientific investigations of cultural heritage objects made from different materials play an important role in understanding the manufacturing process, establishing their chronology, attributing objects to artists, and deciding on conservation methods [3, 56, 161, 183, 184]. Because of the uniqueness of these historical objects, investigations requiring invasive methods (those that involve removing a sample from the object to be analysed either by destructive or non-destructive techniques) are carefully weighed against the potential knowledge gain [3, 62]. Therefore, the demand for non-invasive methods has increased over the past years, and novel techniques are being developed [15, 49, 100, 112, 146, 148, 197]. Amongst these, X-ray-based imaging modalities such as X-ray fluorescence (XRF) spectroscopy [46], radiography [110] and CT imaging [37, 123, 150] are important tools for investigating the chemical composition and the interior structure of art objects. Here, we focus on non-invasive X-ray absorption imaging for the purpose of tree-ring dating as a means to aid in the authentication of

---

This chapter is based on:

F. G. Bossema, M. Domínguez-Delmás, W. J. Palenstijn, A. Kostenko, J. Dorscheid, S. B. Coban, E. Hermens, and K. J. Batenburg. “A novel method for dendrochronology of large historical wooden objects using line trajectory X-ray tomography”. *Scientific Reports* 11, 11024 (2021).

art-historical wooden objects.

Dendrochronology (tree-ring science) is the most exact method to date wood of (pre)historical objects, structures and artifacts [12, 90]. Ring-width series in living trees can be merged to develop reference chronologies anchored in time, which can be used to identify the unique chronological position of tree rings in wood from (pre)historical contexts [65, 78]. This is known as crossdating, whereby each ring is assigned an exact calendar year [12, 78]. In traditional dendrochronology tree rings are measured in the transverse section of the wood. This requires a sample to be extracted from the object and placed under a microscope, or the growth pattern to be accessible in a cross-section so that it can be photographed and measured on the digital photos. Usually, optimal visualisation of the tree rings is only obtained after cleaning the surface with some abrasive method [62]. Such methods range from non-invasive simple brushing to highly-invasive procedures such as sand-blasting or even scraping with scalpel blades. The use of invasive methods is undesirable because they irreversibly alter the object. Furthermore, even when tree-ring patterns are accessible and the measurements can be done without invasive procedures, the longest tree-ring series may not be accessible from the outside. Obtaining the longest possible tree-ring series is crucial to the success of dendrochronological research, as longer series have higher chances to be dated by finding a statistical and visual match with the reference chronologies in a unique position (i.e. in one calendar year) [145]. The shorter the series, the higher the likelihood to obtain spurious matches in random positions, which precludes the possibility to identify which one is the correct date [12]. These considerations have prompted in recent years an increasing demand for the implementation of dendrochronology through non-invasive techniques.

The use of computed tomography (CT) for non-invasive imaging of tree rings has grown over the last decade, as it provides access to the inner structure of the wood when the tree-ring patterns cannot be retrieved by direct inspection on the surface [19, 58, 135, 182]. The 3D information obtained by CT of the internal structure of the object has a decided advantage over 2D images, such as radiographs, yielding additional insights in e.g. the conservation state of a wooden object and previous restoration interventions [47, 134, 149, 150, 178]. Successful investigations using CT scanners at medical facilities, laboratories and synchrotron facilities have been performed on wooden object of varying sizes such as historical instruments [75, 178, 180, 202], painted panels [58, 121], archaeological objects [122] and sculptures [134]. However, the method is in general not well-suited for large objects. A full rotation is needed within the space between source and detector or the source and detector around the object, posing size constraints on the object. Moreover, the size of the detector determines the portion of the object that can stay in the field of view and thus can be imaged during one rotation. In addition, the size of the detector is usually linked to the detector pixel size and therefore a larger detector implies lower spatial resolution. To image large objects in laboratory setups, several CT scans have to be made and merged, requiring large amounts of data and high scanning and computation times [44]. As a result of such constraints, few large wooden objects, such as panel paintings and sculptures, have been scanned using CT thus far [58, 134].

Here, we present a scanning technique for a laboratory setup that is suited for

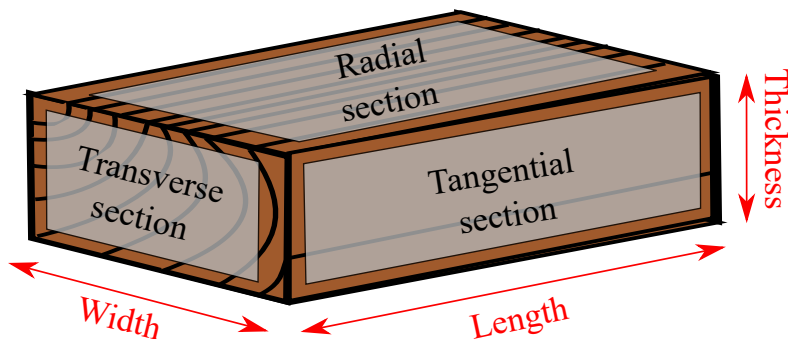


**Figure 3.1:** Schematic figure to illustrate the dendrochronological concepts of transverse, radial and tangential section and the definitions of length, width and thickness as used throughout this chapter.

large objects such as large panel paintings, chests and cabinets. Rather than rotating the object (as is customary in CT), we move it on a linear trajectory between the X-ray source and detector, while recording radiographs. Scanning geometries with linear movement have been previously investigated [80, 84, 176, 210]. Line trajectories in various configurations with one or multiple source-detector pairs have been used for security inspections [80], knot detection in logs [175] and medical applications [208]. Simulations of a line trajectory scan show promising results for imaging features with a planar shape [79]. For rectangular, flat objects, computed laminography is another common method, usually requiring a full rotation of the object or source-detector pair with a tilted rotation axis [91, 92, 112, 133].

The novelty of the proposed line trajectory (LT) scanning technique lies in exploiting the direct link between the features to be imaged and the scanning trajectory. We make use of the specific requirement for dendrochronology, providing a cut through the wood that shows the tree-ring pattern in the transverse section. In the following, we introduce the principles of this method and validate it with simulated data and test objects, discussing possibilities and limitations. Subsequently, a successful case study of an iconic wooden chest from the Rijksmuseum in Amsterdam (The Netherlands) is presented.

## 3.1 Methods

### 3.1.1 Dendrochronology and CT

To date wooden objects or investigate their origin, the science of dendrochronology typically uses the relative width of tree rings. The tree rings are measured on the transverse section of the wood (figure 3.1) However, the transverse section is not always accessible on the outside of the object, for example due to how the plank was processed.

To overcome this limitation, tree rings in a wooden object can be visualised using X-ray absorption imaging, because the differences in density within the wood provide

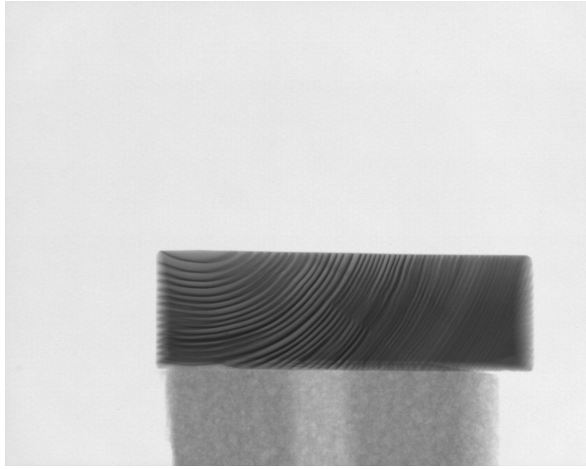


**Figure 3.2:** A radiograph of a wooden block, with the transverse section facing the source.

contrast. The reason for this contrast is that more radiation travels through the less dense areas (earlywood) and less radiation through the denser areas (latewood). On a single radiograph, most rings will be projected at an angle, because of the cone shape of the X-ray beam. This means that on the radiograph denser and less dense areas are overlaid, blurring part of the rings. A single radiograph does therefore not suffice to extract the entire tree-ring pattern (figure 3.2).

During a regular CT scan, radiographs (or projections) are taken over a rotation circle of 360 degrees. A 3D volume can be reconstructed from the 2D projections [48]. This reconstruction consists of 3D pixels, called voxels, that can be visualised as a stack of images (slices) at different depths in the object. For regular CT scans, reconstructions are commonly done using fast analytical algorithms [72], but these are typically tailored to specific acquisition trajectories. Iterative tomographic reconstruction methods on the other hand, are slower but more generally applicable to acquisitions using non-standard trajectories [87].

### 3.1.2 Line trajectory scanning

The proposed scanning trajectory is a linear movement of the object between the source and detector (figure 3.3a). The internal features we want to capture, the tree rings, are curved surfaces along the longitudinal axis of the tree. As the data is not collected over a complete angular range, this will however not yield a perfect reconstruction. The reconstructed 3D image is expected to be smeared out along the source-detector axis. The tree ring surfaces are elongated in the direction of the longitudinal axis. If these are placed parallel to the source-detector axis, the typical smearing effect across slices is along the direction of the longitudinal axis. Although this smearing may have a large quantitative impact on the attenuation values in the reconstruction, due to the high similarity of wood structure in that direction, the

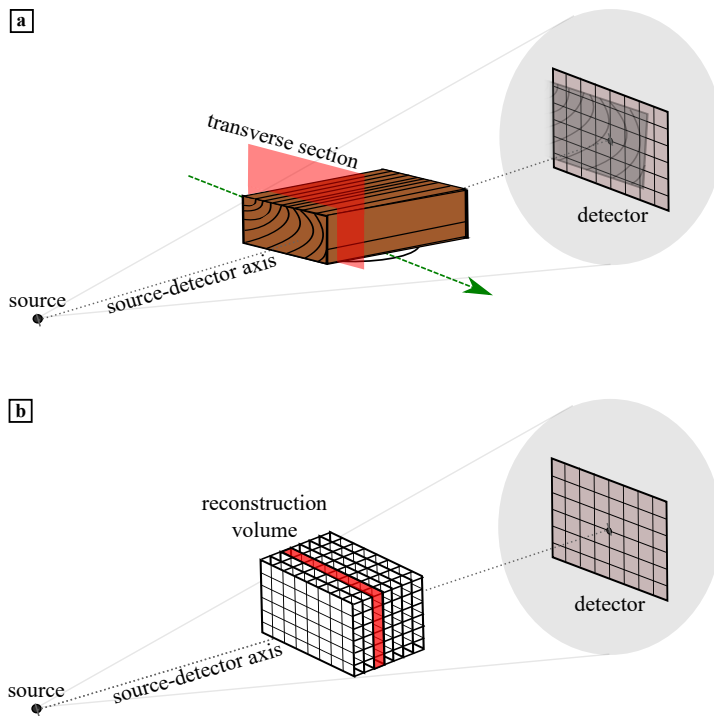


**Figure 3.3:** Schematic figures illustrating the LT scanning method. a) Setup of the LT scan, where the object is placed with the transverse section perpendicular to the source-detector axis and is moved along the green arrow between source and detector. The transverse section is indicated by the red plane. b) Schematic showing the location of the virtual reconstruction volume within the setup, a slice perpendicular to the source-detector axis is indicated in red.

influence of the smearing is effectively small on the slices perpendicular to the source detector axis. This enables a sharp reconstruction of the tree-ring pattern of the transverse section in those slices. If the pith lies outside the plank, the tree ring surfaces are mainly vertically oriented. Images are then taken along and at slight angles of these surfaces. We expect that this will lead to the sharp imaging of the tree rings. If the orientation of the longitudinal axis is sufficiently aligned with the source detector axis, the desired transverse section lies in a reconstruction slice perpendicular to the source-detector axis (figure 3.3b). Slices in this direction should then provide images of the transverse section suitable for tree ring acquisition.

### 3.1.3 3D reconstruction and slice selection

In this chapter, we use the Simultaneous Iterative Reconstruction Algorithm (SIRT) [87] to obtain reconstructions, because of its suitability to deal with non-standard trajectories. This reconstruction algorithm transforms the data into a high dimensional system of linear equations, which is then solved by iteratively updating the reconstruction based on the difference between a forward projection of the current estimate and the acquired data. A possible drawback of the SIRT algorithm is the required computation time and memory. This can partly be overcome by reducing the number of voxels in the reconstruction volume. When the scanned objects are long, this can be achieved by extending the voxels in the length direction, i.e. producing cuboid voxels. The effect on the quality of the transverse slices is negligible because of the high similarity of the wood structure at the scale of the voxels in the direction of the longitudinal axis.

From the reconstructed volume, slices need to be selected for dendrochronological analysis. As the side of the object closest to the source has the highest magnification factor on the detector images, this will have the best image resolution in the reconstruction. The voxel size is therefore chosen based on magnification of the front of the object. Due to the previously described smearing effect, the exact front of the object does not yield the sharpest slice. Based on inspections of results, we choose to investigate slices around 25% from the front of the object. As the features have a strong similarity in the scanning direction, the measurements will be comparable across slices that are close to each other. The measurement of tree rings is a manual process, in which the expert knowledge of a dendrochronologist is required. Through the inspection of images together with a dendrochronologist, slices that would yield the most measurable images (i.e. showing the sharpest tree rings) were selected. Measurements can be performed either on one slice or on multiple slices and averaged subsequently to compensate for slight variation in manual measurements.

### 3.1.4 Scanning procedure and analysis of the wooden test objects

The scans of two wooden test objects were carried out at the FleX-ray laboratory [53] of the Centrum Wiskunde & Informatica (CWI) in Amsterdam (the Netherlands). This scanner in laboratory setup allows for flexible adjustment of the components and

is therefore well suited to investigate new scanning trajectories. It can image objects up to approximately 50cm x 50cm x 50cm.

The wooden test objects were placed on the sample stage, aligning their centre with the centre of the stage. We chose the range of translation as far to the left and right as possible within the space constraints. We determined the source power, energy and exposure time to gain sufficient contrast of the early- and latewood of the tree rings by visually inspecting the projections. Then, we calculated the distance that the object moved between projections, ensuring that a point on the front of the object would move less than one detector pixel in between two projections. Taking a high number of images should provide better reconstruction quality; therefore it is recommended to move the object at short intervals along the trajectory to increase the number of projections. To process the scan, the projection data was first flat- and darkfield corrected. For all the reconstructions the Flexbox software [108] was used, with reconstruction algorithm SIRT. From the reconstruction, one or more slices were selected for measurement.

The transverse surface of both test planks was moreover prepared for dendrochronological research cleaning with sharp scalpel blades. Chalk powder was applied to the surface to enhance the visualisation of the tree-ring boundaries [12, 164]. The surface was photographed with a compact digital camera on macro mode to proceed with the measurement of the tree rings.

Tree-ring widths were measured on the photographs and selected slices from the reconstruction by manually placing the coordinate points on the ring boundaries following a reference line perpendicular to the boundaries using the software package *CooRecorder & Cdendro* [111]. *CooRecorder* registers the distance between two points (which are equivalent in this case to the ring width) as coordinates, and *CDendro* converts the coordinates into metric units, creating a series of ring widths (commonly known as tree-ring series). Next, we used *PAST4 v.4.3* [170] to crossdate the tree-rings series. This software automatically compares pairs of tree-ring series while performing several statistical tests for each overlapping position. To measure the goodness-of-fit we considered in *PAST4* the Student's t-test calculated after normalisation of the data as described by Baillie and Pilcher [13] (TBP), the percentage of parallel variation, or 'Gleichläufigkeit' [68] (GI), which is a non-parametric test that reflects the synchronicity between overlapping portions of tree-ring series, and the significance level of the %PV. The Student's t test is based on the correlation coefficient ( $r$ ). Identical tree-ring series would yield TBP=100 (resulting from a  $r=1$ ) and a GI=100% regardless of the length of the overlap. Tree-ring series obtained from the same sample should be very similar, although never identical due to differences in the manual placement of coordinates points. Still, they should yield high TBP and GI values (e.g. TBP>10 and GI>75%) even for short overlaps.

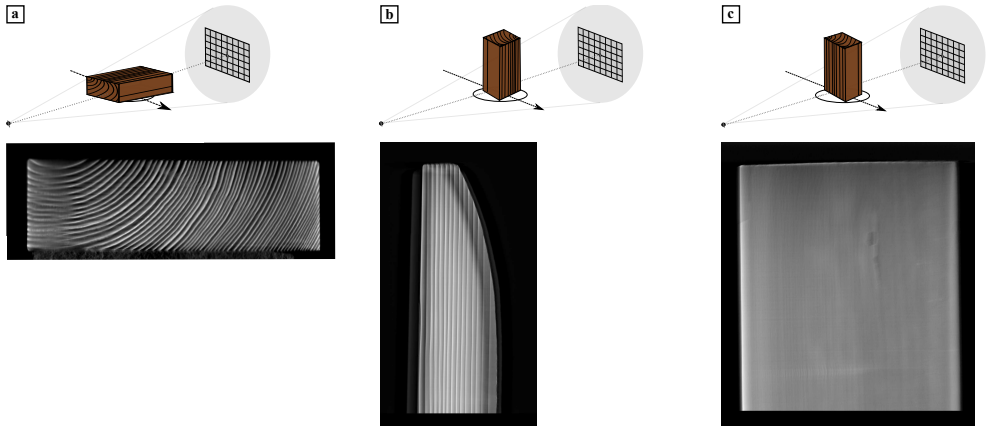


**Figure 3.4:** A reconstruction slice (bottom row) perpendicular to the source-detector axis from three LT scans. The wooden block was placed in 3 different orientations shown on the top row: the transverse section a) perpendicular to the source-detector axis; b) perpendicular to the vertical axis, width aligned with the source-detector axis; and c) perpendicular to the vertical axis, width perpendicular to the source-detector axis. Only (a) is useful for dendrochronological investigation.

## 3.2 Experiments and results

### 3.2.1 Test case 1: small conifer block

A small wooden block of conifer wood (3cm thickness x 10cm width x 12cm length) was first chosen to assess how the positioning of the object affects the reconstruction. For this, we took three LT scans with the wooden object in different orientations [34]. For the LT scans 2,201 projections over translation range (-110mm, 110mm) (figure 3.4a,c) and 2001 (figure 3.4b) projections over translation range (-100mm, 100mm) were taken at tube settings 90kV and 40W. The reconstructions were performed with 100 iterations of SIRT and voxel size 66.9 micron. The results (figure 3.4) clearly show that the LT scanning technique only yields images suitable for dendrochronological measurements, when the transverse section is facing the source (figure 3.4a) and the tree rings are thus parallel to the source detector axis. As the other orientations do not provide measurable images, the question arises how a slight tilt of the tree rings with respect to the source detector axis affects the measurability. In the next section, we will show simulated results to investigate the effect of tree ring tilt.

The size of the first test object allowed a full CT scan to be made to validate that the ring-width pattern measured in a line-trajectory scan (figure 3.5a), a full CT reconstruction (figure 3.5b), and a digital photograph (figure 3.5c) would yield the same tree-ring measurements. Therefore, a CT scan [32] and a digital photograph were also recorded of this object. For the CT scan 2,915 projections over a full rotation were recorded at 90kV and 30W. Similar as for the LT scan, the reconstruction was performed with 100 iterations of SIRT and the voxel size was 66.9 micron for both scans. The object was positioned on the source detector axis in such a way to allow

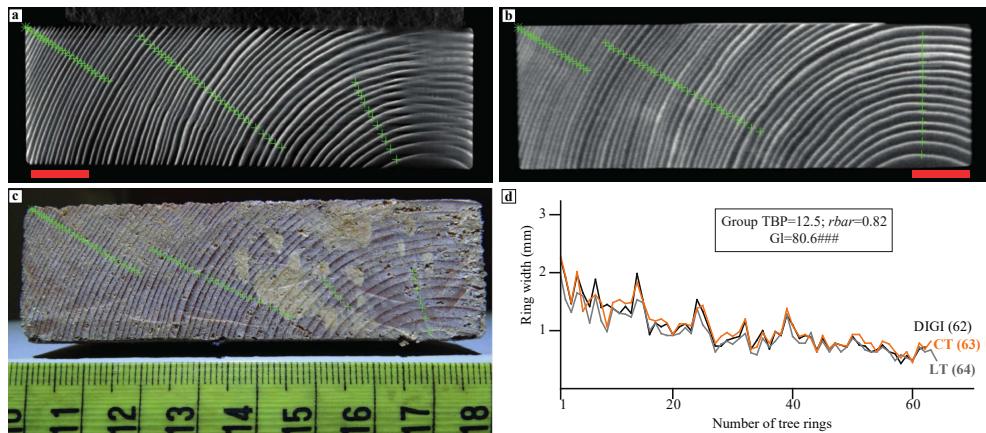


**Figure 3.5:** Results of tree-ring measurements on Test plank 1, crosses are placed at the border between rings. Red scale bars indicate 1cm. a) LT reconstruction, voxel size 66.9 micron. b) CT reconstruction, voxel size 66.9 micron. c) Digital photograph. d) Visual and statistical crossdating between the measurements obtained from the different images. All three measurements show high similarity in pattern and magnitude (manual measuring and measured paths account for the slight differences). TBP, Student's t-value as implemented by Baillie and Pilcher [13] for tree-ring studies;  $r_{bar}$ , mean correlation coefficient; GI, mean percentage of parallel variation between the overlapping portion of the compared tree-ring series [68] accompanied by its signification level (###,  $p < 0.0001$ ).

for a full CT scan while remaining within the field-of-view of the detector for 360 degrees.

The results show that the measurements are indeed comparable in pattern and magnitude (figure 3.5d), and the observed differences can be attributed to different paths of the measurements and inaccuracies related to manual measuring. We observe that the horizontally oriented parts of the tree rings closer to the pith are blurred in the LT image but that this does not hinder the measurement as that is taken perpendicular to the tree-ring boundaries. Both reconstructions provide a good measurement match with the gold standard measurement on the digital photograph, which shows that the results from both reconstruction images are suitable for dendrochronological investigation.

### 3.2.2 Test case 2: simulations

In practice, it is not feasible to have the tree rings exactly aligned with the source detector axis. A tree-ring tilt is common and can be caused by the growth conditions of the tree, by how the wood has been processed (i.e. sawn at an angle) or by imperfect alignment of the wood in the scanner. The question therefore arises what the influence is of a small tree ring tilt on the performance of the LT method. To answer this question, we performed a small simulation study. The tree-ring tilt ( $\alpha$  in figure 3.6) is 0, when the longitudinal growth direction of the tree rings is parallel with the source-detector axis ( $\alpha = 0$ ). The X-rays in the centre of the beam are then parallel

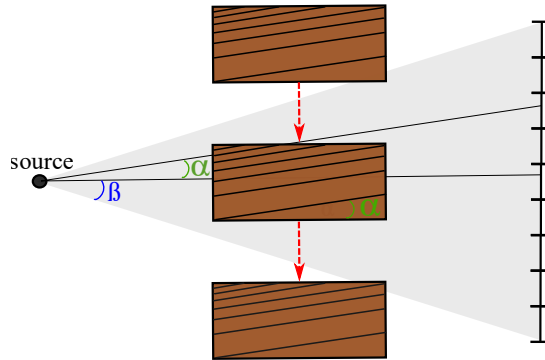


**Figure 3.6:** Schematic representation (seen from above) of the LT scan, with tree-ring tilt  $\alpha$  and cone angle  $\beta$ .

to the rings. The cone-beam X-ray source emits rays in an angular range of  $\beta$  degrees (see  $\beta$  in figure 3.6). For tree-ring tilt smaller than  $\beta$  there are still rays that are parallel to the tree rings. Therefore, we expect the method to perform well if the tree-ring tilt is sufficiently smaller than the cone angle.

We simulated a dataset in a best-case scenario in which the tree rings are perfectly concentric rings. The simulated datasets were created, with a tree-ring tilt  $\alpha$  set at  $0^\circ$ ,  $8^\circ$  and  $15^\circ$  and with a cone angle  $\beta$  of  $9^\circ$ . The simulated data projections (figure 3.7a) were generated with the ASTRA-Toolbox [1]. Reconstructions were made using the SIRT algorithm with 50 iterations and a slice perpendicular to the source detector axis at 25% of the length of the simulated object was selected. Note that on the projection (figure 3.7a) the tree rings parallel to the source-detector axis are sharp, whereas the other rings are blurred because the X-rays travel through the object at an angle, thus overlaying rings on the projection. Results show that for tree-ring tilts smaller than roughly 9 degrees, the reconstructed images are similar (figure 3.7b,c). When the tree-ring tilt is higher, the image becomes blurred (figure 3.7d) and not suitable for tree-ring measurements. It must be noted that the cone beam angle  $\beta$  is not a hard limit for the tree-ring tilt. A key conclusion of the simulations is that the LT method is robust to realistic tree-ring tilt. Moreover, in these simulated images we observe that the horizontally oriented part of the tree rings (bending around the pith) are slightly blurred, similar to the previously shown reconstruction of Test case 1. This effect increases with the tree-ring tilt.

### 3.2.3 Test case 3: conifer plank

A plank of conifer wood of 2cm thickness x 23cm width x 15cm length, which was too large to be imaged in a single CT scan, was selected for the second test. It was scanned using the LT scanning technique with translation range (-150mm, 150mm). The front of the object was placed as close to the source as possible, while ensuring

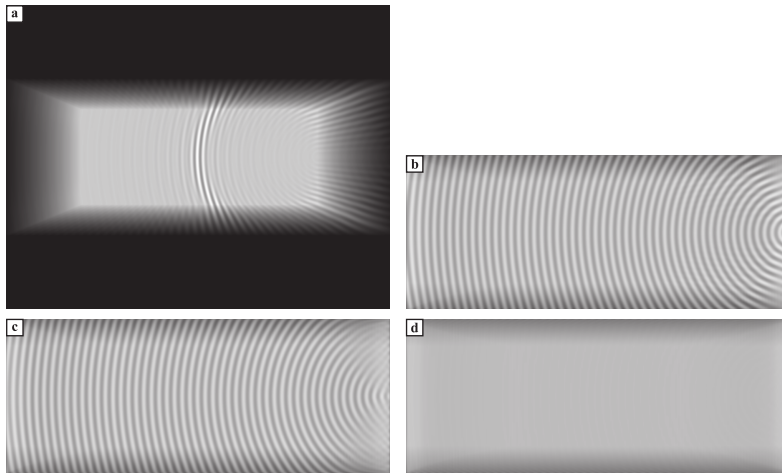


**Figure 3.7:** Simulated data and reconstructions. a) Simulated projection. b) Reconstruction with tree-ring tilt 0 degrees. c) Reconstruction with tree-ring tilt 8 degrees. d) Reconstruction with tree-ring tilt 15 degrees. Brightness and contrast settings are equal for all three reconstructions. The similarity between b) and c) demonstrates that the method is robust for small tilt in the tree rings.

that it still moved from outside the field of view of the detector on one side to outside the field of view on the other side. The scan took eight minutes and 1,875 projections, with tube settings 70kV and 30W [33]. The reconstruction was performed with 400 iterations of SIRT and voxel size 20 micron, the voxels were elongated in the growth direction (1:1:4 scale) to reduce reconstruction time and memory. We inspected the slices at 25% and 30% of the object length and decided to use the slice at 30% for tree-ring measurements (figure 3.8a).

The preparation of the surface of the plank and the acquisition of the tree-ring widths on the digital photograph was done following the same procedures as in Test case 1 (figure 3.8b).

As expected from the simulations and the first test scans, the horizontally oriented tree rings appear blurred in the reconstructed image. Given that tree rings are measured along a path perpendicular to the pith this does not hinder the acquisition of tree-ring widths in that portion of the wood. The crossdating results show a good match between both tree-ring series, which is illustrated by an excellent visual match and high statistical values (figure 3.8c). This validates that the LT scanning method provides accurately measurable images for dendrochronological research. The narrowest ring in this plank is 0.34 mm wide and has been neatly captured in the LT image, proving that this method can be used successfully to retrieve tree-ring patterns of slow-grown trees, which were often used in the production of art works such as sculptures, furniture and panel paintings [76, 89].

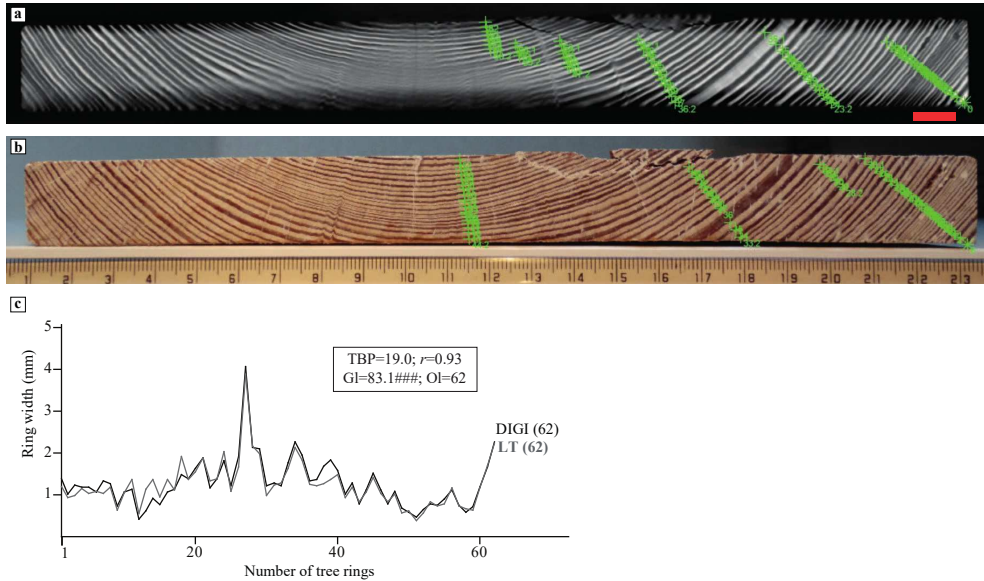


**Figure 3.8:** Dendrochronological results on Test case 3. a) LT reconstruction. Red scale bar indicates 1cm. b) Digital photograph. c) Visual and statistical crossdating between the tree-ring series obtained from both images. The series have the same number of rings and show an outstanding synchronisation. TBP, Student’s t-value as implemented by [13] for tree-ring studies;  $r$ , mean correlation coefficient; GI, mean percentage of parallel variation between the overlapping portion of the compared tree-ring series [68] accompanied by its signification level (###,  $p < 0.0001$ ).

### 3.2.4 Case study: the book chest of Hugo de Groot

Finally, we tested the LT scanning method on an iconic object from Dutch history at the Rijksmuseum collection: a book chest in which Hugo de Groot allegedly hid to escape imprisonment (figure 3.9a) [154]. Hugo de Groot (1583-1645) was a jurist and writer who was sentenced in 1619 to spend the rest of his life in prison in Loevenstein Castle, because of political disputes. He was allowed to write and receive books in large wooden chests, and in 1621, he performed a masterly escape from the castle hiding in one of the chests. The chest in question remained in his family for several decades afterwards, but its trail disappeared in the 18th century [11, 88]. Three chests in Dutch museum collections were potentially the original chest in which Hugo de Groot escaped. Research into the origin of these was broadcast in the TV series ‘Historisch Bewijs’ (Historic Evidence) [11]. In the context of this investigation the opportunity arose to test the LT scanning technique on a large cultural heritage object. The chest is large enough to have contained a person (73 cm width x 160 cm length x 75 cm height). These dimensions hamper scanning possibilities at most CT facilities, including the Flex-ray laboratory. However, the Rijksmuseum houses X-ray equipment within the building dedicated to Conservation and Science (the Ateliergebouw). The dimensions of the chest were too large to rotate it fully, a CT

scan was therefore not possible. We could however carry out an LT scan to validate our technique.

LT scanning was carried out with tube settings 150kV and 525W and 1325 projections were recorded [39]. A ‘ruler’ with metal nails inserted every centimetre was used to register the translation between recorded projections. The magnification was then estimated based on the distance between two nails and the translations using cross correlation of the nail locations [85]. By this approach the accuracy of the experimental parameters is limited, but as demonstrated by the experimental results this does not compromise the robustness of the method. The reconstruction was performed with 100 iterations of SIRT and voxel size 90 micron.

A plank whose transverse edge was not accessible for dendrochronology was selected for the study as an example of a scenario in which dendrochronology could not be carried out on the desired section. Digital photographs of the tree rings were however taken with a compact camera on macro mode from the radial/tangential section of the plank, which was visible on the outside of the chest (figure 3.9b). Due to the fact that the measurement cannot be performed perpendicular to the pith, but only at a slight angle (which becomes larger when closer to the pith), the magnitude of the tree-ring widths could be slightly distorted in the radial/tangential section. The growth pattern should however be the same as the one retrieved from the LT image (figure 3.9c) and could thus provide validation of the LT technique.

Apart from the expected differences in magnitude due to the measuring on the radial/tangential section, crossdating results show an excellent match between both tree-ring series (figure 3.9d). Furthermore, the reconstructed image allowed the visualisation and measurement of more rings on both ends of the plank, which were too distorted or not visible in the digital photos from the radial/tangential section. Consequently, the series obtained from the LT image contains a total of 92 rings, whereas the one from the digital photographs is shorter (88 rings). As the length of the tree ring series can be crucial to the dating of the object, obtaining a longer tree ring series is a valuable result. Although this plank remains undated, these results validate the LT method, and demonstrate that it provides high quality images from large objects for dendrochronological research.

### 3.3 Discussion and conclusions

Our research demonstrates that the proposed LT X-ray tomography method provides reconstructed images suitable for dendrochronological research. We exploit the fact that only a slice (instead of a full 3D image) is needed for dendrochronology, and have validated and demonstrated the method by obtaining accurately measurable images on simulations, test objects and a large wooden chest from the Rijksmuseum collection. By moving the object on a linear trajectory between the source and detector, with the transverse section of the wood facing the source, sharp images have been obtained where tree rings as narrow as 0.34 mm were clearly discernible. The results from our experiments open the door to future investigations of a variety of wooden objects, ranging from large panel paintings and doors from cabinets to chests, tables and large

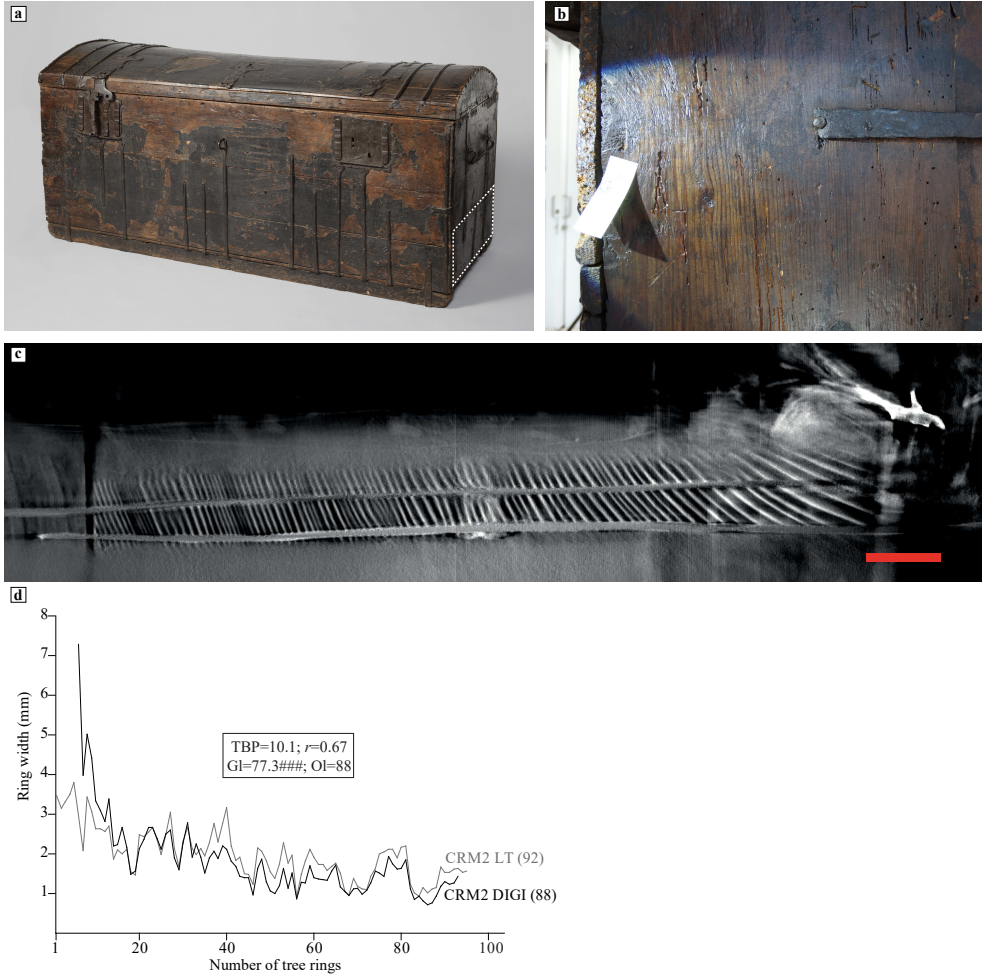


**Figure 3.9:** Results of the case study. a) The Hugo de Groot book chest (the white rectangle indicated the lower plank of the right side of the chest, which was selected for this study). b) Digital photograph on the radial/tangential section. c) One of the LT reconstruction slices of the cross-section used to measure the tree rings, red scale bar indicates 1cm. d) Visual and statistical crossdating results between the tree-ring series obtained from the digital photographs (labelled CRM020\_DIGI) and the one obtained from the LT reconstructed image. The series obtained from the digital image has seven rings less than the one from the LT reconstruction image and shows a slightly distorted pattern (magnitude-wise) due to measuring in the radial/tangential section of the wood.

sculptures.

The LT scanning method has many advantages for dendrochronology on large objects. First of all, there is no need for rotation of the object and only one scan is required, as opposed to CT, where a full rotation is required for multiple scans (tiles) if the object is larger than the detector frame. The method can therefore be implemented in systems with a small detector or a static setup, such as a C-arm, where source and detector cannot be moved independently from each other. This is the typical X-ray imaging setup present in museum research facilities (e.g. The British Museum, London [45] and Rijksmuseum, Amsterdam). Secondly, LT scanning can be carried out relatively fast. A scan can be performed within the order of 10 minutes, considerably reducing the exposure time. CT scans can take several hours up to days depending on the number of tiles and radiographs and the illumination time per radiograph [44]. Thirdly, given that a specific section of the object is selected, structures within the object that are unsuitable for X-ray imaging or that reduce the image quality, such as metals, can be avoided. In CT scanning all those structures are captured in the image during the rotation, causing distortions in the reconstructed image. Another artefact that commonly occurs in CT scans is the so-called ring artefact. If the pith of the wood is aligned with the rotation axis of the CT scanner, these ring artefacts may distort the tree ring pattern. This is avoided in an LT scan because of the scanning direction along the longitudinal growth direction.

For the LT scanning method, it is important that the transverse section of the wood is as perpendicular as possible to the source-detector axis. Still, we have shown that measurable images can be achieved when this alignment is not perfect. This makes the method feasible for practical application, as perfect alignment can be difficult to attain due to the variable shape and direction of the tree rings.

We have illustrated that for each scanned object there were object-specific considerations. Every object is different and therefore it is not possible to give one general set of guidelines that will guarantee measurable results. Optimal tube and detector settings need to be investigated and alignment is different for each object. The acceptable radiation dose should also be considered for each object. The effect of high radiation dose on artworks has not been sufficiently investigated yet, and therefore further tests need to be implemented to understand the short- and long-term effect on X-rays on art-historical materials.

The scanning direction of the LT method can be a limitation. It is necessary to scan in the longitudinal direction of the tree rings, which is often in the length direction of the plank. The total amount of material may be too thick to obtain enough contrast to distinguish the tree rings. Even if contrast can be obtained, high energy and power will be necessary in most cases, increasing the radiation dose.

We moreover found that the metal parts in the chest caused lower reconstruction quality. In this case, the effect was not so severe as to obstruct the measurement of tree rings. This may however be the case for other art objects, as these often contain metal parts. For the test objects in this chapter the pith of the tree lies outside the sample. We have shown that the imaged tree rings become blurry with larger curvature. The method may therefore be less suited for planks with the pith in the sample. However, we expect that this limitation will not often hamper the dating

of the sample in practice, because for a dendrochronological measurement one line perpendicular to the tree ring direction is measured and the younger tree rings further from the pith are the most important for obtaining a felling date.

For the practical application of the LT scanning method, the input of both dendrochronologists and imaging scientists is required. The reconstructions should be discussed to select the slice that is best suited to measure the tree rings. The accuracy of the results increases when multiple reconstructed images at different depths are used for tree-ring measurements. Although the reconstruction of large LT datasets imposes substantial computational demands, we foresee that faster reconstruction may be possible. Additional research is needed to optimise reconstruction time.

In conclusion, LT X-ray tomography caters to the increasing demand for non-invasive research methods providing a novel and powerful technique for dendrochronology of large objects, which due to their size would be deemed unsuitable for CT imaging.





## 4

# Marker-based 3D CT imaging using only basic 2D X-ray equipment

The interior of an art object often contains answers to questions about how and when the object was made, where the materials came from, and in some cases even who made it. This information can potentially be revealed by computed tomography (CT), a powerful technique for creating a three-dimensional (3D) image of the interior of an object. CT imaging was originally developed for health care [103], but also has applications in industry [102] and cultural heritage [123]. Cultural heritage research has used CT imaging of artifacts to determine their manufacturing process [196], current state [64, 113, 180], and origin [63]. Over the past years, the possibilities of CT imaging have been expanded by applying image processing methods to CT data, for example when unfolding unopened documents [59], combining CT data with other 3D imaging methods [77], and applying deep learning techniques to improve resolution [94].

To indirectly observe internal features, most museums have resorted to 2D X-ray imaging equipment, which can be straightforwardly applied to objects of various sizes and shapes. Typically, this equipment is used in a radiation-shielded room, which provides extensive flexibility for imaging of large and irregularly shaped objects that

---

This chapter is based on:

F. G. Bossema, W. J. Palenstijn, A. Heginbotham, M. Corona, T. Van Leeuwen, R. Van Liere, J. Dorscheid, D. O’Flynn, J. Dyer, E. Hermens, and K. J. Batenburg. “Enabling 3D CT-scanning of cultural heritage objects using only in-house 2D X-ray equipment in museums”. *Nature Communications* (accepted, in press).

do not fit in the confines of medical or cabinet-based CT scanners. In 2D radiography, internal features of an object are projected onto a single image, which results in the loss of depth information. A 3D CT reconstruction volume, on the other hand, can be sliced to investigate interior features of the object at their exact 3D location within the object. Performing a CT scan requires a dedicated CT scanner, which acquires a sequence of 2D radiographs from angles all around the object and records the geometrical parameters needed for the mathematical reconstruction algorithm, which computes a 3D image of the object's interior. To facilitate this rotational acquisition, either the X-ray source and detector are mounted on a gantry that rotates around the static object, or the object is placed on a turntable that moves with respect to a static X-ray source and detector. In both cases, the stability and accuracy of all components are dependent on sophisticated system design combined with high quality computer-controlled stages, as well as extensive system calibration to precisely control the orientation and timing of each radiograph.

Despite the capabilities of CT imaging, its use in cultural heritage research is still limited to selected cases, often carried out offsite. For example, clinical CT has been carried out on paintings [121] and mummies [143]. Since costly commercial-class micro-CT systems often provide higher resolution images, these have been used for purposes such as dendrochronology [58, 63], analyzing panel paintings [60, 199], and investigating unopened letters [59]. These systems are focused on a specific object dimension range, due to the detector size and the space within the cabinet, which limits their versatility for the broad range of object sizes and shapes in museum collections. An even less accessible option is synchrotron facilities, which can provide high resolution images of small objects [119].

Although CT scanning provides considerably more information than radiography, there are challenges specific to its use on cultural heritage objects, which are unique, precious, and often fragile. Moving objects to a scanning facility can be costly because of specialized transport and insurance. Another challenge is the objects' wide variety of sizes, shapes, and materials, which means the acquisition has to be tailored to the object [37, 106]. Museums have addressed these challenges with a variety of setups. One example is a portable CT imaging setup which can be moved to investigate the object in situ [4, 124, 136]. Other solutions were sought out by the J. Paul Getty Museum (Los Angeles) which built a custom acquisition setup to investigate a bronze statue [18], and the British Museum (London), who obtained an easily accessible but costly in-house CT scanning facility [196].

In this article, we present a novel alternative approach for creating 3D CT imaging capabilities that can be applied to any existing radiography setup. By using a combination of basic X-ray imaging equipment, a tailored marker-based image acquisition protocol, and sophisticated data-processing algorithms, we can achieve 3D imaging of collection objects, alleviating the need for a costly CT system and making optimal use of the hardware already available. We demonstrate the efficacy of our approach by performing CT scans using the available X-ray imaging equipment at the British Museum, London; the J. Paul Getty Museum, Los Angeles; and the Rijksmuseum, Amsterdam. We imaged a small wooden block as test object in all three museum radiography suites as well as in the FleX-ray lab micro-CT facility, situated at the

Center for Mathematics and Computer Science in Amsterdam. We compared the results of our algorithms with those obtained using the well-calibrated in-house CT system already in use at the British Museum and the micro-CT system at the FleX-ray lab. The capacities of this technique and the new research possibilities it provides are further demonstrated by imaging a case study object at the J. Paul Getty Museum: a 19th-century plaster model *Python Killing a Gnu* by French artist Antoine-Louis Barye (1796 - 1875). Our approach enables 3D CT imaging for the first time at the Getty Museum and Rijksmuseum radiography suites.

## 4.1 Results

Our approach for creating accurate CT reconstructions uses only basic 2D radiography equipment and does not require precision operation of the moving parts, but instead relies on a set of markers (small metal balls) that are used to track all geometrical system parameters during image acquisition. This enables us to computationally derive the geometric system parameters that are typically hardware-calibrated in standard CT systems [22]. The radiographs acquired and system parameters calculated are combined to obtain a 3D CT reconstruction, which can be inspected to gain information about the interior features of the object.

### 4.1.1 CT workflow

Our complete workflow for computing a 3D CT reconstruction from a series of standard 2D radiography measurements is illustrated in figure 4.1. The work carried out in the X-ray suite starts by placing small metal balls or *markers* in a piece of foam that surrounds the object. The object and marker holder are then placed on the rotation stage. The next step is the acquisition of radiographs in a full circular range, which yields a dataset with the markers in view. The computational workflow performed afterwards consists of the following steps: 1) marker detection and labeling; 2) system parameter derivation; 3) preprocessing (flat- and dark-field correction) and removing the markers by inpainting; and 4) 3D reconstruction. The outputs corresponding to each of these steps are 1) labeled marker trajectories, 2) accurate system parameters, 3) preprocessed radiographs with the markers removed, and 4) 3D reconstruction based on the two previous outputs. For details on the methods and implementation, please refer to section 4.3 and appendix A.

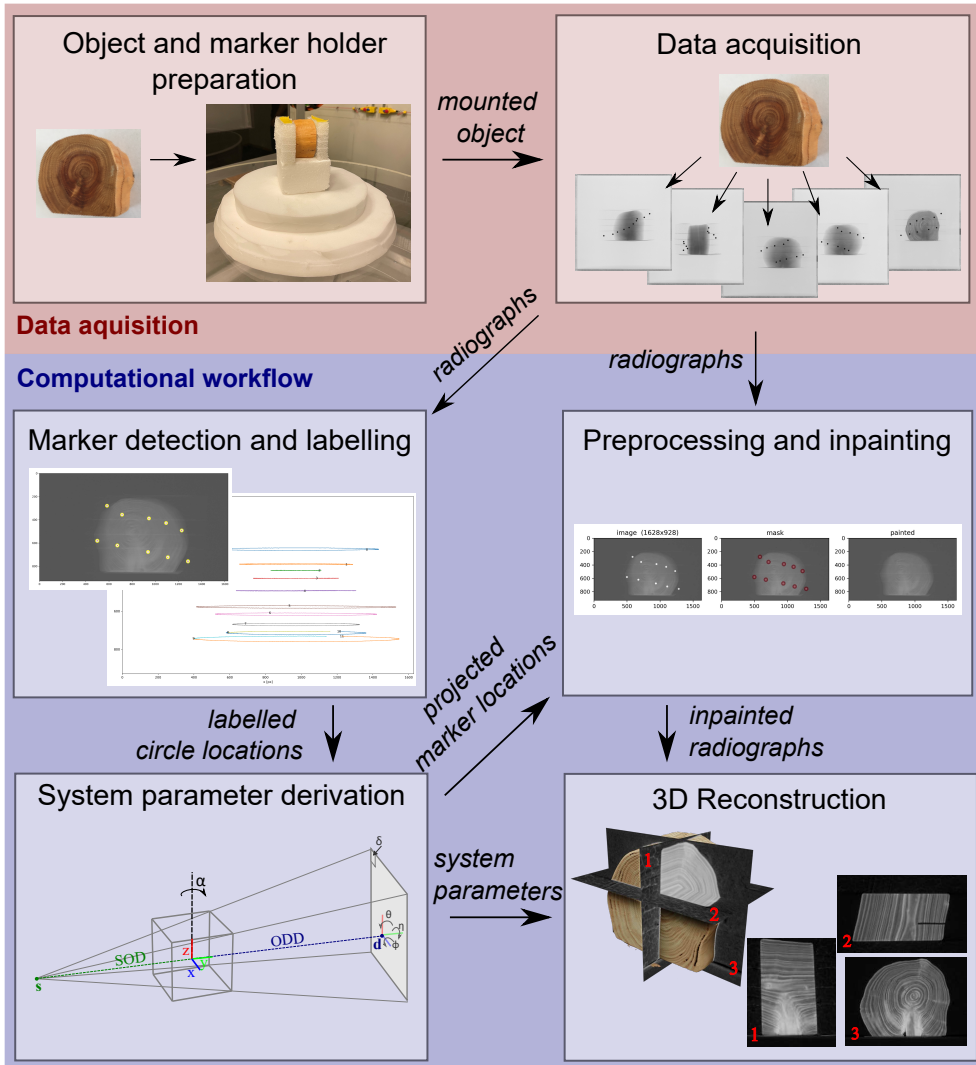


**Figure 4.1:** Steps in the workflow for post-scan marker-based parameter derivation method for 3D reconstruction.

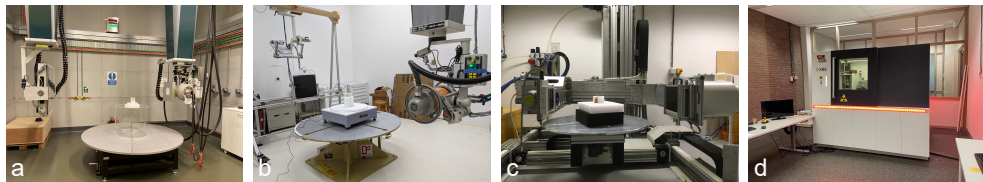


**Figure 4.2: X-ray imaging facilities.** a) the British Museum (London), b) the J. Paul Getty Museum (Los Angeles), c) the Rijksmuseum (Amsterdam) and d) the FleX-ray laboratory (Amsterdam).

#### 4.1.2 Comparison of one object imaged at three museum radiography suites and a micro-CT facility

We applied our methods to radiography datasets recorded at the research facilities of three prestigious museums: the British Museum (London) [27], the J. Paul Getty Museum (Los Angeles) [25], the Rijksmuseum (Amsterdam) [24], and a micro-CT facility: the FleX-ray laboratory (Amsterdam)[23], see figure 4.2. A small wooden object (h 5cm x w 6cm x d 3cm, figure 4.3a, was scanned at all four facilities. The woodblock used for reconstructions was microscopically identified as yew (*Taxus* spp.) [169]. The details on the scanning parameters can be found in table 4.1. In figure 4.3b-d we show sample radiographs of the object from each facility and in figure 4.4 five cross-sections of the CT reconstruction of the wooden block obtained from 1) the British Museum setup with system reported parameters, 2) the British Museum setup with post-scan marker-based parameter retrieval, 3) the J. Paul Getty Museum setup with post-scan marker-based parameter retrieval, 4) the Rijksmuseum setup with post-scan marker-based parameter retrieval and 5) the FleX-ray CT system with system reported parameters. As expected, the CT reconstructions obtained from the museum facilities using post-scan marker-based parameter retrieval do not reach the same effective resolution that can be observed in the micro-CT. The images show that the reconstruction with markers reveals the same internal structures as the reference reconstruction from the British Museum, which is based on their usual workflow for CT reconstructions.

There are several factors that potentially influence the image quality, such as the focal spot size of the source and the distances between the source, object and detector. For example, the effect of the larger focal spot size in the J. Paul Getty Museum setup is visible on the radiograph (figure 3c), on which the markers are more blurred than in the other two facilities. Here, the source to detector distance and object to detector distance were chosen to match the British Museum distances for comparability, but these could be determined differently to improve the acquisition. We find that the angular increment is constant at the British Museum facility, but shows a more step-like profile in the other two facilities. Please see the Supplementary table A.3 and figure A.4. The interior features of interest are shown in all reconstructed 3D images: the tree rings in the wood and the saw cut. The line profiles show that the contrast is

sufficient to distinguish the tree rings. We observe that the image quality and detail in the line profile is considerably higher in the British Museum setup, whose system was intended for CT imaging. As we were working with uncalibrated systems in which multiple hardware and software factors may play a role, we cannot exactly pinpoint the reasons for the differences in image quality. Compared to the radiographs (figure 4.3), where the internal features are superimposed, the added advantage of the CT image is evident, since we gain depth information about the internal features and can slice the object open digitally. These CT slices allow further analysis of internal features.

Although the relatively low CT image quality at the J. Paul Getty Museum and Rijksmuseum facilities limits the use of automated post-processing tools to extract quantitative metrics from the data, the marker-based 3D reconstruction makes it possible to obtain digital cross-sections of objects and is highly useful for visual inspection of the interior features of objects. For cultural heritage objects, this implies a considerable knowledge gain with respect to radiographs. This will be further illustrated in the next section, with a case study scanned at the J. Paul Getty Museum. Notably, this is the first time the basic in-house radiography setups at the J. Paul Getty Museum and Rijksmuseum have been used for 3D X-ray CT reconstruction.

Scan settings	BM	GM	RM	FleX-ray
Tube voltage (kV)	60	60	65	60
Tube current (mA)	3	15	4.5	800
Focal spot size (mm)	0.4	2.5	0.5	0.17
number of projections	1800	1469	1350	1440
number of rounds	1	3.05	2	1
exposure time (s)	1.0	0.9	0.1	0.4
total scanning time (min)	99	295	3.5	13

**Table 4.1: Scan settings of the small wooden block.** Scan settings as used at the British Museum (BM), the J. Paul Getty Museum (GM), the Rijksmuseum (RM) and the FleX-ray laboratory.

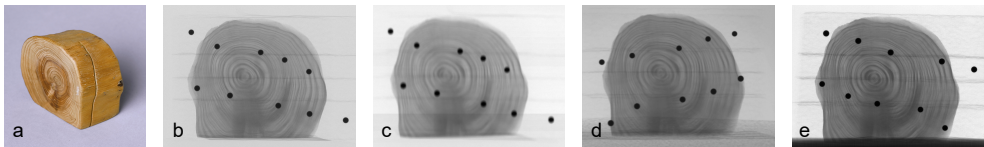


**Figure 4.3: The wooden test object.** a) Wooden object (h 5cm x w 6cm x d 3cm). Zoomed radiographs of the wooden test object at b) the British Museum, c) the J. Paul Getty Museum, d) the Rijksmuseum and e) the FleX-ray lab.

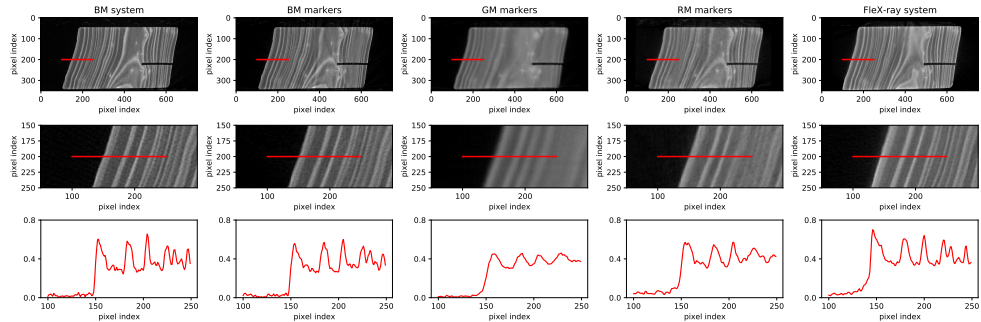


**Figure 4.4: Scan results of the wooden test object.** Top row. Single horizontal CT slice from reconstructions using the British Museum standard reconstruction workflow based on system feedback (BM system), all three museum systems with marker-based parameter retrieval (BM markers, GM markers and RM markers) and the FleX-ray setup with system feedback. After reconstruction, the resulting 3D volumes have been scaled and registered in order to show a similar slice through the object using the FleXbox toolbox [108]. The intensities were normalized. The red line measures 1.5cm. The tree rings and the saw cut are visible in all reconstructions. Middle row. Zoomed-in CT slices. Bottom row. A line profile of the normalized intensities corresponding to the red line in the reconstruction.

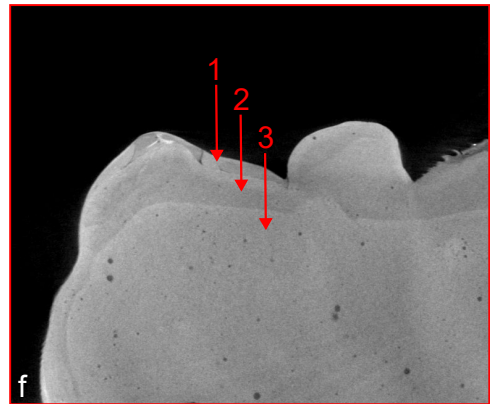
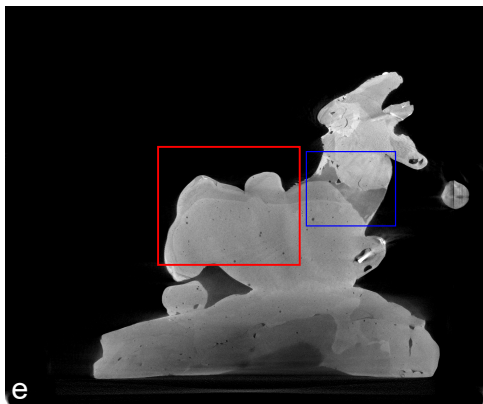
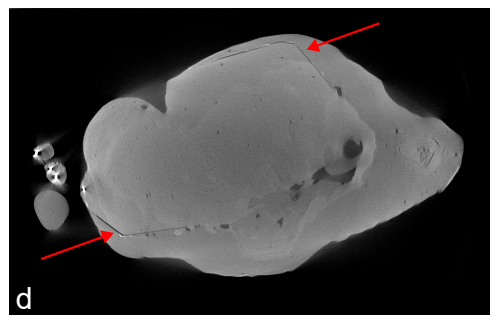
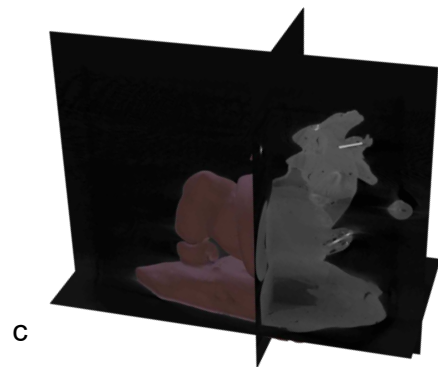
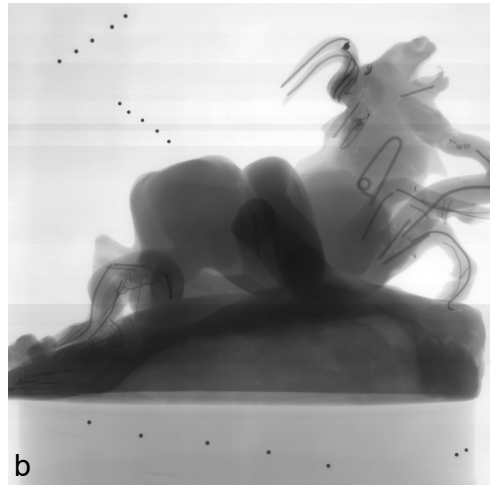
### 4.1.3 Case study at the J. Paul Getty Museum

To further test the capabilities of the 3D CT reconstruction method and its application to the investigation of museum objects, we chose a case study from the J. Paul Getty Museum’s collection: the plaster model *Python Killing a Gnu* by Antoine-Louis Barye (1796 - 1875) (figure 4.5a, collection number 85.SE.48), h 27.9 cm, w 39.1 cm, d 20.5 cm, here referred to as *the Barye model*. The Barye model is a complex construction consisting of plaster, metal armature, modeling wax, paint, and adhesive, and contains numerous repairs executed in unknown materials. An ongoing technical study of this sculpture focuses on its complex history of use and its relationship with several related Barye bronzes in other collections.

The earliest Barye sculpture of a python killing a gnu (or wildebeest) is a bronze that was part of one of the artist’s earliest and largest commissions: a *surtout de table* (centerpiece) commissioned by Ferdinand Philippe, duc d’Orleans, in 1834 [101]. This bronze (Walters Art Museum, accession number 27.152) is a lost-wax cast that depicts the animals in a compact format, attached to a rectangular plaster base. The current composition of the Barye model in the J. Paul Getty Museum collection and later bronzes (including sand casts at the Walters Art Museum (accession number 27.4510) and Baltimore Museum of Art (object number 1996.46.45)) are significantly different from the *surtout* bronze, with changes to the shape, length, and posture of both animals and the addition of a larger rocky outcrop. Close examination under visible and ultraviolet light, comparisons of 3D surface scans, and radiographs led to the hypothesis that the Barye model was originally hollow and conformed to the more compact *surtout* composition, but was later broken into sections and reconfigured

to be used as a working model for the elongated sand-cast versions. However, the radiographs of this highly complex object proved to be difficult to interpret with certainty, so definitive confirmation of this hypothesis was not possible. The Barye model was scanned at the in-house facility of the J. Paul Getty Museum [26]. It was mounted on the rotation stage with the center of rotation positioned so that only a small part of the base would rotate out of the field of view on some radiographs. The part of the base not covered by all projections was not significant for the investigation of the hypotheses and therefore a lower image quality in that region was considered acceptable. Seventeen markers were inserted in foam and placed next to the object at the top and the bottom, to avoid overlap with the denser parts of the object in the radiographs (see figure 4.5b). Tube voltage and current were 450kV and 2mA respectively. The exposure time was 2.85 seconds per capture, and to reduce noise, each radiograph was the result of averaging four captures. In total, 718 radiographs were recorded over two revolutions of the rotation stage. The 3D CT reconstruction of the Barye model revealed several key features that could not have been observed with traditional radiography and other noninvasive examination techniques. One significant question at the start of the study was how closely the composition of the Barye model matched that of the *surtout* bronze. The radiographs showed small gaps that suggested that the rectangular base of the original Barye model might have been embedded in added plaster to create the larger rocky outcrop. The CT reconstruction (see figure 4.5c) confirmed this observation quickly and easily; horizontal slices clearly reveal an embedded rectangular area of plaster of a different density than the surrounding plaster that matches the positioning of the original base, see figure 4.5d.

**Figure 4.5: Results of scanning the case study.** a) The sculpture *Python Killing a Gnu* (1840s–1860s), Antoine-Louis Barye (French, 1796 - 1875), the J. Paul Getty Museum collection number 85.SE.48, h 27.9 cm, w 39.1 cm, d 20.5 cm. b) Single radiograph of the Barye model *Python Killing a Gnu*, including the markers used to determine the system parameters for CT reconstruction. c) Three orthogonal slices of the CT reconstruction. d) Horizontal slice, red arrows indicating the lines that show where the original square base is contained in the sculpture. e) Vertical slice, blue box indicates where gaps in the reconfigured neck were filled with wax instead of plaster. f) Enlargement of the red box in (e), the arrows indicate the three different layers of plaster used to create the sculpture.



Another initial inquiry was focused on the metal armature and how it was embedded in sections of plaster. 2D radiographs showed varying plaster densities in different areas, suggesting that the model may have originally been hollow and was later filled with a second pour of plaster; however, it was difficult to be certain that this was a valid interpretation because of overlapping features and digital artifacts in the radiographs. The 3D CT data, on the other hand, not only validated this theory by allowing clear observation of the two different plaster densities throughout the model, but also revealed a third layer of plaster that was previously unidentified. The data allowed conservators to confirm that the object was initially a hollow sculpture with two layers of plaster: an initial fine, thin layer that was likely slushed into a mold to capture surface detail, and a secondary, thicker layer for support. This sculpture was then filled with a third layer of high porosity plaster in order to embed the metal armature after the reconfiguration (see figure 4.5e, red box, and 4.5f with an enlargement and arrows indicating the different layers). Large structural gaps that resulted from the reconfiguration but could not be easily replaced with plaster were instead filled with wax. This material change can be seen most prominently on the neck of the gnu, where the difference in density between the plaster and the wax is clear (see figure 4.5e, blue box). Modeling wax was also added to the surface of the gnu in several areas to alter the animal's musculature and match its reconfigured position.

Several other features that were difficult or impossible to observe in the 2D data were also discovered during examination of the 3D reconstruction, such as exact positioning of armature endpoints and density variation between materials in complicated internal regions. The case study of the Barye model proved to be successful, allowing Getty conservators to confirm aspects of the construction method for this object and to better document evidence of changes made by the artist.

## 4.2 Discussion

Our major results are twofold. First, we developed a method that enables 3D CT scanning with standard 2D radiography equipment, significantly increasing the accessibility of CT imaging within the museum research field by making optimal use of available hardware. The novelty of our approach is that compared to existing CT methods, it does not rely on pre-calibrated system parameters and is flexible with respect to the hardware components. Second, the technique was used to perform CT imaging in the in-house X-ray suites in the J. Paul Getty Museum and the Rijksmuseum for the first time without extra hardware investment. Until now, these systems had only been employed for radiography.

The interior of a cultural heritage object holds valuable information on the object's origin, artist's methods, previous conservation treatments and current state, which can be revealed by CT imaging without damaging the object. By deploying in-house X-ray systems, one can avoid costly and difficult transportation of precious objects to CT facilities located in hospitals or laboratories. An important advantage of our method is that limited hardware investments are required, making it accessible to all

museum research facilities with a standard radiography setup, for whom the purchase of dedicated CT systems is often out of reach. Our method incurs negligible costs and uses only the available basic X-ray equipment as well as small metal balls, foam, and tailored algorithms.

Inaccuracies in the geometrical parameters lead to blurring, shape distortion and streaks in the resulting reconstruction image [2]. Therefore, several studies have investigated the calibration of existing CT systems. Marker-based approaches have been employed previously, for example with motion correction in medical C-arm CT [127] and the geometrical calibration of CT systems [73, 204, 205]. In most cases, a dedicated calibration phantom is used, in which the position of the markers is precisely controlled during fabrication [114] or measured with high precision after fabrication [96, 207]. Some approaches have more flexibility in the marker positions, for example when using an adaptable LEGO phantom [128] or arbitrary marker locations [86]. These methods usually rely on a pre-scan of a marker phantom. They moreover assume the rotation stage is sufficiently reliable to produce accurate equidistant rotation angles between radiographs and calculate the other system parameters [204]. This is an important difference with our method, which was designed to include the estimation of rotation angles such that there is no dependency on the accuracy of the hardware.

Calibration is also important for non-standard trajectories, which are for example encountered in robotic CT [14]. Highly flexible robotic arms have been designed that can allow for adapting the acquisition trajectory to the object. A calibration step is performed by tracking a reference object to compensate for inaccuracies the trajectory [142]. Our method currently assumes a circular trajectory. In principle, it could be extended to include more degrees of freedom in the calculated parameters to facilitate handling of more general acquisition trajectories.

Apart from marker-based methods, efforts have been made to compensate for inaccuracies in the acquisition parameters using optimisation methods. These methods are usually applied to increase image quality by minor alterations in the parameters given by the CT system and are therefore dependent on the suitability of the internal features of the object (e.g. containing sharp edges) [105]. Other studies investigate methods to perform iterative reconstruction and alignment simultaneously [138]. The optimisation is often applied to a subset of the parameters set used in our approach [73, 138, 139].

Obtaining a 3D reconstruction provides information on the internal features than 2D radiographs. In the case of wood, for example, when a cross-section of sufficiently high resolution has been obtained, this could be used by dendrochronologists to measure the tree rings and date them through comparison with reference chronologies [19]. The resolution should be high enough to capture the thinnest rings in the transverse section of the sample [19, 38].

Through the datasets acquired at three different museum research facilities and a micro-CT facility, we show the flexibility of our approach. An important feature of our method is that, in addition to the system parameters, the marker positions are

included as parameters in this optimisation. Therefore no tailored, specifically made calibration phantoms are needed and the marker foam can be adjusted to suit the object. The calculation of the angular increments makes this approach applicable to systems that cannot be relied upon to produce equidistant angles. If the system does produce equidistant angles, the markers could be used for a pre-calibration step to obtain the parameters that stay the same (source-detector-distance, object-detector-distance, detector tilts), eliminating the need for keeping markers in the scan with the object and using an inpainting step afterwards (see Supplementary figures A.8-reffig:inpaintingGM). Including the markers in the object scan, however, allows our approach to be applied in a wide range of uncalibrated X-ray setups and may also be used to validate assumptions on the system geometry of existing CT setups, e.g. by checking if the projection angles are indeed equally spaced.

The method presented in this manuscript has three main limiting factors. First, the resolution of the final image is dependent on the available hardware, mainly the X-ray tube focal spot size as well as the possible distances between source, object and detector, which will be different for each setup and scan. The current method provides a 3D reconstruction and does not determine an absolute scale. In order to perform measurements on the reconstruction, either one feature on the object, the distance between markers or an included dummy object with known size needs to be measured to adjust the absolute scale. Second, the field of view of the detector determines the size of the objects that can be scanned. Third, the flexibility in motion of the hardware components will limit the possibility to perform tiled scans.

In future work, we would like to include horizontal and vertical tiling, which involves recording multiple datasets with different positions of the source and detector and computationally tying them together to image larger objects. Many factors can play a role when acquiring tiled scans. For systems where the detector can move independently from the source, stitching can be performed relatively easily. The projections are sampled based on the same source position and can therefore be stitched to on large projection [37]. A limiting factor here is the cone angle and fan angle of the beam, the detector may move to a position where it is not fully illuminated by the X-rays. For systems where the source and detector are linked (such as is the case in the BM and RM for instance) stitching becomes more complicated, since the data is sampled based on different source positions and horizontal tiles have to be reconstructed simultaneously. This requires the data to be processed simultaneously by the reconstruction algorithm, for which stitching algorithms have been developed previously, for instance within the FleX-box toolbox [108] or Astra toolbox [1].

Notably, all instructions for the acquisition phase at the J. Paul Getty Museum took place in online meetings, without any need for the computer scientists to be physically present in the X-ray suite. The computational workflow was carried out afterwards in Amsterdam. We aim to reduce the involvement of computer scientists in the processing workflow by further automating the method and providing a user-friendly interface, which would stimulate the adoption of our method in other research

facilities. This would greatly increase the amount of knowledge gained from CT imaging in the cultural heritage sector in general and will also play an important role in bringing research results to public attention.

By expanding the capabilities of existing hardware with post-scan parameter derivation, CT imaging will become more accessible to a wider cultural heritage community, thus further bridging the gap between digital methods and cultural heritage research. Our method may also be useful for the development of portable X-ray systems, since no pre-calibration of components is needed. Enabling CT scanning in pre-existing radiography setups in museums also increases the options for applying post-scan image processing methods to a wider range of objects.

The application of 3D X-ray imaging on a broader scale will challenge conservators and museum professionals to incorporate the previously inaccessible interiors of objects as part of their research on museum objects, encouraging new perspectives on how we investigate and conserve cultural heritage. Our method has shown the potential of computational methods to upgrade existing hardware with previously unimplemented capabilities. This step toward further integration of computational methods with traditional techniques will promote the development of both research fields.

## 4.3 Methods

### 4.3.1 Computed tomography reconstruction

X-ray imaging setups for scanning static objects typically consist of an X-ray source, an X-ray detector and a rotation stage in between, on which the object is mounted. For our workflow, we use a cone-beam X-ray source and a digital flat-panel detector. The detector measures the intensity of the X-ray beam profile after it is attenuated by the object, resulting in a projection of the object's internal structure. Apart from the material composition and location of internal features within the object, the measurement of the projection image further depends on the geometrical system parameters: the precise location of the source, object and detector, as well as the orientation of the object and the acquisition angles. A CT dataset consists of a set of these projection images, or *radiographs*, typically hundreds to thousands acquired across a full rotational range. After data acquisition, a CT reconstruction algorithm computes a 3D volumetric image of the scanned object based on the acquired radiographs and the system parameters. In commercial CT systems, the system components are managed by high quality computer-controlled motors to precisely control the orientation and timing of each radiograph. The rotation stage supporting the object is at an accurately known position, and rotates at a constant speed around an axis that can be assumed to be exactly aligned with the vertical axis of the detector plane, enabling the use of the Feldkamp-David-Kress algorithm for efficient and accurate 3D reconstruction [72].

In contrast to dedicated CT scanners, when attempting to perform a CT scan using a basic X-ray imaging system designed for live radiography inspection, a range of parameters governing the geometry of the acquisition are unknown at the time of

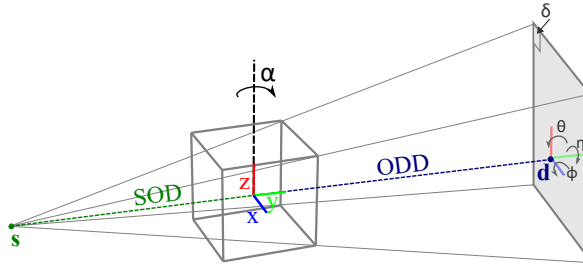


**Figure 4.6: Schematic representation of the X-ray setup.** X-ray setup with annotated system components and parameters required for accurate 3D reconstruction indicated: Source-detector-distance (SOD), Object-detector-distance (ODD), coordinate system  $(x,y,z)$ , rotation angle  $\alpha$ , detector tilts  $(\eta, \theta, \phi)$ .

measurement (see figure 4.6). The 2D X-ray imaging system can be combined with any kind of rotation stage, with varying control mechanisms. This variety makes a solution that is independent of specific hardware components highly desirable.

The acquisition process can be modeled as a system of equations. The so-called *forward operator*  $\mathbf{A}_\Theta$  contains all the geometric information on the scanning process and therefore depends on the vector  $\Theta$ , which contains the *unknown* system parameters, such as the distances between source, center of rotation, and detector; the projection angles; and the detector tilts. The vector  $\mathbf{x}$  is the digital representation of the object and  $\mathbf{b}$  is the projection data acquired [48]. The goal is to find the representation of the image that leads to the acquired projection data, and in the process to minimize the difference between the forward projected image representation and the data:

$$\min_{\mathbf{x}} |\mathbf{A}_\Theta \mathbf{x} - \mathbf{b}|^2. \quad (4.1)$$

We first computationally derive the system parameters  $\Theta$  using the marker-based approach detailed in section 4.3.2 and then solve equation 4.1 by using the algebraic SIRT algorithm, a standard iterative reconstruction method in the CT field [87]. The SIRT algorithm operates by performing a gradient descent to minimize the residual, which is determined by forward-projecting the current estimate of the object representation and comparing it to the data.

source location	$\mathbf{s} = (s_x, SOD, s_z)$
detector location	$\mathbf{d} = (d_x, d_y, d_z)$
detector tilt	$\theta, \phi$
detector in-plane rotation	$\eta$
detector pixel size	$\delta$
projection angles	$A = \{\alpha_0, \dots, \alpha_{n-1}\}$
set of all system parameters	$\Theta = \{\mathbf{s}, \mathbf{d}, \theta, \phi, \eta, \delta, A\}$
marker positions	$\mathbf{m}_1, \dots, \mathbf{m}_N$

**Table 4.2:** Parameters used in the marker-based post-scan parameter derivation.

### 4.3.2 Marker-based post-scan parameter derivation

In our workflow, the markers are used not to refine given system parameters or calibrate an existing CT system, but rather to estimate all of the parameters necessary, thus obtaining 3D CT reconstructions from systems that were not designed for this purpose. In standard CT systems, the projection angles are equidistant. However, since we are working with non-calibrated systems, the projection angles can be non-equidistant and are therefore part of the parameter set that is derived. Moreover, the positions of the markers in the foam are configurable. They can therefore be easily adapted to the diversity of museum objects, and are also part of the parameter set. The positions of the markers in the foam are not precisely controlled or measured, but placed vertically spaced to avoid overlap on the radiographs. In appendix A, we give some general guidelines on the positioning of the markers within the foam. On the radiographs, we can detect the projected marker location (PML). We aim to computationally find the positions of the markers and the system parameters to match these detected PMLs.

Given a set of system parameters and marker positions, we can calculate a *predicted PML*, by taking the intersection of a line through the source and the marker with the detector plane. The modeled system parameters are shown in figure 4.6 and given in table 4.2. The positions of the markers in the foam are considered unknown, and therefore constitute additional parameters. The aim is to find the system parameters and marker positions for which the predicted PML  $\mathbf{p}_{ij}^{pred}(\Theta, \mathbf{m}_j) = (x_{ij}^{pred}(\Theta, \mathbf{m}_j), y_{ij}^{pred}(\Theta, \mathbf{m}_j))$  for each marker  $j$  on radiograph  $i$  is as close as possible to the measured PML  $\mathbf{p}_{ij}^{meas} = (x_{ij}^{meas}, y_{ij}^{meas})$ .

We therefore want to find the parameters  $\Theta$  which minimize the following value:

$$\sum_i \sum_j |\mathbf{p}_{ij}^{meas} - \mathbf{p}_{ij}^{pred}(\Theta, \mathbf{m}_j)|^2 \quad (4.2)$$

We approximate the parameters  $\Theta$  by employing a least squares solver. These parameters are then used to obtain a 3D reconstruction of the object by using the algebraic SIRT algorithm to solve equation 4.1 [87]. Our method obtains a 3D reconstruction and does not determine the actual physical dimensions. Excluding voxel dimensions, this does not impact the CT reconstruction. An object of known

size can be included in the acquisition or a feature on the object can be measured to determine the scale. Details regarding the theory underlying our method and the practical and computational implementation can be found in appendix A.

### 4.3.3 Radiography suites

The setups that were used in this research (see figure 4.2) each consisted of an X-ray tube, rotation stage and digital flat-panel detector. Below, we briefly describe the characteristics of each facility; the individual specifications can be found in table 4.3.

System characteristics	British Museum	J. Paul Getty Museum	Rijksmuseum	FleX-ray
Minimum focal spot size (mm)	0.4	2.5	0.5	0.017
Maximum voltage (kV)	450	450	225	90
Detector size (cm x cm)	40.96 x 40.96	40.96 x 40.96	24.58 x 19.66	14.59 x 11.49
Detector pixel size ( $\mu\text{m}$ )	200	200	128	74.8
Maximum source-detector distance (m)	2.5	3	1.5	1.1
Projection angles equidistant	Yes	No	No	Yes
Rotation mode	Start-stop	Start-stop	Continuous	Continuous
Approximate object size (cm x cm x cm)	25 x 25 x 30	25 x 25 x 30	15 x 15 x 10	10 x 10 x 8

**Table 4.3:** System specifications of the radiography suites.

#### British Museum, London

The British Museum X-radiography suite contains an Yxlon Access Y.100 industrial radiography system (Yxlon, Germany), with digital radiography and CT scanning capabilities. The system utilizes a Y.TU 450-D11 bipolar cone-beam X-ray tube, with tungsten target, nominal tube voltage of 450 kV and focal spot size of 0.4 mm at 700 W output. The X-rays are projected onto a PerkinElmer XRD 1621 AN15 ES flat-panel detector (40.96 x 40.96 cm), which consists of 2048 x 2048 pixels, 200 $\mu\text{m}$  pixel pitch. The source and detector are suspended from a gantry by a retractable belt system, and they move together in the horizontal and vertical axes. The system provides feedback on the X-ray tube, detector and turntable positions. The X-ray tube and detector positions are adjusted by the user with either a pendant or joystick system, and the turntable position is automatically controlled by the system software throughout CT acquisition. The turntable pauses during the acquisition of each radiograph, and the number of radiographs (thus the rotation angle per step) for a scan is predetermined by the user. CT reconstruction is conducted automatically by the system following a scan using the VGSTUDIO 3.2 software package (Volume Graphics, Germany).

#### J. Paul Getty Museum, Los Angeles

The system at the J. Paul Getty Museum is a radiography system for live inspection of objects. The X-ray source is a General Electric system, consisting of a pair of Isovolt Titan E generators driving a cone-beam bipolar Isovolt 450/10 X-ray tube, with a voltage range of 5-450kV. There are two focal spot sizes of 5.5mm and 2.5mm, with maximum power of 4.5kW and 1.68kW respectively. The X-ray detector is a

GE DXR250U-W digital panel with detector area measuring 40.96 x 40.96 cm, with a pixel size of 200 $\mu$ m yielding images of 2048 x 2048 pixels. The tube and detector are mounted on independent carriages on a remotely operable gantry. Images are acquired one at a time using GE Rhythm software. Objects are rotated on an Ortery Photocapture 360M computer-controlled turntable with 1° rotation intervals; 0.5° intervals are acquired by first acquiring 360 images at 1° intervals, then manually rotating the turntable by approximately 0.5°, and then acquiring a second set of 360 images at 1° intervals. Coordination between the image capture software and the turntable control software is accomplished using RoboTask automation software.

### **Rijksmuseum, Amsterdam**

The system is designed for live radiographic inspection of objects. The apparatus is a Balteau Baltograph X-ray system, which consists of a Baltograph Generator XSD225 with cone-beam X-ray tube TSD225/0, with voltage range 2-225kV and a focal spot size of 1mm (640W max.) or 5.5mm (3000W max.), and Control Unit LS1. The X-rays are projected onto a flat-panel detector (Balteau Baltoscope FPDIGIT13-127), with detector area 19.5cm x 24.4cm, which consists of 1920 x 1536 pixels, with a pixel size of 127 $\mu$ m. The source and detector are mounted on either side of a gantry and are thus moved together. The system can record radiographs in mp4 video format, while the rotation stage moves continually. The angular increment per radiograph is not constant during the acquisition. There is moreover no way to determine accurately when a full 360° rotation has been recorded. The recording is continued long enough to make sure information is gathered over at least a full rotation. The motors are externally controlled by a Seifert DP435 system, using joysticks that control vertical and horizontal movement and tilts of the X-ray tube and detector, move the rotation stage in two directions, set the rotation speed and control the rotational movement. For the last of these functions, the joystick needs to be manually pushed throughout the recording to make the stage move continually. There is, however, no feedback on the location of the components or displacement. It is not possible to accurately choose parameters such as rotation speed or locations of source and detector.

### **FleX-ray, Amsterdam**

The cabinet-based system from TESCAN XRE is a highly flexible system designed to develop and test different acquisition trajectories. The system features a cone-beam microfocus X-ray point source with energy range of 20–90 kV with a maximum of 90W at 90kV. The focal spot size is 17  $\mu$ m. The flat-panel detector is a CMOS (complementary metal-oxide semiconductor) detector with CsI(Tl) scintillator (Dexela1512NDT), with 1944x1536 pixels (14.59 cm x 11.49 cm). The detector pixel size is 74.8  $\mu$ m. Datasets can be recorded at angular intervals of 0.1° with continuous rotation.



# 5

## Interactive visualisation of the interior and exterior of cultural heritage objects

A thorough understanding of the physical make-up of cultural heritage objects plays an increasingly significant role within material and art historical studies, as well as in conservation research. In tandem with scientific analytical methods, several 3D imaging methods are increasingly employed to obtain knowledge about an objects' manufacture, internal structure, origin and current state of conservation. Pieraccini and colleagues [144], for instance, identify five reasons for digitising collections using 3D imaging techniques: (1) to create digital archives; (2) to create physical replicas of artworks; (3) to provide remote accessibility; (4) to facilitate digital restoration; and (5) to monitor artworks over time. The exterior of objects can be imaged using surface scanning (e.g. structured light scanning or photogrammetry), producing a 3D representation which includes colour and texture information on the surface. The interior surface and internal structure on the other hand, can be captured using X-ray computed tomography (CT).

In recent years, surface scanning has become a popular tool in cultural heritage institutions to record and investigate archaeological and museum objects [6, 147]. Photogrammetry – a method that extracts a 3D surface model from a collection of

---

This chapter is based on:

F. G. Bossema, P. J. Van Laar, K. Meechan, D. O'Flynn, J. Dyer, T. Van Leeuwen, S. Meijer, E. Hermens, and K. J. Batenburg. "Inside out: Fusing 3D imaging modalities for the internal and external investigation of multi-material museum objects". *Digital Applications in Archaeology and Cultural Heritage* 31 (2023), e00296.

overlapping 2D images – has proved to be an accessible technique, since the acquisition can be performed with any camera, and by professionals as well as by the general public. Hence, many 3D models of cultural heritage objects can be found on popular online interfaces, such as Sketchfab [179], which, among others, hosts models by the British Museum [189] and the Metropolitan Museum of Art [118]. Some museums and institutions also use handheld structured light scanners to image their objects in 3D. 3D models are well-suited for outreach purposes and can increase accessibility of museum collections to audiences across the world [126]. X-ray CT is an absorption-based technique that provides a greyscale 3D image of an object, based on the density of its constituent materials. This 3D image can be sliced open virtually to reveal internal features. Investigations using CT imaging for cultural heritage objects have revealed valuable and sometimes surprising information, leading to, for example, a more accurate attribution to workshops or makers, a more detailed visualisation of the manufacturing process, or information on the present condition of the objects [37, 64, 81, 196]. The technique is not as easily accessible, both technologically and economically, as 3D scanning, since it generally requires objects to be brought to a specialised X-ray facility.

Besides their difference in capturing external and internal features, 3D surface scans and CT scans provide complementary information in regards to the models' surface as well. For example, if an object consists of a higher density material and lower density layers, a surface scan could capture the shape more accurately than the CT scan. On the other hand, CT scanning can recover a shape that was hard to capture using a surface scan due to glossy or transparent surfaces. Though both exterior and interior imaging techniques are used to investigate cultural heritage objects, few attempts have been made to combine various 3D imaging modalities [7, 77, 196]. Capturing and registering both external and internal features promises to be a powerful research tool for object-based investigation as well as for their digitisation [77]. It is challenging to fuse multiple 3D imaging modalities due to the diversity in shapes, sizes, and materials of cultural heritage objects and the different output formats of the various imaging techniques. There is also a lack of accessible and free software solutions that are capable of registering multiple datasets and visualising them interactively. To address this, a software solution has been developed to facilitate the fusion of 3D imaging datasets and provide an interactive environment for data analysis.

## 5.1 Related work and common practice

Working with surface scans, or 3D meshes in general, has a long history in fields outside of the cultural heritage sector. As a result, there is a wide range of software solutions available that allow for the editing and display of surface scans. Besides specialised commercial packages, such as Autodesk Maya [9] and ZBrush [117], there is a large community revolving around free and open source solutions. Two widely used examples are Blender [20], and MeshLab [52]. Furthermore, recent laptops and phones can come with native software able to open and display most 3D file types,

greatly facilitating the dissemination of such models.

There are multiple options for investigating and visualising CT data. Within the medical world, specialised software tailored to the scanner and purpose, is regularly supplied by the manufacturer of the hardware. Within laboratory settings, the use of free and open source software ImageJ [166] is widespread. While it is easy to view the data as a sequence of slices in ImageJ, its 3D capabilities are limited. For 3D visualisations of CT data, Slicer3D [71] is an open source solution that is used for both medical and academic purposes. There are also commercial options available, such as the versatile 3D visualisation programs VGStudio [201] and Avizo/Amira [192] but their cost limits their availability and suitability in cultural heritage institutions lacking sufficient funding. Another non-commercial option for volume rendering is Dragonfly [66], which offers a non-commercial licence for academic research. The fusion of different 3D data modalities, in particular CT and surface scanning has, to a limited degree, been addressed in other disciplines. For example, NASA launched the website Astromaterials3D [7], which provides interactive visualisations of space rocks, based on both a mesh of the exterior and X-ray CT data showing internal properties. However, no detailed protocol on how such registration was achieved has yet been made available. Other examples include forensic research [70, 200] and craniofacial modelling [99, 203].

In the cultural heritage field, different 3D data imaging modalities have also been combined. For example, Fried and colleagues [77], used CT scanning and photography to create 3D models of antique glass figures. These imaging modalities were chosen in order to overcome particular complexities that arise when attempting to scan transparent materials with 3D imaging techniques such as photogrammetry and structured light scanning. In their work, the CT data was used to provide the surface mesh if this was inadequately captured by the photography. To process the resulting images, multiple software packages were used, some commercial and some free and open source. Another example is the scan of the Sherit mummy (Rosicrucian Egyptian Museum), in which CT data and a structured light scan were combined using VGStudio [8]. Vandenbeusch et al.[196], acquired both a CT scan and a structured light scan of an Egyptian mummy mask from the British Museum collection. The two datasets were manually aligned in VGStudio [201] to obtain a combined dataset. That project, and the desire to optimise and automate this alignment process, was the inspiration for this work. As will be shown, the dataset of the Egyptian mummy mask will serve as one of the case studies for automated alignment and visualisation. Fusion of CT datasets and surface scans is not yet common practice for cultural heritage objects. The reasons for this are, firstly, that X-ray scanning facilities are not easily accessible due to the cost and the need to transport fragile objects, and secondly that, since the two datasets are recorded independently, a post-acquisition registration step is necessary. The latter often involves manual steps and the use of multiple software packages, sometimes open access, but also often commercial. This is labour-intensive and, depending on the packages used, can be costly. The lack of interactive data visualisation hampers optimal use by a wide range of users.

In this chapter, the second obstacle for integrating fusion of 3D imaging modalities into cultural heritage research is addressed via the development of an open-source

software package that provides tools for the multi-modal visualisation of CT scans, automatic registration with a surface scan, and interactive visualisation of the aligned 3D images.

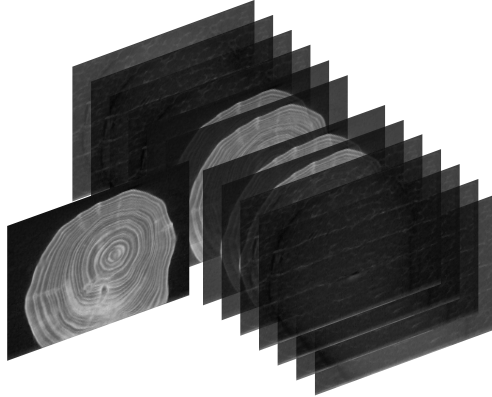


**Figure 5.1:** Stack of CT slices of a small wooden block.

## 5.2 Contributions and data availability

A plugin was developed within the open source and free 3D imaging software package Blender, enabling the combination of several 3D datasets. The reason for developing a new plugin is four-fold: i) existing single (commercial) visualisation packages often do not include all the required functionalities, such as the registration of multiple imaging modalities; ii) in existing commercial packages it is often impossible to access the source code and add or change functionalities; iii) by providing an open source plugin for an open source software package, it is accessible to all users and institutions; and iv) it is possible to continue development of the plugin and to add new features based on user experiences, with customisation and contribution open to all users. The plugin's acronym is INTACT - visualising the INTerior of Art through CT. The visualisation tool was developed as a collaboration between the Rijksmuseum and the British Museum. Four case study objects from the collections of these museums are presented, showing that the tool is versatile and cross validating that it can be used in different imaging facilities. The code is published at Zenodo, together with detailed step-by-step guidelines and a practice dataset (Figure 5.1, 5.2 and 5.5), including a CT scan and a surface scan that correspond to the provided instructions.

## 5.3 Material and methods

The INTACT plugin was developed for the open access software Blender. The decision to work with Blender was made for the following reasons: i) Blender runs on the

programming language Python, which allows users to easily build custom functions and plugins according to their own needs; ii) Blender is free and open source; and iii) the Blender Foundation safeguards older versions of the software, ensuring future compatibility of the tool, even if newer versions are released.

### 5.3.1 Data formats and visualisation

CT datasets consist of voxels, each with an assigned greyscale value based on the attenuation of the material of the object. These datasets are often represented as stacks of 2D slices (figure 5.1), each representing a cross section through the object. Two standard data formats are DICOM, commonly used in the medical field, and TIFF, commonly used in the computational imaging field. The cross sections are extremely useful for investigating detailed interior features that lie on a plane but it can be difficult to interpret due to the inherent limitations of looking at 2D cross-sections of a 3D object. It is, for example, difficult to find how internal features on the slice relate to the exterior and what their exact location is within the larger 3D object. Furthermore, characteristics that shed light on conservation issues or the process of making, are generally quite large and are not uniquely visible on a 2D plane. Visualising these features in 3D facilitates their interpretation, especially by cultural heritage professionals who are trained to look at materials and objects in 3D, and not as 2D cross-sections. For the plugin, the desired visualisation options of the CT data included both the 2D slices (figure 5.2b) and a 3D volumetric representation (figure 5.2c). Furthermore, in terms of functionality, there was a requirement for the tool to be able to dissect the volume representation in any direction, to focus on certain features, while allowing the corresponding 2D slice at the location of interest to be shown.

Surface scans are displayed as meshes consisting of a large set of triangles or faces, with associated colours and textures (figure 5.2d). A common type is the wavefront OBJ file format (.obj), which stores vertex coordinates, texture coordinates (UV) and normal. OBJ files can reference associated Material Template Library files (.mtl), that define material properties as color, reflectivity, transparency, and ambient, diffuse and specular coefficients. The Material Template Library files reference texture files (.png/.jpg/.tiff) to be applied to the 3D model. The way in which these files are created and their resulting quality/resolution is dependent on the hardware and method of data collection (e.g. photogrammetry with an affordable phone or structured light scanner with an expensive premium handheld scanner). For the plugin, the implemented option is an .obj file with material and texture files stored in the same folder. It should be noted, however, that it is possible to skip this step in the plugin user interface and instead use Blender's native capacity to load a large number of other types of 3D meshes. These, once loaded, can consequently be used in the next steps of the plugin. This opens up the possibility to use this plugin with any of the presently 3D mesh filetypes currently available in Blender.

When the surface and CT scans are aligned, the plugin is designed so that both the surface scan and the volume representation can be sliced through in tandem (figure 5.2e,f), to facilitate the evaluation of the relationship between the exterior

and interior features. As such, the visualisation is easy to manipulate and inspect interactively. Since the surface scan and CT scan are different data modalities, there is a requirement for a mesh to be generated from the CT data prior to registration of the two datasets. Surface scanning and CT scanning are not always available or co-located at the same institution. Therefore, through the plugin it is also possible to visualise data of either imaging modality individually. The presented visualisation tool is a post-processing tool, for use after the collection of datasets.

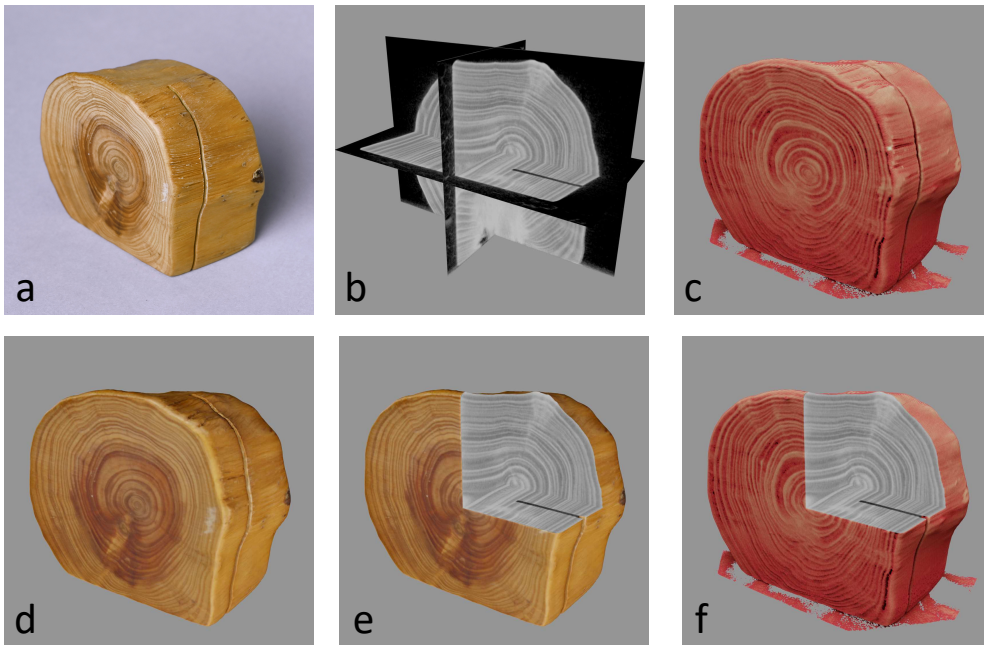


**Figure 5.2:** a) Photograph of a small wooden block (h 5cm x w 6cm x d 3cm), b) X-ray CT scan represented as orthogonal slices, c) CT 3D volume render, d) surface scan, e) combined image modalities showing surface scan and slices, f) CT 3D volume render and slices.

### 5.3.2 Code

The INTACT plugin was programmed in Python and builds upon and extends previous work. For CT data visualisation, both a volume representation and slice representation were desired. Furthermore, a function to generate a mesh from the voxel data was required to allow automatic alignment with the surface scan. The BDENTAL [57] plugin provided these functions and was therefore used as a base for the INTACT plugin. The code for loading DICOMs, generating the CT mesh and CT slices stems from there. The volumetric visualisation of the CT scan is achieved through displaying the data as a stack of thin slices. The user can choose the lower threshold of the displayed CT values. To align the two meshes (CT mesh, surface mesh), an iterative closest point (ICP) algorithm [207] was employed. In the plugin this alignment was done using an ICP implementation by Niels Klop [107]. Both these plugins have been released under GNU GPL licence, which means they can be used and modified freely.

The functionality of the INTACT plugin was extended by adding the capability to load CT data in TIFF format, to choose the colour of the CT volume render and to load a surface scan. Next, an interactive visualisation was designed. First, a clipping box was created using Blender's 'boolean' modifier. This modifier allows the box to cut into the surface scan and CT data, removing everything within its bounds from view. The CT slices were then parented to the clipping box, so that when it was moved, the corresponding slices could be shown on the three orthogonal sides of the box. In the final step, several image and video creation tools were included to make media for presentations and outreach. In this step the user can place the camera and render images from the same standpoint, choose the background colour of these images and make rotational videos along the  $x$ ,  $y$  or  $z$  axes. The functionalities of the plugin were arranged in the user interface (UI) to make each tab correspond to a step in the workflow described below and to prompt the user to undertake actions in the right order.

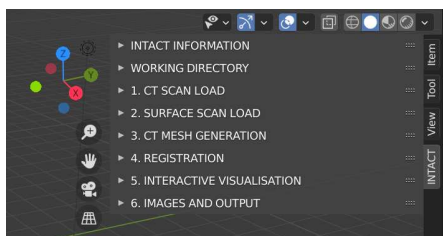


**Figure 5.3:** The plugin UI, each step in the workflow corresponds to a drop-down menu.

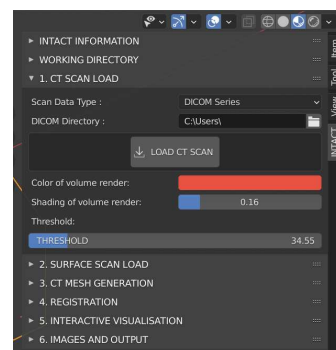


**Figure 5.4:** Example of the UI, the drop-down menus for loading the data and adjusting the visualisation of the CT volume representation.

## 5.4 Results

### 5.4.1 Workflow for generation of the interactive visualisation

To use the INTACT plugin, the user first needs to install Blender and download the .zip file containing the plugin. After installation, the workflow to set up the interactive visualisation interface consists of the steps outlined below. Within the plugin UI, each step is represented by a drop-down menu (see figure 5.3, 5.4). The workflow is also represented as a flowchart in figure 5.5 and detailed steps can be found in the guidelines in appendix B. A video recording of the workflow for the wooden block used to create figures 5.1, 5.2 and 5.5 is provided in the online Supplementary Material of [43], along with a short output video.

1. Load the CT data (DICOM or TIFF).
2. Load the surface scan data (.obj).
3. Determine a threshold value for the CT volume representation and generate a CT mesh.
4. Register the surface scan to the CT mesh by first performing an initial manual alignment and then using the ICP algorithm to refine the alignment. Several options for this step are provided. The user can enable/disable the scaling of the surface scan, in case of imperfectly calibrated scanning hardware. Furthermore, several parameters of the ICP algorithm can be altered, such as the number of iterations and the percentage of outlying vertices that is allowed. While these options may be of interest to advanced users, the standard settings have proven to work for our case studies. Lastly, if either the surface scan or CT scan are incomplete, manual selection of parts of the two meshes can be carried out to ensure registration occurs only based on correctly scanned sections. Carry out visual inspection to determine whether sufficient registration accuracy has been achieved.
5. Set up the interactive visualisation environment:
  - (a) Generate CT slices.
  - (b) Generate a clipping box that allows the simultaneous slicing of the CT volume representation and surface scan.
  - (c) Link the CT slices to the clipping boxes. The side of the box then shows the cross-section of the object at that location.
  - (d) Cut the CT slices to only show the interior (making the surrounding air transparent). Either based on the surface scan, if available, or based on the chosen threshold, if only a CT is loaded.
6. Set up camera and video options to create images and videos.

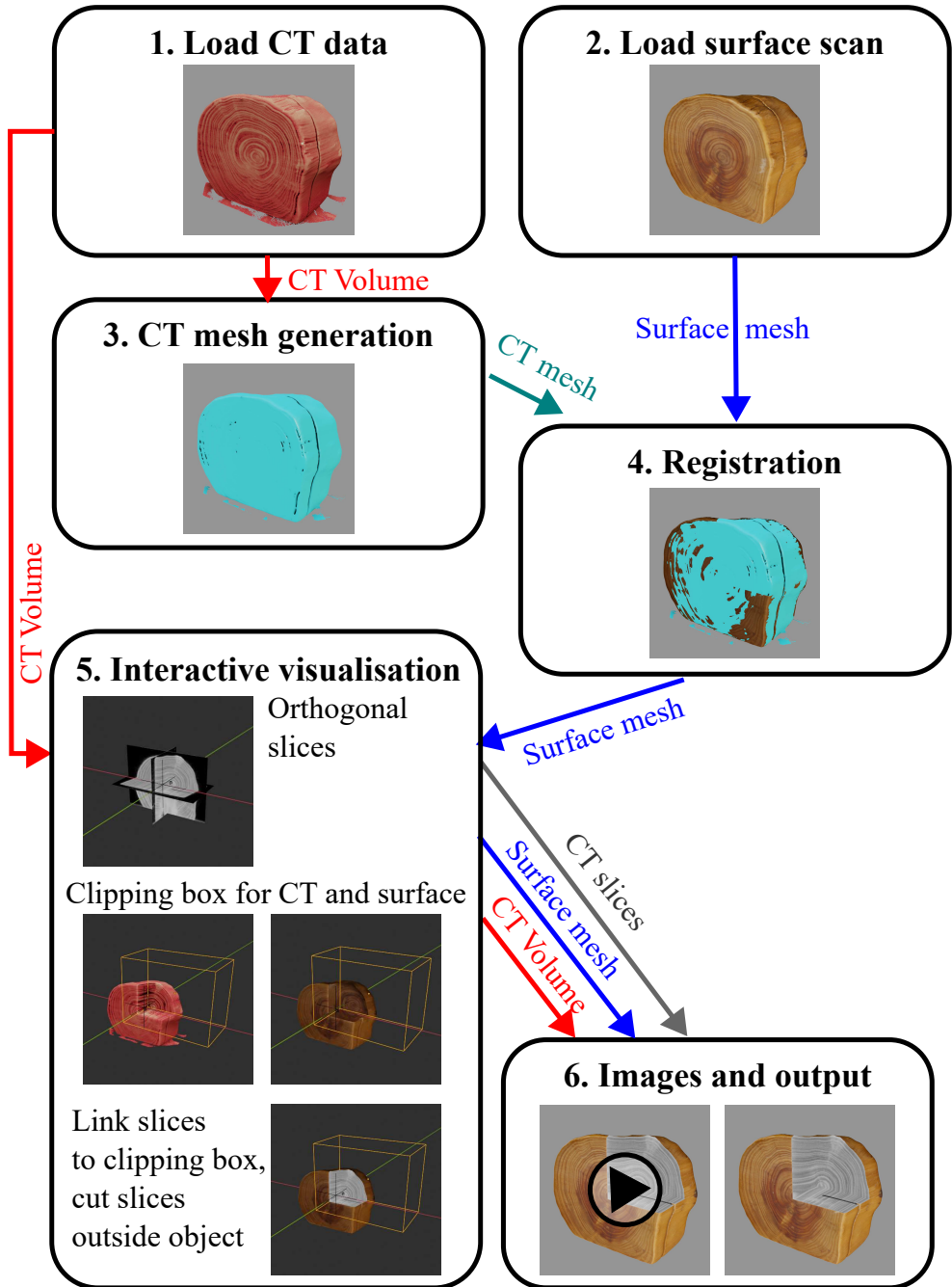


**Figure 5.5:** Flowchart of the workflow to combine CT datasets and surface scans. The results of the application of the visualisation tool developed to the case study objects are presented in figures and videos.

### 5.4.2 Case studies

The versatility of the visualisation tool is demonstrated with four case studies (figure 5.6), showing the diversity of sizes, shapes and materials the plugin can be applied to. Below, the objects and the challenges related to each are described, as well as the questions that guided the data acquisition and analysis. The objects were investigated to answer questions about their manufacture, their material nature, and their current conservation state.

The objects from the Rijksmuseum collection were CT scanned at the FleX-ray laboratory [53], and those of the British Museum objects were carried out at the in-house CT facility of the Scientific Research Department at the museum. The structured light scans of all four objects were acquired using an Artec Space Spider [97]. For the visualisations, the CT scans and surface scans were downscaled to allow investigation without the need for a powerful computer. The parameters of the case study datasets can be found in the online Supplementary Material of [43].



**Figure 5.6:** Case study objects. 1. Jaguar figure (British Museum, Am,+ .165). 2. Cutlery case (Rijksmuseum collection, object nr. BK-NM-3086). 3. Bottle in the shape of a whale (Rijksmuseum collection, object nr. BK-KOG-1382) 4. Mummy mask (British Museum, EA 29472). Images 1 and 4 are © The Trustees of the British Museum, 2 and 3 © Rijksmuseum, Amsterdam.

### 1. Turquoise Mosaic jaguar figure

*Size: h 17cm x w 9 cm x d 14cm.*

The Turquoise Mosaics are a group of objects from Mesoamerica, dating between the 14th Century and 1521, nine of which are housed in the British Museum. The group includes a seated figure (Am,+ .165), thought to be a jaguar, fashioned from wood (Cedrela odorata) and intricately decorated with tesserae of multiple different materials including turquoise, malachite, pyrite and mother-of-pearl (*Pinctada mazatlanica*) shell [187]. The tesserae are attached to the figure by a layer of pine resin covering most of the wood surface. Ongoing research into this object is focussed on its method of manufacture, its constituent materials and its current condition.

The CT images and 3D surface render visualise the interior of the jaguar and give insights into its construction, showing that several pieces of wood were used in making the figure, rather than a single piece (figure 5.7). A key advantage of combining the CT and surface scans of the figure is the connection between the material properties and their appearance: tesserae with visually similar colours have clearly different densities, readily showing a distinction between, for example, (less dense) turquoise and (more dense) malachite, without the need for destructive analysis or time-consuming point-by-point analysis. The figure is under further investigation and further findings will be part of a forthcoming publication on the Turquoise Mosaic objects.

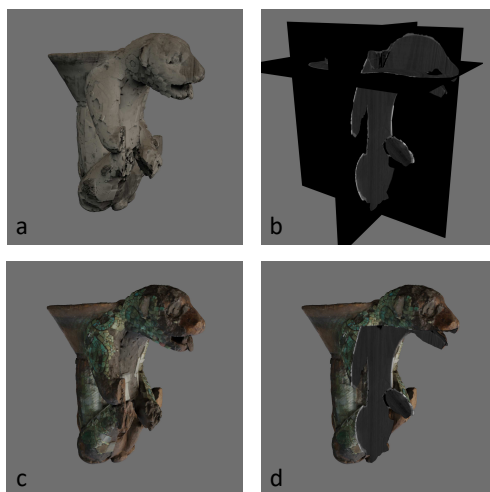


**Figure 5.7:** Images made with the INTACT plugin of the Turquoise Mosaic jaguar figure: a) CT volume render, b) orthogonal CT slices, c) surface scan, d) registered surface scan on CT volume and cut through the object showing orthogonal slices.

## 2. A 17th-century cutlery case

*Size: h 22cm x w 2,5cm x d 3,4cm.*

This early 17th-century encasement [158] has three cavities that once held pieces of cutlery. The case is made up of a variety of materials, with a stiffened paper internal structure covered by a purple velvet exterior, which is elaborately decorated with silver thread, gold thread, and small pearls in floral motifs. Questions about this object were related to its manufacturing process, in particular, how the internal compartments are constructed, what materials were used throughout the object, and whether the velvet exterior was pre-embroidered or not. The challenges during CT scanning arose from the materials in this object, as the metal threads caused image artefacts in the 3D reconstruction, which were mitigated by filtering the X-ray beam [106]. For the registration of the CT scan and surface scan, a further challenge was the rotational symmetry of this object (both the front and back of the case had similar decorations), making an accurate initial, manual, alignment necessary based on distinct features such as missing pearls. The lid and case were surface-scanned separately (figure 5.8a), to also show the intricately decorated part of the case that slides into the lid (figure 5.8b). Both scans needed to be registered to different parts of the CT scan. This was done by manually selecting the registration area for the ICP algorithm (see for more detail the INTACT User Guidelines in appendix B).

The CT scan of the 17th-century cutlery case allowed us to gain insight into how a variety of materials were used in its construction. The inner compartment, divided into three, is made from (stiffened) paper, and is held together by a surrounding outer shell made of leather. The absence of any holes in this leather outer shell suggests that the velvet exterior was pre-embroidered, and then attached using glue, not stitched onto the case. The registration of the surface scan to the CT scan in particular allowed the path of materials that are visible on the exterior to be traced as they are folded inside. An example of this is the golden threaded decoration running vertically along the object, as well as around the rim of the cap. Being able to access the 3D model exactly at this point (figure 5.8d), to reveal the corresponding slice (figure 5.8f), clearly showed that gold thread extends into the object only very slightly, which strengthened the hypothesis they were in fact glued, rather than stitched onto the velour.



**Figure 5.8:** a) Surface scan of the cutlery case and lid - aligned using the CT of the full object, b) surface scan of the case only, c) CT volume representation and surface scan of lid, d) surface scan, cut open to show the CT slices, e) corresponding vertical slice, f) corresponding horizontal slice.

### 3. Bottle in the shape of a whale

*Size: h25 x w30cm x d11.*

A 17th-century whale shaped object with a shoe sole and cork-tail that functions as a bottle [155], is a rather curious object hypothesised to have been made as part of a test to become a master in the cobbler's guild. The object is mostly made of leather, alongside a wooden heel, a cork, and metal reinforcements. Questions related to the object were focused on its crafting process and use: how and why was it made? Is the object fully hollow, which would have allowed it to hold liquid, or is it merely suggestive of a bottle? The challenges for CT scanning were mainly its odd shape. To obtain a full CT image, multiple scans were recorded with the source and detector at different positions, also called 'tiled scanning' [37]. The object was held upright in a plastic container, to facilitate tiled scanning and to make sure the tail, which contains metal, did not overlap with the rest of the object on any radiographs acquired throughout its rotation to avoid metal streaking artefacts on the main body of the whale. For structured light scanning, the dark and reflective surface provided a challenge, as well as the object's deep mouth that made it difficult to reach all the corners with the light beam.

3D visualisation of the CT data provided valuable insight into the construction of the object, such as the fact that the top part of the whale is constructed from just one intricately shaped piece of leather stitched along the back of the whale's tail. Inside the object, we can trace this stitching along the inner sole, where multiple pieces of leather from the bottom converge and are attached to one another (figure 5.9a). Furthermore, it quickly became clear the object is in fact fully hollow, even under the tongue (figure 5.9b), indicating that it could have in fact been used as a bottle and perhaps was not merely decorative. The overlay of the 3D surface scan and the CT data visualised features that had previously gone unnoticed when inspecting this object with the naked eye alone. While the presence of circular features reminiscent of eyes had been noted before, the overlay of data clearly revealed two additional circular marks on top of the whale's body (figure 5.10). What their function was or what these represent exactly is unclear at this stage, but they might be a pair of blowholes.

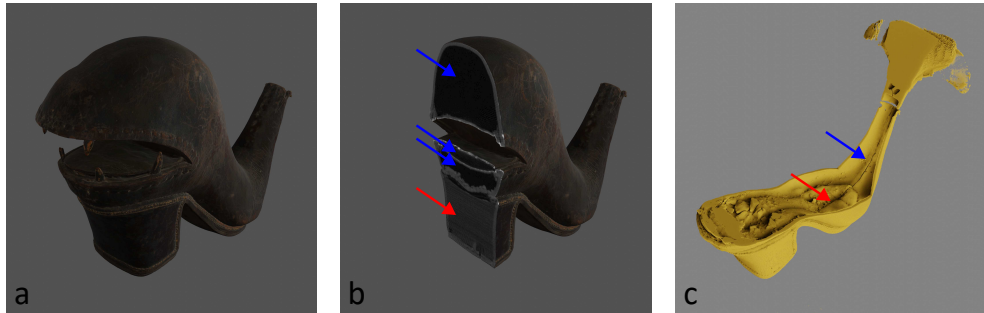


**Figure 5.9:** a) 3D surface scan of the body part of the whale. b) Slicing through the 3D surface scan, showing the corresponding CT slice, revealing the hollow spaces inside the object (blue arrows) and tree rings in the heel (red arrow). c) The volumetric representation of CT data cut through, to visualise the stitch along the back of the tail (blue arrow) as well as multiple pieces of leather converging in the insole (red arrow).

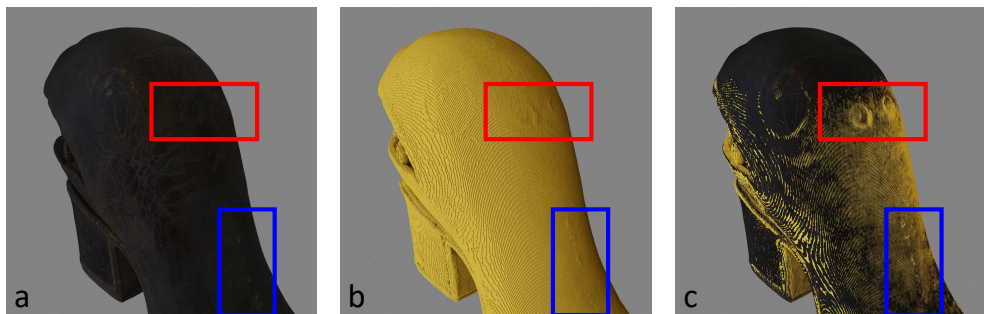


**Figure 5.10:** Detail, showing eye and blowholes, a) Surface scan, b) CT scan, c) CT and surface scan overlay. The volumetric representation of the CT data (in yellow) clearly reveals two circular features that had previously gone unnoticed (red box). In the blue box we see marks that are presumably made by stitches.

#### 4. Mummy mask

*Size: h 44cm x w 22cm x d 31cm.*

The ancient Egyptian mummy mask [188] is dated from the mid to late Ptolemaic Period (second to first century BCE). The mask is made in cartonnage: layers of textile covered with plaster, onto which a layer of paste was applied before its decoration with painting and gilding. Due to the mask's width being greater than the field of view of the X-ray imaging detector, a region of interest CT scan was performed, capturing the mask in the region of the face only (Vandenbeusch et al., 2021). The reflective gold surface was a challenge for surface scanning. For the fusion of the two scans, moreover, the hollow interior, thin mask walls and partial CT data posed a challenge. Accurate registration of the scans required focusing on areas captured by both methods. The CT segmentation captured both the inner and outer surfaces of the mask within the region of interest, while the surface scan captured the outer surface of the entire mask. Accurate registration therefore required manual selection of vertices only within the region of interest and outer mask layer for both the surface scan and CT segmentation. This was a challenge because the outer and inner layers of the mask are very close together due to the thinness of the mask walls (for more detail please refer to the guidelines in appendix B).

In figure 5.11 the results of registration and visualisation using the INTACT plugin are shown. The CT slices give insight into the construction, for example the nose is made up of more layers of textile than the rest of the mask; these layers act to thicken and reinforce this potentially fragile region. On this object the colours and decorations are of importance, and the combination of the imaging modalities is of high value. An example is shown in figure 5.12: on the CT images, patches can be identified within the vertical stripes. Switching to the surface scan and cutting the object open, shows that these patches correspond to the gold and that they are visible where the gold leaf overlaps. This shows that the gold was applied as sheets and then polished.

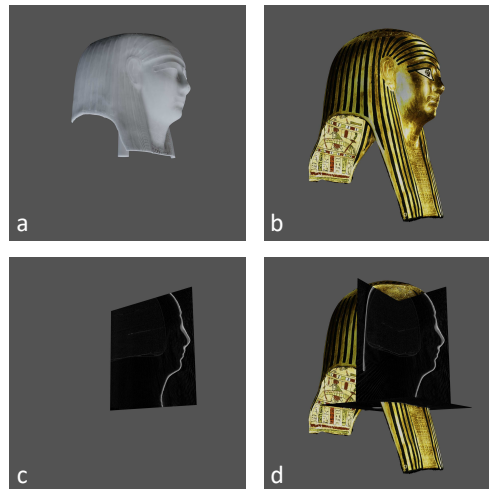


**Figure 5.11:** Images of the mummy mask, generated using the INTACT plugin. A) CT volume render, b) surface scan (note: the interior of the object could not be captured with structured light scanning; a mirror of the outside surface is represented here, rather than its actual undecorated interior), c) a CT slice, d) the surface scan registered with the CT scan, showing orthogonal slices (coronal and sagittal views are visible) where the object is cut open.

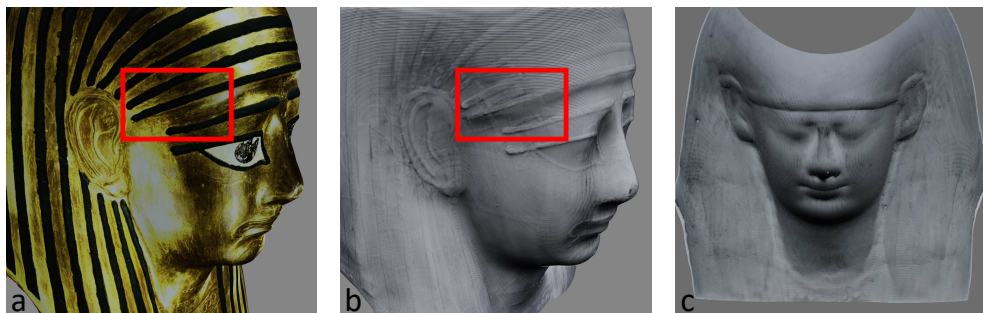


**Figure 5.12:** a) Surface scan of the mummy mask, b) CT scan of the mask, registered to the surface scan (red boxes indicate regions of overlapping gold leaf), c) CT scan showing the mould impression on the mask's interior surface.

## 5.5 Discussion and conclusions

The objective of this work was to create a single open-source and free workspace for cultural heritage experts to inspect two different types of 3D data in tandem: surface scans and CT scans. It combines colour and texture information on the exterior with the interior features, relating what can be seen with the naked eye to the structural composition, which leads to knowledge gain, optimised object analysis and improved digitization of objects. The plugin provides a free and simple to use interactive environment to examine 3D images for museums and heritage institutions. The plugin is openly available for use and fully enables customisation/extension, therefore it is hoped that it will be further developed based on user experience.

The INTACT plugin provides a way to interactively visualise and analyse 3D CT data, with a few simple steps. Users can view the volumetric representation of the data, as well as virtually cut the object open to see the 2D slices. This facilitates the inspection of internal features both in 2D and 3D. If a surface scan is available, the INTACT plugin provides all the tools and an easy step-by-step guideline to register this onto the CT data and to simultaneously inspect and cut open both datasets. After alignment is complete, the resulting transformation parameters can also be exported and used in other visualisation software packages. The processing times and file size limitations are dependent on the hardware used. For the case studies, we decided to downscale the CT scans and surface scans to ensure the workflow and interactive visualisation could be carried out on a laptop for accessibility to a broad audience. The processing time of the registration was then in the order of minutes and the entire workflow to obtain the interactive visualisation takes less than 15 minutes. Higher resolution visualisation and output images could be created when a more powerful computer is available.

The INTACT plugin was developed with ease-of-use for a broad audience in mind. The diversity in size, shape and materials of cultural heritage objects makes generalisability a challenge, since each unique object may require object-specific tailoring of acquisition and visualisation. Experienced Blender users can freely use the large sets of tools already included in Blender alongside the plugin to improve their data and the visualisation, for example by the mesh repair tools if the surface scan contains holes. The plugin is provided fully open-source, so other researchers are invited to extend it to the users' specific use cases. The versatility of Blender will allow dedicated and experienced 3D software users to self-optimize the potential of the plugin, by for example designing more complex, sophisticated and object-specific visualisations and videos. To this end, the plugin is provided fully open-source on GitHub and those who would like to contribute are encouraged to do so via that platform. The version used for the images in this manuscript is provided on Zenodo, along with the sample dataset that was used to create the Guidelines and the images in this article.

During the development of the INTACT plugin, datasets of a small wooden block and four accessioned museum objects were used, from two different facilities. The case studies show the importance of 3D imaging techniques for cultural heritage research, as

well as the added value of combining multiple techniques to retrieve more information for research. Additionally, the resulting images and videos are exceptionally well suited for outreach purposes. Future work could include extending the features of the visualisation tool with automatic quantified assessment of registration accuracy, automatic segmentation of materials, overlaying of multiple meshes in cases where multiple surface scans were acquired [152], and integration of output with other platforms, such as interactive PDFs [186] and open access online platforms for dissemination purposes.



# Conclusion and outlook

In this thesis, we identified the challenges and opportunities related to CT scanning of cultural heritage objects and to contribute to the broader adoption of this imaging technique within the museum research context by developing algorithms and techniques tailored to cultural heritage. In this chapter we will first summarize the contributions and limitations of the work presented in this thesis. We then present the research that was initiated or inspired by the work presented in this thesis. In the last section we provide perspectives on future work and identify where the main possibilities and challenges lie.

## 6.1 Contributions and limitations

The contributions of this thesis can be classified into two categories: 1) technique development and 2) application in the cultural heritage domain. Each chapter outlined a novel method or approach, which was consequently applied to a case study from a museum collection. Below we will outline the contributions and limitations per chapter, first on the topic of the technique development and then on the application in the cultural heritage domain.

### 6.1.1 Technique development

In **chapter 2**, we discussed the key characteristics of cultural heritage objects that require flexibility of the CT scanning setup. To be able to capture the multi-scale features in the interior of cultural heritage objects, it is necessary for the setup to be flexible in image resolution. Because of the varying shapes and sizes, the CT scanner needs to have adjustable source and detector position, to facilitate tiled scans of larger and irregularly shaped objects. The diversity in materials in art objects poses

a challenge due to the image artefacts that can arise with higher density components in particular. It is therefore important that there is flexibility in object positioning to find the optimal orientation for each object. The requirements for a scanning setup that are discussed in this chapter may not be feasible to obtain for most museums due to the cost of highly flexible laboratory scanners. However, we show the importance of the close collaboration between imaging experts and art experts to move this interdisciplinary field forward.

In **chapter 3**, we developed a novel method for the dendrochronological investigation of large wooden objects with X-ray imaging. Instead of a full circular acquisition trajectory, the object is moved on a linear trajectory. The images thus acquired span a small angular range. If the object is placed so that the section faces the source, we showed that it is possible to obtain sharp images of the tree rings that lead to similar tree ring measurements as the traditional method of high resolution photographs. This method is of high importance, because it opens up a wide range of objects for dendrochronological investigation, which were undatable before due to the inaccessibility of the tree rings from the outside. The technical limitation lies mostly in the needed orientation of the wood. This is usually along the length of a wooden plank, which means that high X-ray energy and power is needed. Moreover, it means that the length of the plank needs to fit between the source and detector, limiting the size of the object. Our method does provide the means to scan larger objects than with regular CT imaging, but more research could be performed to further eliminate barriers for the X-ray imaging of large objects for dendrochronological investigation.

In **chapter 4**, we proposed a marker-based acquisition protocol combined with sophisticated post-processing algorithms to use in-house X-ray facilities for 3D CT imaging. The goal was to make optimal use of existing hardware to obtain 3D reconstructions of objects. We obtained a standard reconstruction from the in-house CT scanner at the British Museum. We then compared the results of this CT-scan to the results obtained by applying our method in the British Museum, the J. Paul Getty Museum and the Rijksmuseum. Although these facilities have different hardware and thus the resolution of the reconstruction differs, we were able to show that the same features are visible in the reconstruction of a small wooden test object throughout the three facilities. This method is still limited to those museums that have an in-house X-ray imaging facility. The algorithms that were developed are moreover not user friendly for cultural heritage professionals. The impact of this work could be increased by developing user interfaces. Despite these limitations, this novel method allows for the application of 3D CT imaging in-house in more museums.

In **chapter 5**, we presented a software solution to provide an interactive environment for the visualisation of CT scans and surface scans. The object experts are used to handling the objects and looking at them closely. The addition of a surface scan that shows the colours and textures of the object therefore greatly enhances their engagement with the CT data, which is often represented as 2D greyscale slices through a colourful 3D object. The solution presented is a plugin for 3D visualisation software Blender. It provides all the tools for loading the different data types, making a mesh out of the CT scan and registering the surface scan to the CT scan. It then guides the user through the steps to setup an interactive environment to inspect

the different data types simultaneously, also giving the option to slice the volumes open and show the CT slices. In the last step, a few tools are provided for making simple images and video's for presentation, documentation and outreach purposes. To facilitate further analysis of data, additional tools should be added to the plugin. In next projects, the tools should be tested and evaluated by cultural heritage professionals. The application of this tool requires some knowledge of software Blender and is therefore not directly accessible for all users. By providing an extensive user guide and a step-by-step user interface, we have however attempted to mitigate this drawback.

### 6.1.2 Application in the cultural heritage domain

In **chapter 2**, we showed the added value of an expert-led acquisition process by scanning a musical instrument, a 17th century cornett. The feedback loops in which the object experts inspected live X-ray images and intermediate reconstruction results allowed us to adjust the scanning process. We acquired high resolution region of interest scans based on the intermediate analyses that would not have been acquired if the experts had not been present on the spot to steer the process. This not only answered the initial question, but additionally questions that arose during the scanning process. Thus more information about the object was gained by actively involving the object experts.

In **chapter 3**, the line trajectory acquisition method was applied to a large chest from the Rijksmuseum collection. It was reported to be the chest in which Hugo de Groot escaped his imprisonment at Castle Loevestijn. Using the new method, we were able to capture more tree rings than were visible on a photograph of the same plank. Although this proved the efficacy of our approach, unfortunately, it did not lead to a tree ring series that was long enough to cross-date with reference chronologies.

In **chapter 4**, the marker-based imaging protocol was applied to an object from the J. Paul Getty Museum collection. The 3D reconstruction obtained using our new methods led to knowledge about the production process that was unknown before. Different layers of plaster and metal rods were clearly visible. From the CT scans it could be deduced that the object had been reconfigured from an earlier model to its current shape by breaking it up and adding layers of material to create a new shape.

In **chapter 5**, several objects were used to illustrate the added value of a visualisation tool that combines CT imaging with surface scanning. Two objects from the British Museum collection were presented: a mummy mask and a turquoise mosaic jaguar. From the Rijksmuseum collection we presented two other objects: a shoe in the shape of a whale, that is also a bottle, and a cutlery case. In all these case studies, new information was gathered by the scanning and visualisation about the making process, material use and relation between external and internal features.

## 6.2 Continued research

In this thesis we have shown the knowledge gain from applying our newly developed methods and techniques on case studies from museum collections. The research presented in this thesis often sparked new questions which led to further research on objects and publications in the cultural heritage domain. Each of the chapters has led to a related publication by colleagues from the cultural heritage domain. Although these publications are not presented as part of this thesis, they were a direct result of the research presented here.

The CT scan of the cornett in chapter 2, led to further research into its making process and the question whether the combination of two woodtypes could have been original or more likely a later restoration [64]. The *Holy woman with lantern*, which was also featured in that chapter, was dated and its provenance was determined based on the CT scan. This led to insights in the Dutch wood trade [63]. The success of this CT scan led to a new project, investigating a panel painting attributed to Rubens' studio for dendrochronological dating. The CT scan contained a surprise: the painting was not painted on the oak backboard as originally thought, but on a tropical wood board that was glued onto the oak board. This result has important implications for the analysis and dating of panel paintings [60].

The acquisition technique presented in chapter 3 led to further investigation of the chest to determine its age and provenance [61], was featured in the NPO (Dutch national television) television series *Historisch Bewijs* (Historical Evidence)[11]. The research team received the NWO Team Science Award for this interdisciplinary collaboration in 2021 [51, 67].

The newly acquired knowledge about the making process of the *Python Killing a Gnu* in chapter 4, will be included in a catalogue detailing the sculpture collection of the J. Paul Getty Museum (author: Madeline Corona). The challenges for CT scanning the cutlery case for chapter 5 were the metal threads in the object, which led to streaking artefacts in the reconstruction. These image artefacts were mitigated by filtering the X-ray beam, which led to a publication on the topic of tailoring the acquisition process to the object [106]. The other objects presented in chapter 5 are under further investigation and the conclusions of data analysis may lead to further publications.

## 6.3 Outlook

As outlined above, there is much to be won by integrating CT scanning as a research tool within the cultural heritage research practice. There are however challenges for broad implementation of CT scanning for cultural heritage, such as the accessibility of scanning facilities and the difficulty of moving precious collection objects. In the future, hopefully CT will become more accessible to museums for the investigation of their objects. A first step was made by making optimal use of existing hardware in museums in chapter 4. To increase the impact of this work, the developed algorithms should be accompanied by user friendly interfaces that are implemented in the X-ray

suites. It is important to increase the accessibility of the algorithms developed in this thesis, such that on the longer term these can be used by museum professionals independently from a computational expert.

The interpretation of the data should be more accessible to increase the impact of CT imaging in the cultural heritage domain. We have provided a starting point with the plugin for Blender in chapter 5. The addition of colour information, three dimensional representation of the object and an interactive environment to inspect these datasets will lead to better understanding of the data and consequently more information can be retrieved from the datasets. In future projects, the fusion of other - 3D and 2D - imaging methods in an interactive way may be investigated. In the past years, the reproduction of art objects by employing 3D printing techniques and the perception of these reproductions has been investigated [130]. It would be interesting to explore the potential of these techniques for making CT scans more accessible for both researchers and the wider public.

One aspect that is often discussed in the cultural heritage field is the potential damage to objects due to the radiation. The energy of the X-rays and the exposure time influence the quality of the data and determine the effective radiation dose the object receives. The potential effect of the radiation exposure depends on the settings of the scan and the characteristics of the object [17, 83]. This potential effect has not yet been sufficiently investigated and would be an important topic for the investigation of cultural heritage with CT imaging.

Apart from the implementations of existing methods within the museum context, it is interesting to develop novel algorithms and data processing tools to automatically detect features within the data. Over the last years, image processing has been applied for example to read unopened letters [59]. Using machine learning methods, automated feature detection could be achieved. For example, it would be possible to look into automated tree ring detection, tool mark detection, classification of objects and many other applications.

The algorithms and case studies presented in this thesis show the importance of close collaboration between imaging experts and object experts. On the one hand, investigation by CT scans leads to new insights, new questions and further analyses of cultural heritage objects. On the other hand, the specific challenges presented by the diversity of cultural heritage objects give rise to the need to tailor acquisition processes and develop new algorithms. Thus, both the cultural heritage field and the CT imaging field benefit from this interdisciplinary research.



# Bibliography

- [1] W. V. Aarle, W. J. Palenstijn, J. Cant, E. Janssens, F. Bleichrodt, A. Dabravolski, J. D. Beenhouwer, K. J. Batenburg, and J. Sijbers. “Fast and flexible X-ray tomography using the ASTRA toolbox”. *Optics Express* 24.22 (2016), pp. 25129–25147 (cit. on pp. 50, 70).
- [2] M. Abella, C. Martinez, I. Garcia, P. Moreno, C. De Molina, and M. Desco. “Tolerance to geometrical inaccuracies in CBCT systems: A comprehensive study”. *Medical Physics* 48.10 (Oct. 2021), pp. 6007–6019 (cit. on p. 69).
- [3] A. Adriaens. “Non-destructive analysis and testing of museum objects: An overview of 5 years of research”. *Spectrochimica Acta - Part B Atomic Spectroscopy* 60.12 (2005), pp. 1503–1516 (cit. on p. 41).
- [4] F. Albertin, M. Bettuzzi, R. Brancaccio, M. P. Morigi, and F. Casali. “X-Ray Computed Tomography In Situ: An Opportunity for Museums and Restoration Laboratories”. *Heritage* 2.3 (2019), pp. 2028–2038 (cit. on pp. 27, 60).
- [5] J. Anderson and D. Antoine. “Scanning Sobek, Mummy of the Crocodile God”. In: *Creatures of Earth, Water and Sky: Essays on Animals in Ancient Egypt and Nubia*. Leiden: Sidestone Press, 2019, pp. 31–37 (cit. on pp. 23, 24).
- [6] F. I. Apollonio, F. Fantini, S. Garagnani, and M. Gaiani. “A Photogrammetry-Based Workflow for the Accurate 3D Construction and Visualization of Museums Assets”. *Remote Sensing* 13.3 (2021), p. 486 (cit. on p. 77).
- [7] ARES. *Astromaterials 3D*. URL: <https://ares.jsc.nasa.gov/astromaterials3d/> (visited on Nov. 9, 2023) (cit. on pp. 78, 79).
- [8] Artec 3D. *Egyptian mummy turned into 3D model*. 2017. URL: <https://www.artec3d.com/news/computed-tomography-3d-scanning-egyptian-mummy> (visited on Nov. 9, 2023) (cit. on p. 79).
- [9] Autodesk. *Maya Software*. URL: <https://www.autodesk.eu/products/maya/overview> (visited on Nov. 9, 2023) (cit. on p. 78).
- [10] *Autograd*. URL: <https://github.com/HIPS/autograd> (visited on Nov. 9, 2023) (cit. on p. 127).
- [11] Avrotros. *Historisch Bewijs - De boekenkist van Hugo de Groot*. URL: <https://www.avrotros.nl/archive/historisch-bewijs-de-boekenkist-van-hugo-de-groot-04-03-2020~osixpw0e/> (visited on Nov. 9, 2023) (cit. on pp. 52, 100).
- [12] M. G. L. Baillie. *Tree-ring dating and archaeology*. Vol. 3. 1982 (cit. on pp. 42, 47).
- [13] M. G. L. Baillie and J. R. Pilcher. “A simple crossdating program for tree-ring research”. *Tree-Ring Bulletin* 33 (1973), pp. 7–14 (cit. on pp. 47, 49, 52).

- [14] F. Bauer, D. Forndran, T. Schromm, and C. U. Grosse. “Practical Part-Specific Trajectory Optimization for Robot-Guided Inspection via Computed Tomography”. *Journal of Nondestructive Evaluation* 41.3 (2022), p. 55 (cit. on p. 69).
- [15] L. Beck. “Recent trends in IBA for cultural heritage studies”. *Nuclear Instruments and Methods in Physics Research, Section B: Beam Interactions with Materials and Atoms* 332 (2014). Publisher: Elsevier, pp. 439–444 (cit. on p. 41).
- [16] G. Bekes, E. Máté, L. G. Nyúl, A. Kuba, and M. Fidrich. “Geometrical model-based segmentation of the organs of sight on CT images: Geometrical model-based segmentation of the organs of sight”. *Medical Physics* 35.2 (2008), pp. 735–743 (cit. on pp. 5, 24).
- [17] L. Bertrand, S. Schöeder, D. Anglos, M. B. Breese, K. Janssens, M. Moini, and A. Simon. “Mitigation strategies for radiation damage in the analysis of ancient materials”. *TrAC Trends in Analytical Chemistry* 66 (2015), pp. 128–145 (cit. on pp. 26, 101).
- [18] M. Bettuzzi, F. Casali, M. P. Morigi, R. Brancaccio, D. Carson, G. Chiari, and J. Maish. “Computed tomography of a medium size Roman bronze statue of Cupid”. *Applied Physics A* 118.4 (2015), pp. 1161–1169 (cit. on pp. 26, 60).
- [19] J. Bill, A. Daly, Ø. Johnsen, and K. S. Dalen. “DendroCT - Dendrochronology without damage”. *Dendrochronologia* 30.3 (2012), pp. 223–230 (cit. on pp. 12, 24, 42, 69).
- [20] Blender Foundation. *blender.org - Home of the Blender project*. URL: <https://www.blender.org/> (visited on Nov. 9, 2023) (cit. on p. 78).
- [21] F. E. Boas and D. Fleischmann. “CT artifacts: causes and reduction techniques”. *Imaging in Medicine* 4.2 (2012), pp. 229–240 (cit. on p. 26).
- [22] F. Bossema. *Code for 3D tomography using only basic X-ray equipment and metal markers*. 2024. URL: <https://zenodo.org/records/8379920> (visited on Mar. 19, 2024) (cit. on pp. 61, 150).
- [23] F. Bossema. *Radiographic data of a wooden block with metal markers at the FleX-ray laboratory (high resolution)*. 2024. URL: <https://zenodo.org/records/10557034> (visited on Mar. 19, 2024) (cit. on pp. 63, 150).
- [24] F. Bossema. *Radiographic data of a wooden block with metal markers at the Rijksmuseum X-ray facility*. 2024. URL: <https://zenodo.org/records/8379870> (visited on Mar. 19, 2024) (cit. on pp. 63, 150).
- [25] F. Bossema and A. Heginbotham. *Radiographic data of a wooden block with metal markers at the J. Paul Getty Museum X-ray facility*. 2024. URL: <https://zenodo.org/records/8379880> (visited on Mar. 19, 2024) (cit. on pp. 63, 150).
- [26] F. Bossema, A. Heginbotham, and M. Corona. *Radiographic data of 'Python killing a Gnu' by Antoine-Louis Barye, The J. Paul Getty Museum collection*. 2024. URL: <https://zenodo.org/records/8379913> (visited on Mar. 19, 2024) (cit. on pp. 66, 150).

- [27] F. Bossema and D. O’Flynn. *Radiographic data of a wooden block with metal markers at the British Museum X-ray facility*. 2024. URL: <https://zenodo.org/records/8379910> (visited on Mar. 19, 2024) (cit. on pp. 63, 150).
- [28] F. Bossema, J. Retrê, S. Pereira, and P. Russo. “Your night out under the stars: Reaching beyond native audiences”. *Communicating Astronomy with the Public* (2018) (cit. on p. 150).
- [29] F. Bossema and P. Van Laar. *CT reconstruction and structured light scan of a small wooden block*. 2023. URL: <https://zenodo.org/records/8041816> (visited on Nov. 9, 2023) (cit. on p. 151).
- [30] F. Bossema, P. Van Laar, and K. Meechan. *IntACT plugin for Blender*. 2023. URL: <https://zenodo.org/records/8041844> (visited on Nov. 9, 2023) (cit. on p. 151).
- [31] F. Bossema, C. Zwetsloot, and I. Smeets. “Math in the City: Designing a Math Trail for High School Students”. In: *World Scientific Series on Science Communication*. Vol. 03. WORLD SCIENTIFIC, 2023, pp. 53–72 (cit. on p. 149).
- [32] F. G. Bossema. *A CT dataset of a small wooden block*. 2021. URL: <https://zenodo.org/record/4533882> (visited on Nov. 9, 2023) (cit. on pp. 48, 151).
- [33] F. G. Bossema. *A line trajectory X-ray tomography dataset of a wooden plank*. 2021. URL: <https://zenodo.org/record/4533887> (visited on Nov. 9, 2023) (cit. on pp. 51, 151).
- [34] F. G. Bossema. *Three line trajectory X-ray tomography datasets of a small wooden block*. 2021. URL: <https://zenodo.org/record/4541555> (visited on Nov. 9, 2023) (cit. on pp. 48, 151).
- [35] F. G. Bossema, P. Burger, L. Bratton, A. Challenger, R. C. Adams, P. Sumner, J. Schat, M. E. Numans, and I. Smeets. “Expert quotes and exaggeration in health news: a retrospective quantitative content analysis”. *Wellcome Open Research* 4 (2019), p. 56 (cit. on p. 150).
- [36] F. G. Bossema and S. B. Coban. *Three tomographic CT datasets of a woven fabric*. 2020. URL: <https://zenodo.org/records/3741311> (visited on Nov. 9, 2023) (cit. on pp. 28, 151).
- [37] F. G. Bossema, S. B. Coban, A. Kostenko, P. van Duin, J. Dorscheid, I. Garachon, E. Hermens, R. van Liere, and K. J. Batenburg. “Integrating expert feedback on the spot in a time-efficient explorative CT scanning workflow for cultural heritage objects”. *Journal of Cultural Heritage* 49 (2021), pp. 38–47 (cit. on pp. 23, 41, 60, 70, 78, 90, 149).
- [38] F. G. Bossema, M. Domínguez-Delmás, W. J. Palenstijn, A. Kostenko, J. Dorscheid, S. B. Coban, E. Hermens, and K. J. Batenburg. “A novel method for dendrochronology of large historical wooden objects using line trajectory X-ray tomography”. *Scientific Reports* 11, 11024 (2021) (cit. on pp. 41, 69, 149).

- [39] F. G. Bossema, J. Dorscheid, A. Kostenko, and S. B. Coban. *A line trajectory X-ray tomography dataset of the Hugo de Groot bookchest*. 2021. URL: <https://zenodo.org/record/4533923> (visited on Nov. 9, 2023) (cit. on pp. 53, 151).
- [40] F. G. Bossema, A. Kostenko, and S. B. Coban. *A five-tile tomographic micro-CT dataset of the oak sculpture "Holy woman with lantern" - part 1 of 2*. 2020. URL: <https://zenodo.org/record/3747192> (visited on Nov. 9, 2023) (cit. on pp. 30, 151).
- [41] F. G. Bossema, A. Kostenko, and S. B. Coban. *A five-tile tomographic micro-CT dataset of the oak sculpture "Holy woman with lantern" - part 2 of 2*. 2020. URL: <https://zenodo.org/record/3747327> (visited on Nov. 9, 2023) (cit. on pp. 30, 151).
- [42] F. G. Bossema, W. J. Palenstijn, A. Heginbotham, M. Corona, T. Van Leeuwen, R. Van Liere, J. Dorscheid, D. O’Flynn, J. Dyer, E. Hermens, and K. J. Batenburg. “Enabling 3D CT-scanning of cultural heritage objects using only in-house 2D X-ray equipment in museums”. *Nature Communications* (accepted, in press) (cit. on pp. 59, 121, 149).
- [43] F. G. Bossema, P. J. Van Laar, K. Meechan, D. O’Flynn, J. Dyer, T. Van Leeuwen, S. Meijer, E. Hermens, and K. J. Batenburg. “Inside out: Fusing 3D imaging modalities for the internal and external investigation of multi-material museum objects”. *Digital Applications in Archaeology and Cultural Heritage* 31 (2023), e00296 (cit. on pp. 77, 84, 86, 133, 149).
- [44] R. Brancaccio, M. Bettuzzi, F. Casali, M. P. Morigi, G. Levi, A. Gallo, G. Marchetti, and D. Schneberk. “Real-time reconstruction for 3-D CT applied to large objects of cultural heritage”. *IEEE Transactions on Nuclear Science* 58.4 (2011), pp. 1864–1871 (cit. on pp. 42, 55).
- [45] *British Museum - Scientific techniques*. URL: <https://www.britishmuseum.org/our-work/departments/scientific-research/scientific-techniques> (visited on Nov. 9, 2023) (cit. on p. 55).
- [46] M. Brookhouse, S. Ives, P. Dredge, D. Howard, and M. Bridge. “Mapping Henry: Dendrochronological Analysis of a Sixteenth-Century Panel Painting Based Upon Synchrotron-Sourced X-ray Fluorescence Mapping”. *Studies in Conservation* (2020), pp. 1–13 (cit. on p. 41).
- [47] J. V. d. Bulcke, D. V. Loo, M. Dierick, B. Masschaele, L. V. Hoorebeke, and J. V. Acker. “Nondestructive research on wooden musical instruments: From macro- to microscale imaging with lab-based X-ray CT systems”. *Journal of Cultural Heritage* 27.Supplement (2017), S78–S87 (cit. on pp. 13, 24, 26, 42).
- [48] T. Buzug. *Computed tomography: From photon statistics to modern cone-beam CT*. Springer-Verlag Berlin Heidelberg, 2008 (cit. on pp. 6, 24, 26, 44, 72).
- [49] M. Carl and M. L. Young. “Complementary analytical methods for analysis of Ag-plated cultural heritage objects”. *Microchemical Journal* 126 (2016). Publisher: Elsevier Inc., pp. 307–315 (cit. on p. 41).

- [50] F. Casali. “Chapter 2 X-ray and neutron digital radiography and computed tomography for cultural heritage”. In: *Physical Techniques in the Study of Art, Archaeology and Cultural Heritage*. Vol. 1. Elsevier, 2006, pp. 41–123 (cit. on pp. 6, 24, 26).
- [51] Centrum Wiskunde & Informatica. *NWO Team Science Award for CWI with UvA and Rijksmuseum*. URL: <https://www.cwi.nl/en/news/nwo-team-science-award-for-cwi-and-research-partners/> (visited on Nov. 9, 2023) (cit. on p. 100).
- [52] P. Cignoni, M. Callieri, M. Corsini, M. Dellepiane, F. Ganovelli, and G. Ranzuglia. “MeshLab: an Open-Source Mesh Processing Tool”. In: *Eurographics Italian Chapter Conference*. Ed. by V. Scarano, R. D. Chiara, and U. Erra. The Eurographics Association, 2008 (cit. on p. 78).
- [53] S. B. Coban, F. Lucka, W. J. Palenstijn, D. Van Loo, and K. J. Batenburg. “Explorative Imaging and Its Implementation at the FleX-ray Laboratory”. *Journal of Imaging* 6.4 (2020), p. 18 (cit. on pp. 27, 46, 86).
- [54] A. Netherlands Institute for Conservation and Science. *CT for Art*. URL: <https://www.nicas-research.nl/projects/impact4art/> (visited on Nov. 9, 2023) (cit. on p. 25).
- [55] B. Cornelis, T. Ruzzić, E. Gezels, A. Doods, A. Pixzurica, L. Platixsa, J. Cornelis, M. Martens, M. De Mey, and I. Daubechies. “Crack detection and inpainting for virtual restoration of paintings: The case of the Ghent Altarpiece”. *Signal Processing* 93.3 (2013), pp. 605–619 (cit. on p. 23).
- [56] B. Cornelis, A. Doods, I. Daubechies, and P. Schelkens. “Report on Digital Image Processing for Art Historians”. In: *SAMPTA’09, Marseille, France. Special session on sampling and (in)painting*. 2009 (cit. on pp. 23, 41).
- [57] I. Dakir. *BDENTAL*. 2022. URL: <https://github.com/issamdakir/BDENTAL> (visited on Nov. 9, 2023) (cit. on p. 83).
- [58] A. Daly and N. L. W. Streeton. “Non-invasive dendrochronology of late-medieval objects in Oslo: refinement of a technique and discoveries”. *Applied Physics A* 123.6 (2017), p. 431 (cit. on pp. 12, 24, 42, 60).
- [59] J. Dambrogio, A. Ghassaei, D. S. Smith, H. Jackson, M. L. Demaine, G. Davis, D. Mills, R. Ahrendt, N. Akkerman, D. van der Linden, and E. D. Demaine. “Unlocking history through automated virtual unfolding of sealed documents imaged by X-ray microtomography”. *Nature Communications* 12.1 (2021). Number: 1 Publisher: Nature Publishing Group, p. 1184 (cit. on pp. 59, 60, 101).
- [60] M. Domínguez-Delmás, F. G. Bossema, J. Dorscheid, M. Hall-Acquitania, S. B. Coban, K. J. Batenburg, and E. Hermens. “X-ray computed tomography for non-invasive dendrochronology reveals concealed double paneling on a painting from Rubens’ studio”. *PLOS ONE* (2021) (cit. on pp. 11, 60, 100, 150).

- [61] M. Domínguez-Delmás, P. Van Duin, J. Dorscheid, F. G. Bossema, K. J. Batenburg, and R. Van Langh. “Unravelling a 17th-century prison escape: The quest to identify the original Hugo Grotius bookchest”. In: *Working Towards a Sustainable Past*. ICOM-CC 20th Triennial Conference Preprints, Valencia, 18–22 September 2023, J. Bridgland. Paris: International Council of Museums, 2023 (cit. on pp. 100, 149).
- [62] M. Domínguez-Delmás. “Seeing the forest for the trees: New approaches and challenges for dendroarchaeology in the 21st century”. *Dendrochronologia* 62. October 2019 (2020). Publisher: Elsevier, p. 125731 (cit. on pp. 41, 42).
- [63] M. Domínguez-Delmás, F. G. Bossema, B. van der Mark, A. Kostenko, S. B. Coban, S. van Daalen, P. van Duin, and K. J. Batenburg. “Dating and provenancing the Woman with lantern sculpture – A contribution towards attribution of Netherlandish art”. *Journal of Cultural Heritage* 50 (2021), pp. 179–187 (cit. on pp. 3, 12, 23, 30, 59, 60, 100, 150).
- [64] J. Dorscheid, F. G. Bossema, P. van Duin, S. B. Coban, R. van Liere, K. J. Batenburg, and G. P. Di Stefano. “Looking under the skin: multi-scale CT scanning of a peculiarly constructed cornett in the Rijksmuseum”. *Heritage Science* 10, 161.1 (2022) (cit. on pp. 38, 59, 78, 100, 149).
- [65] A. Douglass. “Crossdating in Dendrochronology”. *Journal of Forestry* 39.10 (1941) (cit. on p. 42).
- [66] *Dragonfly*. URL: <https://www.theobjects.com/dragonfly/index.html> (visited on Nov. 9, 2023) (cit. on pp. 11, 79).
- [67] Dutch Research Council (NWO). *Winners NWO Science Awards 2021 announced*. URL: <https://www.nwo.nl/en/news/winners-nwo-science-awards-2021-announced> (visited on Nov. 9, 2023) (cit. on p. 100).
- [68] D. Eckstein and J. Bauch. “Beitrag zur Rationalisierung eines dendrochronologischen Verfahrens und zu Analyse seiner Aussagesicherheit”. *Forstwissenschaftliches Centralblatt* 88 (1969), pp. 230–250 (cit. on pp. 47, 49, 52).
- [69] *Ethafoam - CAMEO*. URL: <https://cameo.mfa.org/wiki/Ethafoam> (visited on Nov. 9, 2023) (cit. on p. 33).
- [70] S. Fahrni, L. Campana, A. Dominguez, T. Uldin, F. Dedouit, O. Delémont, and S. Grabherr. “CT-scan vs. 3D surface scanning of a skull: first considerations regarding reproducibility issues”. *Forensic sciences research* 2.2 (2017), pp. 93–99 (cit. on p. 79).
- [71] A. Fedorov, R. Beichel, J. Kalpathy-Cramer, J. Finet, J.-C. Fillion-Robin, S. Pujol, C. Bauer, D. Jennings, F. Fennessy, M. Sonka, J. Buatti, S. Aylward, J. V. Miller, S. Pieper, and R. Kikinis. “3D Slicer as an image computing platform for the Quantitative Imaging Network”. *Magnetic Resonance Imaging* 30.9 (2012), pp. 1323–1341 (cit. on pp. 11, 79).
- [72] L. A. Feldkamp, L. C. Davis, and J. W. Kress. “Practical cone-beam algorithm”. *Journal of the Optical Society of America A* 1.6 (1984), pp. 612–619 (cit. on pp. 9, 44, 71).

- [73] M. Ferrucci, R. K. Leach, C. Giusca, S. Carmignato, and W. Dewulf. “Towards geometrical calibration of x-ray computed tomography systems—a review”. *Measurement Science and Technology* 26.9 (Sept. 2015), p. 092003 (cit. on p. 69).
- [74] M Feser, J Gelb, H Chang, H Cui, F Duewer, S. H. Lau, A Tkachuk, and W Yun. “Sub-micron resolution CT for failure analysis and process development”. *Measurement Science and Technology* 19.9 (2008), p. 094001 (cit. on p. 24).
- [75] M. Fioravanti, G. Di Giulio, G. Signorini, G. R. Rognoni, N. Sodini, G. Tromba, and F. Zanini. “Non-invasive wood identification of historical musical bows”. *IAWA Journal* 38.3 (2017), pp. 285–296 (cit. on p. 42).
- [76] P. Fraiture. “Contribution of dendrochronology to understanding of wood procurement sources for panel paintings in the former Southern Netherlands from 1450 AD to 1650 AD”. *Dendrochronologia* 27.2 (2009). Publisher: Elsevier, pp. 95–111 (cit. on p. 51).
- [77] P. Fried, J. Woodward, D. Brown, D. Harvell, and J. Hanken. “3D scanning of antique glass by combining photography and computed tomography”. *Digital Applications in Archaeology and Cultural Heritage* 18 (2020), e00147 (cit. on pp. 23, 59, 78, 79).
- [78] H. C. Fritts. *Tree rings and climate*. Academic Press, London, 1976 (cit. on p. 42).
- [79] H. Gao, L. Zhang, Z. Chen, Y. Xing, J. Cheng, and Z. Qi. “Direct filtered-backprojection-type reconstruction from a straight-line trajectory”. *Optical Engineering* 46.5 (2007), p. 057003 (cit. on p. 43).
- [80] H. Gao, L. Zhang, Z. Chen, Y. Xing, H. Xue, and J. Cheng. “Straight-line-trajectory-based x-ray tomographic imaging for security inspections: System design, image reconstruction and preliminary results”. *IEEE Transactions on Nuclear Science* 60.5 (2013), pp. 3955–3968 (cit. on p. 43).
- [81] I. Garachon. “Some technical aspects of the terracotta models from the estate of Johan Gregor van der Scharde”. *Simiolus Neth. Q. Hist. Art* 41 (2020), pp. 177–190 (cit. on pp. 13, 24, 78).
- [82] I. Garachon and L. Van Valen. “The matter of tang tomb figures: A new perspective on a group of terracotta animals and riders”. *Rijksmuseum Bulletin* (2014), pp. 218–239 (cit. on pp. 23, 24, 26).
- [83] P. Garside and S. O’Connor. “Assessing the risks of radiographing culturally significant textiles”. *e-Preservation science* (2007) (cit. on p. 26, 101).
- [84] S. Gondrom, J. Zhou, M. Maisl, H. Reiter, M. Kröning, and W. Arnold. “X-ray computed laminography: An approach of computed tomography for applications with limited access”. *Nuclear Engineering and Design* 190 (1999), pp. 141–147 (cit. on p. 43).
- [85] R. C. Gonzalez and R. E. Woods. *Digital Image Processing*. 3rd Editio. Prentice-Hall, 2007 (cit. on p. 53).

- [86] J. Graetz. “Auto-calibration of cone beam geometries from arbitrary rotating markers using a vector geometry formulation of projection matrices”. *Physics in Medicine & Biology* 66.7 (2021). Publisher: IOP Publishing, p. 075013 (cit. on p. 69).
- [87] J. Gregor and T. Benson. “Computational analysis and improvement of SIRT”. *IEEE Transactions on Medical Imaging* 27.7 (2008), pp. 918–924 (cit. on pp. 9, 44, 46, 72, 73).
- [88] G. Van der Ham. “De boekenkist van Hugo de Groot (1621)”. In: *Verzameld verleden: veertig gedenkwaardige momenten en figuren uit de vaderlandse geschiedenis*. Verloren, Hilversum, 2004 (cit. on p. 52).
- [89] K. Haneca, R. d. Boodt, V. Herremanas, H. d. Pauw, J. V. Acker, C. v. d. Velde, and H. Beekman. “Late Gothic Altarpieces As Sources of Information on”. *IAWA Journal* 26.3 (2005), pp. 273–298 (cit. on p. 51).
- [90] K. Haneca, K. Cufar, and H. Beekman. “Oaks, tree-rings and wooden cultural heritage: a review of the main characteristics and applications of oak dendrochronology in Europe”. *Journal of Archaeological Science* 36.1 (2009), pp. 1–11 (cit. on p. 42).
- [91] L. Helfen, A. Myagotin, P. Mikulk, P. Pernot, A. Voropaev, M. Elyyan, M. D. Michiel, J. Baruchel, and T. Baumbach. “On the implementation of computed laminography using synchrotron radiation”. *Review of Scientific Instruments* 82 (2011), p. 063702 (cit. on p. 43).
- [92] L. Helfen, T. F. Morgeneyer, F. Xu, M. N. Mavrogordato, I. Sinclair, B. Schillinger, and T. Baumbach. “Synchrotron and neutron laminography for three-dimensional imaging of devices and flat material specimens”. 103 (2012), pp. 170–173 (cit. on p. 43).
- [93] K. Hiller. “Krummer Zink, gerade Stäbchen”. *Restauro* 8 (2018), pp. 34–38 (cit. on pp. 33, 36).
- [94] Y. Hou, M. Canul-Ku, X. Cui, and M. Zhu. “Super-resolution reconstruction of vertebrate microfossil computed tomography images based on deep learning”. *X-Ray Spectrometry* (2023), xrs.3389 (cit. on p. 59).
- [95] J. Hsieh. *Computed Tomography: Principles, Design, Artifacts, and Recent Advances*. SPIE PRESS, 2015 (cit. on pp. 5, 6, 24, 26).
- [96] J. Hwang, H. Kim, T. Lee, D.-i. Choi, T. Kwon, and S. Cho. “Geometry calibration for a dental cone-beam CT system with an offset detector”. *Precision Engineering* 79 (2023), pp. 264–276 (cit. on p. 69).
- [97] *Industrial 3D Scanner, Space Spider*. URL: <https://www.artec3d.com/portable-3d-scanners/artec-spider> (visited on Nov. 9, 2023) (cit. on p. 86).
- [98] P. P. Jaju, M. Jain, A. Singh, and A. Gupta. “Artefacts in cone beam CT”. *Open Journal of Stomatology* 03.05 (2013), pp. 292–297 (cit. on p. 26).

- [99] Y. S. N. Jayaratne, C. P. J. McGrath, and R. A. Zwahlen. “How Accurate Are the Fusion of Cone-Beam CT and 3-D Stereophotographic Images?” *PLOS ONE* 7.11 (2012). Publisher: Public Library of Science, e49585 (cit. on p. 79).
- [100] C. Johnson, E. Hendriks, I. Berezhnoy, E. Brevdo, S. Hughes, I. Daubechies, J. Li, E. Postma, and J. Wang. “Image processing for artist identification”. *IEEE Signal Processing Magazine* 25.4 (2008), pp. 37–48 (cit. on pp. 23, 41).
- [101] W. R. Johnston and S. Kelly. *Untamed. The Art of Antoine-Louis Barye*. Exhibition Catalogue. Baltimore: The Walters Art Museum, 2006 (cit. on p. 65).
- [102] G. van Kaick and S. Delorme. “Computed tomography in various fields outside medicine”. *European Radiology Supplements* 15.S4 (2005), pp. d74–d81 (cit. on pp. 5, 23, 59).
- [103] W. A. Kalender. “CT: the unexpected evolution of an imaging modality”. *European Radiology Supplements* 15.S4 (2005), pp. d21–d24 (cit. on pp. 24, 59).
- [104] F. Kharfi. “Mathematics and Physics of Computed Tomography (CT): Demonstrations and Practical Examples”. In: *Imaging and Radioanalytical Techniques in Interdisciplinary Research - Fundamentals and Cutting Edge Applications*. IntechOpen, 2013 (cit. on p. 126).
- [105] A. Kingston, A. Sakellariou, T. Varslot, G. Myers, and A. Sheppard. “Reliable automatic alignment of tomographic projection data by passive auto-focus”. *Medical Physics* 38.9 (2011), pp. 4934–4945 (cit. on p. 69).
- [106] M. Kiss, F. G. Bossema, P. J. Van Laar, S. Meijer, F. Lucka, T. Van Leeuwen, and K. J. Batenburg. “Beam filtration for object-tailored X-ray CT of multi-material cultural heritage objects”. *Heritage Science* 11, 130 (2023) (cit. on pp. 7, 8, 16, 60, 88, 100, 149).
- [107] N. Klop. *ICP (iterative closest point) registration / alignment - Blender Market*. URL: <https://blendermarket.com/products/icp-iterative-closest-point-registration-addon> (visited on Nov. 9, 2023) (cit. on p. 83).
- [108] A. Kostenko, W. Palenstijn, S. Coban, A. Hendriksen, R. van Liere, and K. Batenburg. “Prototyping X-ray tomographic reconstruction pipelines with FleXbox”. *SoftwareX* 11 (2020), p. 100364 (cit. on pp. 10, 28, 47, 65, 70, 128).
- [109] A. Kostenko, V. Andriiashen, and K. J. Batenburg. “Registration-based multi-orientation tomography”. *Optics Express* 26.22 (2018), p. 28982 (cit. on p. 28).
- [110] J. Lang and A. Middleton. *Radiography of Cultural Material*. Publication Title: Radiography of Cultural Material. Elsevier Butterworth-Heinemann, 2005 (cit. on pp. 23, 41).
- [111] A. Larsson. *Cybis CooRecorder - Image Coordinate Recording program & CDendro - Cybis dendro dating program*. 2017. URL: [www.cybis.se](http://www.cybis.se) (visited on Nov. 9, 2023) (cit. on p. 47).

- [112] S. Legrand, F. Vanmeert, G. Van der Snickt, M. Alfeld, W. De Nolf, J. Dik, and K. Janssens. “Examination of historical paintings by state-of-the-art hyperspectral imaging methods: from scanning infra-red spectroscopy to computed X-ray laminography”. *Heritage Science* 2.1 (2014) (cit. on pp. 23, 41, 43).
- [113] S. Longo, E. Mormina, F. Granata, D. Mallamace, M. Longo, and S. Capuani. “Investigation of an Egyptian Mummy board by Using Clinical Multi-slice Computed Tomography”. *Studies in Conservation* 63.7 (2018), pp. 383–390 (cit. on pp. 23, 24, 59).
- [114] M. Lüthi, B. A. Bircher, F. Meli, A. Küng, and R. Thalmann. “X-ray flat-panel detector geometry correction to improve dimensional computed tomography measurements”. *Measurement Science and Technology* 31.3 (2019). Publisher: IOP Publishing, p. 035002 (cit. on p. 69).
- [115] B. Masschaele, M. Dierick, D. V. Loo, M. N. Boone, L. Brabant, E. Pauwels, V. Cnudde, and L. V. Hoorebeke. “HECTOR: A 240kV micro-CT setup optimized for research”. In: *Journal of Physics: Conference Series*. Vol. 463. ISSN: 17426596 Issue: 1. 2013 (cit. on p. 27).
- [116] A. Masson-Berghoff and D. O’Flynn. “Absent, invisible or revealed ‘relics’? X-radiography and CT scanning of Egyptian bronze votive boxes from Naukratis and elsewhere”. *British Museum Studies in Ancient Egypt and Sudan* 24 (2019), pp. 159–174 (cit. on p. 26).
- [117] Maxon. *ZBrush*. URL: <https://www.maxon.net/en/zbrush> (visited on Nov. 9, 2023) (cit. on p. 78).
- [118] *Metropolitan-museum-of-art 3D models*. URL: <https://sketchfab.com/tags/metropolitan-museum-of-art> (visited on Nov. 9, 2023) (cit. on p. 78).
- [119] S. Mizuno, R. Torizu, and J. Sugiyama. “Wood identification of a wooden mask using synchrotron X-ray microtomography”. *Journal of Archaeological Science* 37.11 (2010), pp. 2842–2845 (cit. on pp. 24, 60).
- [120] V. Mocella, E. Brun, C. Ferrero, and D. Delattre. “Revealing letters in rolled Herculaneum papyri by X-ray phase-contrast imaging”. *Nature Communications* 6.1 (2015), p. 5895 (cit. on p. 23).
- [121] L. Montaina, S. Longo, G. Galotta, G. Tranquilli, R. Saccuman, and S. Capuani. “Assessment of the Panel Support of a Seventeenth-Century Dutch Painting by Clinical Multislice Computed Tomography”. *Studies in Conservation* 66.3 (2021), pp. 174–181 (cit. on pp. 24, 42, 60).
- [122] M. Mori, S. Kuhara, K. Kobayashi, S. Suzuki, M. Yamada, and A. Senoo. “Non-destructive tree-ring measurements using a clinical 3T-MRI for archaeology”. *Dendrochronologia* (2019) (cit. on p. 42).
- [123] M. P. Morigi, F. Casali, M. Bettuzzi, R. Brancaccio, and V. D’Errico. “Application of X-ray Computed Tomography to Cultural Heritage diagnostics”. *Applied Physics A* 100.3 (2010), pp. 653–661 (cit. on pp. 23, 24, 41, 59).

- [124] M. P. Morigi, F. Casali, A. Berdondini, M. Bettuzzi, D. Bianconi, R. Brancaccio, A. Castellani, V. D’Errico, A. Pasini, A. Rossi, C. Labanti, and N. Scianna. “X-ray 3D computed tomography of large objects: investigation of an ancient globe created by Vincenzo Coronelli”. In: *O3A: Optics for Arts, Architecture, and Archaeology*. ISSN: 0277786X. 2007 (cit. on p. 60).
- [125] M. Morigi, F. Casali, M. Bettuzzi, D. Bianconi, R. Brancaccio, S. Cornacchia, A. Pasini, A. Rossi, A. Aldrovandi, and D. Cauzzi. “CT investigation of two paintings on wood tables by Gentile da Fabriano”. *Nuclear Instruments and Methods in Physics Research Section A: Accelerators, Spectrometers, Detectors and Associated Equipment* 580.1 (2007), pp. 735–738 (cit. on p. 23).
- [126] H. A. Museums. *Prince Shōtoku: The Secrets Within*. URL: <https://harvardartsmuseums.org/tour/prince-shotoku-the-secrets-within/slide/10799> (visited on Nov. 9, 2023) (cit. on pp. 23, 78).
- [127] K. Müller, M. Berger, J.-H. Choi, S. Datta, S. Gehrisch, T. Moore, M. P. Marks, A. K. Maier, and R. F. Müller. “Fully Automatic Head Motion Correction for Interventional C-arm Systems using Fiducial Markers”. *Proceedings of the 13th Fully Three-Dimensional Image Reconstruction in Radiology and Nuclear Medicine* (2015), pp. 1–4 (cit. on p. 69).
- [128] V. Nguyen, J. De Beenhouwer, J. G. Sanctorum, S. Van Wassenbergh, S. Bazrafkan, J. J. J. Dirckx, and J. Sijbers. “A low-cost geometry calibration procedure for a modular cone-beam X-ray CT system”. *Nondestructive Testing and Evaluation* 35.3 (2020), pp. 252–265 (cit. on p. 69).
- [129] P. Niemz and D. Mannes. “Non-destructive testing of wood and wood-based materials”. *Journal of Cultural Heritage* 13.3 (2012), S26–S34 (cit. on pp. 23, 24).
- [130] L. N.M. Tissen. “3D Printing and the Art World: Current Developments and Future Perspectives”. In: *Advances in 3D Printing*. Ed. by A. Sharma. IntechOpen, 2023 (cit. on p. 101).
- [131] *Numpy*. URL: <https://numpy.org/> (visited on Nov. 9, 2023) (cit. on p. 127).
- [132] D. Nykonenko, O. Yatsuk, L. Guidorzi, A. Lo Giudice, F. Tansella, L. P. Cesareo, G. Sorrentino, P. Davit, M. Gulmini, and A. Re. “Glass beads from a Scythian grave on the island of Khortytsia (Zaporizhzhia, Ukraine): insights into bead making through 3D imaging”. *Heritage Science* 11.1 (2023), p. 238 (cit. on p. 13).
- [133] N. S. O’Brien, R. P. Boardman, I. Sinclair, and T. Blumensath. “Recent advances in X-ray cone-beam computed laminography”. *Journal of X-Ray Science and Technology* 24 (2016), pp. 691–707 (cit. on p. 43).
- [134] T. Okochi. “A nondestructive dendrochronological study on japanese wooden shinto art sculptures using micro-focus X-ray Computed Tomography (CT): Reviewing two methods for scanning objects of different sizes”. *Dendrochronologia* 38 (2016), pp. 1–10 (cit. on pp. 13, 42).

- [135] T. Okochi, Y. Hoshino, H. Fujii, and T. Mitsutani. “Nondestructive tree-ring measurements for Japanese oak and Japanese beech using micro-focus X-ray computed tomography”. *Dendrochronologia* 24.2-3 (2007), pp. 155–164 (cit. on pp. 12, 42).
- [136] R. Oliveira, A. de Paula, F. Gonçalves, R. Bueno, T. Calgam, S. Azeredo, O. Araújo, A. Machado, M. Anjos, R. Lopes, and D. Oliveira. “Development and characterization of a portable CT system for wooden sculptures analysis”. *Radiation Physics and Chemistry* (2022), p. 110409 (cit. on p. 60).
- [137] J. Padfield, D. Saunders, J. Cupitt, and R. Atkinson. “Improvements in the Acquisition and Processing of X-Ray Images of Paintings”. *National Gallery Technical Bulletin* 23 (2002), pp. 62–75 (cit. on p. 23).
- [138] K. Pande, J. J. Donatelli, D. Y. Parkinson, H. Yan, and J. A. Sethian. “Joint iterative reconstruction and 3D rigid alignment for X-ray tomography”. *Optics Express* 30.6 (2022), p. 8898 (cit. on p. 69).
- [139] D. Panetta, N. Belcari, A. D. Guerra, and S. Moehrs. “An optimization-based method for geometrical calibration in cone-beam CT without dedicated phantoms”. *Physics in Medicine & Biology* 53.14 (2008), p. 3841 (cit. on p. 69).
- [140] C. Parisi, C. Pelosi, U. Santamaria, P. Pogliani, G. Agresti, and S. Longo. “The conservation project of a liturgical object: The case of infant Jesus of Prague in the church of Saint Mary of providence at Macchia Giarre (Italy)”. *European Journal of Science and Theology* (2016) (cit. on pp. 13, 24).
- [141] E. M. Payne. “Imaging Techniques in Conservation”. *Journal of Conservation and Museum Studies* 10.2 (2013), pp. 17–29 (cit. on p. 23).
- [142] E. Pekel, F. Schaff, M. Dierolf, F. Pfeiffer, and T. Lasser. “X-ray computed tomography with seven degree of freedom robotic sample holder”. *Engineering Research Express* 4.3 (2022), p. 035022 (cit. on p. 69).
- [143] E. Petrella, S. Piciucchi, F. Feletti, D. Barone, A. Piraccini, C. Minghetti, G. Gruppioni, V. Poletti, M. Bertocco, and M. Traversari. “CT Scan of Thirteen Natural Mummies Dating Back to the XVI-XVIII Centuries: An Emerging Tool to Investigate Living Conditions and Diseases in History”. *PLOS ONE* 11.6 (2016). Ed. by J. Tuukkanen, e0154349 (cit. on pp. 24, 60).
- [144] M. Pieraccini, G. Guidi, and C. Atzeni. “3D digitizing of cultural heritage”. *Journal of Cultural Heritage* 2 (2001), pp. 63–70 (cit. on p. 77).
- [145] J. R. Pilcher. “Sample preparation, cross-dating and measurement”. In: *Methods of Dendrochronology: Applications in the Environmental Sciences*. Springer Science & Business Media, 1990, pp. 40–51 (cit. on p. 42).
- [146] R. Pintus, K. Pal, Y. Yang, T. Weyrich, E. Gobbetti, and H. Rushmeier. “A Survey of Geometric Analysis in Cultural Heritage: Geometric Analysis in Cultural Heritage”. *Computer Graphics Forum* 35.1 (2016), pp. 4–31 (cit. on pp. 23, 41).

- [147] S. T. Porter, N. Huber, C. Hoyer, and H. Floss. "Portable and low-cost solutions to the imaging of Paleolithic art objects: A comparison of photogrammetry and reflectance transformation imaging". *Journal of Archaeological Science: Reports* 10 (2016), pp. 859–863 (cit. on p. 77).
- [148] B. Raj, S. Ranganathan, and B. Venkatraman. "Non-Destructive Testing of Art Objects". In: *Reference Module in Materials Science and Materials Engineering*. Elsevier, 2017, B9780128035818022347 (cit. on p. 41).
- [149] A. Re, F. Albertin, C. Avataneo, R. Brancaccio, J. Corsi, G. Cotto, S. De Blasi, G. Dughera, E. Durisi, W. Ferrarese, A. Giovagnoli, N. Grassi, A. Lo Giudice, P. Mereu, G. Mila, M. Nervo, N. Pastrone, F. Prino, L. Ramello, M. Ravera, C. Ricci, A. Romero, R. Sacchi, A. Staiano, L. Visca, and L. Zamprota. "X-ray tomography of large wooden artworks: the case study of "Doppio corpo" by Pietro Piffetti". *Heritage Science* 2.1 (2014), p. 19 (cit. on pp. 13, 23, 42).
- [150] A. Re, A. L. Giudice, M. Nervo, P. Buscaglia, P. Luciani, M. Borla, and C. Greco. "The importance of tomography studying wooden artefacts: A comparison with radiography in the case of a coffin lid from ancient Egypt". *International Journal of Conservation Science* 7.S12 (2016), pp. 935–944 (cit. on pp. 13, 23, 41, 42).
- [151] C. Richmond. "Sir Godfrey Hounsfield". *BMJ* 329.7467 (2004), p. 687.1 (cit. on pp. 5, 23, 24).
- [152] Rigsters. *Multispectral Photogrammetry*. URL: <https://rigsters.com/portfolio/multispectral-photogrammetry/> (visited on Nov. 9, 2023) (cit. on p. 95).
- [153] Rijksmuseum. *Beurs van groen fluweel met trekkoord en afgezet met gouddraad op een doosje in de vorm van een schaar (fallus?) van dito fluweel en passement, voorzien van twee metalen ogen, anonymous, after 1580*. URL: <https://www.rijksmuseum.nl/en/collection/BK-KOG-29> (visited on Nov. 9, 2023) (cit. on p. 14).
- [154] Rijksmuseum. *Book chest of Hugo de Groot, anonymous, c. 1600 - c. 1615*. URL: <https://www.rijksmuseum.nl/nl/collectie/NG-KOG-1208> (visited on Nov. 9, 2023) (cit. on pp. 14, 19, 52).
- [155] Rijksmuseum. *Bottle in the form of a shoe*. URL: <https://www.rijksmuseum.nl/en/collection/BK-KOG-1382> (visited on Nov. 9, 2023) (cit. on pp. 14, 90).
- [156] Rijksmuseum. *Cadmus, Guided by Minerva, Observes the Spartoi Fighting, Peter Paul Rubens (after), before 1747*. URL: <https://www.rijksmuseum.nl/en/collection/SK-A-4051> (visited on Nov. 9, 2023) (cit. on p. 14).
- [157] Rijksmuseum. *Cornett, anonymous, c. 1600 - c. 1650 - Rijksmuseum*. URL: <https://www.rijksmuseum.nl/en/collection/BK-AM-62-B> (visited on Nov. 9, 2023) (cit. on pp. 13, 14, 33, 36).

- [158] Rijksmuseum. *Langwerpig, taps toelopend foedraal met dop*. URL: <https://www.rijksmuseum.nl/nl/collectie/BK-NM-3086> (visited on Nov. 9, 2023) (cit. on pp. 8, 14, 16, 88).
- [159] Rijksmuseum. *Woman with Lantern (Midwife or Persian Sibyl), from a Nativity or Adoration of the Sheperds, anonymous, c. 1500 - c. 1515 - Rijksmuseum*. URL: <https://www.rijksmuseum.nl/en/collection/BK-NM-9253> (visited on Nov. 9, 2023) (cit. on pp. 2, 5, 14, 30, 31).
- [160] C. T. Rueden, J. Schindelin, M. C. Hiner, B. E. DeZonia, A. E. Walter, E. T. Arena, and K. W. Eliceiri. “ImageJ2: ImageJ for the next generation of scientific image data”. *BMC Bioinformatics* 18.1 (2017), p. 529 (cit. on p. 28).
- [161] L. Sabbatini and I. D. v. d. Werf. *Chemical Analysis in Cultural Heritage*. De Gruyter, 2020 (cit. on p. 41).
- [162] Z. Sabetsarvestani, B. Sober, C. Higgitt, I. Daubechies, and M. R. D. Rodrigues. “Artificial intelligence for art investigation: Meeting the challenge of separating x-ray images of the *Ghent Altarpiece*”. *Science Advances* 5.8 (2019), eaaw7416 (cit. on p. 23).
- [163] A. Sallam, S. Hemedi, M. S. Toprak, M. Muhammed, M. Hassan, and A. Uheida. “CT Scanning and MATLAB Calculations for Preservation of Coptic Mural Paintings in Historic Egyptian Monasteries”. *Scientific Reports* 9.1 (2019), p. 3903 (cit. on p. 23).
- [164] U. Sass and D. Eckstein. “Preparation of large thin sections and surfaces of wood for automatic image analysis”. *Holzforschung* 48 (1994), pp. 117–118 (cit. on p. 47).
- [165] J. Schat, F. Bossema, M. E. Numans, I. Smeets, and P. Burger. “Overdreven gezondheidsnieuws: Relatie tussen overdrijving in academische persberichten en in nieuwsmedia”. *Nederlands Tijdschrift voor Geneeskunde* (2018) (cit. on p. 150).
- [166] J. Schindelin, I. Arganda-Carreras, E. Frise, V. Kaynig, M. Longair, T. Pietzsch, S. Preibisch, C. Rueden, S. Saalfeld, B. Schmid, J.-Y. Tinevez, D. J. White, V. Hartenstein, K. Eliceiri, P. Tomancak, and A. Cardona. “Fiji: an open-source platform for biological-image analysis”. *Nature Methods* 9.7 (2012), pp. 676–682 (cit. on pp. 11, 79).
- [167] D. Schorsch, L. Becker, and F. Caro. “Enlightened technology: Casting divinity in the Gupta age”. *Arts of Asia* 49.2 (2019), pp. 131–143 (cit. on p. 24).
- [168] R. Schulze, U. Heil, D. Groß, D. Bruellmann, E. Dranischnikow, U. Schwanecke, and E. Schoemer. “Artefacts in CBCT: a review”. *Dentomaxillofacial Radiology* 40.5 (2011), pp. 265–273 (cit. on pp. 26, 128).
- [169] F. Schweingruber. *Anatomie Europäischer Hölzer. - Anatomy of European Woods*. Haupt, 1990 (cit. on p. 63).
- [170] *SCIEM. PAST4 – Personal Analysis System for Treering research*. 2009. URL: [www.sciem.com](http://www.sciem.com) (visited on May 2, 2021) (cit. on p. 47).

- [171] *Scikit Image - Canny Edge detector*. URL: [https://scikit-image.org/docs/stable/auto\\_examples/edges/plot\\_canny.html](https://scikit-image.org/docs/stable/auto_examples/edges/plot_canny.html) (visited on Nov. 9, 2023) (cit. on p. 126).
- [172] *Scikit Image - Hough\_circle*. URL: [https://scikit-image.org/docs/stable/api/skimimage.transform.html#skimimage.transform.hough\\_circle](https://scikit-image.org/docs/stable/api/skimimage.transform.html#skimimage.transform.hough_circle) (visited on Nov. 9, 2023) (cit. on p. 126).
- [173] *Scikit Image - Inpainting*. URL: [https://scikit-image.org/docs/stable/auto\\_examples/filters/plot\\_inpaint.html](https://scikit-image.org/docs/stable/auto_examples/filters/plot_inpaint.html) (visited on Nov. 9, 2023) (cit. on p. 128).
- [174] *Scipy Optimize - Least\_squares*. URL: [https://docs.scipy.org/doc/scipy/reference/generated/scipy.optimize.least\\_squares.html](https://docs.scipy.org/doc/scipy/reference/generated/scipy.optimize.least_squares.html) (visited on Nov. 9, 2023) (cit. on p. 127).
- [175] M. M. Seger and P. E. Danielsson. “Scanning of logs with linear cone-beam tomography”. *Computers and Electronics in Agriculture* 41 (2003), pp. 45–62 (cit. on p. 43).
- [176] E. Y. Sidky, Y. Zou, and X. Pan. “Volume image reconstruction from a straight-line source trajectory”. *IEEE Nuclear Science Symposium Conference Record* 5 (2005), pp. 2441–2444 (cit. on p. 43).
- [177] A. T. d. Silva, S. Legrand, G. v. d. Snickt, R. Featherstone, K. Janssens, and G. Bottinelli. “MA-XRF imaging on René Magritte’s La condition humaine: Insights into the artist’s palette and technique and the discovery of a third quarter of La pose enchantée”. *Heritage Science* 5.1 (2017) (cit. on p. 23).
- [178] S. A. Sirr and J. R. Waddle. “Use of CT in Detection of Internal Damage and Repair and Determination of Authenticity in High-Quality Bowed Stringed Instruments”. *RadioGraphics* 19.3 (1999), pp. 639–646 (cit. on pp. 13, 24, 42).
- [179] *Sketchfab - The best 3D viewer on the web*. URL: <https://sketchfab.com> (visited on Nov. 9, 2023) (cit. on p. 78).
- [180] N. Sodini, D. Dreossi, A. Giordano, J. Kaiser, F. Zanini, and T. Zikmund. “Comparison of different experimental approaches in the tomographic analysis of ancient violins”. *Journal of Cultural Heritage* 27 (2017), S88–S92 (cit. on pp. 24, 42, 59).
- [181] J. Stelzner, F. Gauß, and P. Schuetz. “X-ray computed tomography for non-destructive analysis of early Medieval swords”. *Studies in Conservation* 61.2 (2016), pp. 86–101 (cit. on pp. 24, 26).
- [182] J. Stelzner and S. Million. “X-ray Computed Tomography for the anatomical and dendrochronological analysis of archaeological wood”. *Journal of Archaeological Science* 55 (2015), pp. 188–196 (cit. on pp. 12, 24, 42).
- [183] J. H. Stoner and R. Rushfield. *The Conservation of Easel Paintings*. Routledge: London and New York, 2012 (cit. on p. 41).
- [184] H. Strudwick and J. Dawson, eds. *Ancient Egyptian Coffins*. Oxbow Books, 2019 (cit. on p. 41).

- [185] P. Targowski, B. Rouba, M. Wojtkowski, and A. Kowalczyk. “The application of optical coherence tomography to non-destructive examination of museum objects”. *Studies in Conservation* 49.2 (2004) (cit. on p. 23).
- [186] M. Tesaxrová, E. Heude, G. Comai, T. Zikmund, M. Kaucká, I. Adameyko, S. Tajbakhsh, and J. Kaiser. “An interactive and intuitive visualisation method for X-ray computed tomography data of biological samples in 3D Portable Document Format”. *Scientific Reports* 9.1 (2019), p. 14896 (cit. on p. 95).
- [187] The British Museum. *mosaic; figure; vessel*. URL: [https://www.britishmuseum.org/collection/object/E\\_Am-165](https://www.britishmuseum.org/collection/object/E_Am-165) (visited on Nov. 9, 2023) (cit. on pp. 14, 87).
- [188] The British Museum. *mummy-mask*. URL: [https://www.britishmuseum.org/collection/object/Y\\_EA29472](https://www.britishmuseum.org/collection/object/Y_EA29472) (visited on Nov. 9, 2023) (cit. on pp. 14, 92).
- [189] *The British Museum (@britishmuseum)*. URL: <https://sketchfab.com/britishmuseum> (visited on Nov. 9, 2023) (cit. on p. 78).
- [190] The J. Paul Getty Museum. *Python Killing a Gnu, Antoine-Louis Barye*. URL: <https://www.getty.edu/art/collection/object/103RQ1> (visited on Nov. 9, 2023) (cit. on pp. 14, 20).
- [191] *The See-through Museum*. URL: <https://www.nwo.nl/projecten/341-60-001-0> (visited on Nov. 9, 2023) (cit. on p. 25).
- [192] Thermofisher. *Avizo Software | Materials Characterization Software - NL*. URL: <https://www.thermofisher.com/uk/en/home/electron-microscopy/products/software-em-3d-vis/avizo-software.html> (visited on Nov. 9, 2023) (cit. on pp. 11, 79).
- [193] J. Thornton, N. Umney, G. Landrey, M. Baumber, and S. May. “Other materials and structures”. In: *Conserv. Furnit.* 2007, pp. 194–237 (cit. on p. 26).
- [194] *Trackpy*. URL: <http://soft-matter.github.io/trackpy/v0.3.0/index.html> (visited on Nov. 9, 2023) (cit. on p. 126).
- [195] C. Tuniz, F. Bernardini, I. Turk, L. Dimkaroski, L. Mancini, and D. Dreossi. “Did neanderthals play music? X-ray computed micro-tomography of the divje babe ’flute’”. *Archaeometry* 54.3 (2012), pp. 581–590 (cit. on p. 24).
- [196] M. Vandenbeusch, D. O’Flynn, and B. Moreno. “Layer by Layer: The Manufacture of Graeco-Roman Funerary Masks”. *The Journal of Egyptian Archaeology* 107.1-2 (2021), pp. 281–298 (cit. on pp. 59, 60, 78, 79).
- [197] A. Vandivere, A. van Loon, K. A. Dooley, R. Haswell, R. G. Erdmann, E. Leonhardt, and J. K. Delaney. “Revealing the painterly technique beneath the surface of Vermeer’s *Girl with a Pearl Earring* using macro- and microscale imaging”. *Heritage Science* 7.1 (2019), p. 64 (cit. on pp. 23, 41).

- [198] A. Vannoppen, S. Maes, V. Kint, T. De Mil, Q. Ponette, J. Van Acker, J. Van den Bulcke, K. Verheyen, and B. Muys. “Using X-ray CT based tree-ring width data for tree growth trend analysis”. *Dendrochronologia* 44 (2017), pp. 66–75 (cit. on p. 24).
- [199] D. Vavrik, V. Antuskova, S. Chlumska, I. Kumpova, R. Sefcu, and M. Vopalensky. “Non-destructive exploration of late Gothic panel painting using X-ray tomography and flattening of the reconstructed data”. *The European Physical Journal Plus* 138.7 (2023), p. 618 (cit. on p. 60).
- [200] C. Villa, M. J. Flies, and C. Jacobsen. “Forensic 3D documentation of bodies: Simple and fast procedure for combining CT scanning with external photogrammetry data”. *Journal of Forensic Radiology and Imaging* 12 (2018), e2–e7 (cit. on p. 79).
- [201] Volume Graphics. *VGSTUDIO*. URL: <https://www.volumegraphics.com/en/products/vgstudio.html> (visited on Nov. 9, 2023) (cit. on pp. 11, 79).
- [202] R. Wagner, T. Fuchs, G. Scholz, C. Kretzer, R. Schielein, M. Firsching, S. Kirsch, M. Wolters, M. Raquet, and F. P. Bär. “Dual-energy computed tomography of historical musical instruments made of multiple materials.” In: *8th Conference on Industrial Computed Tomography*. 2018 (cit. on p. 42).
- [203] P. Xin, H. Yu, H. Cheng, S. Shen, and S. G. F. Shen. “Image Fusion in Craniofacial Virtual Reality Modeling Based on CT and 3dMD Photogrammetry”. *Journal of Craniofacial Surgery* 24.5 (2013), p. 1573 (cit. on p. 79).
- [204] K. Yang, A. L. C. Kwan, D. F. Miller, and J. M. Boone. “A geometric calibration method for cone beam CT systems: A geometric calibration method for cone beam CT”. *Medical Physics* 33.6Part1 (2006), pp. 1695–1706 (cit. on p. 69).
- [205] Y. Yang, L. Li, and Z.-Q. Chen. “A review of geometric calibration for different 3-D X-ray imaging systems”. *Nuclear Science and Techniques* 27.3 (2016), p. 76 (cit. on p. 69).
- [206] R. Yin, B. Cornelis, G. Fodor, N. Ocon, D. Dunson, and I. Daubechies. “Removing Cradle Artifacts in X-Ray Images of Paintings”. *SIAM Journal on Imaging Sciences* 9.3 (2016), pp. 1247–1272 (cit. on p. 23).
- [207] F. Zhang, J. Du, H. Jiang, L. Li, M. Guan, and B. Yan. “Iterative geometric calibration in circular cone-beam computed tomography”. *Optik* 125.11 (2014), pp. 2509–2514 (cit. on pp. 69, 83).
- [208] T. Zhang, Y. Xing, L. Zhang, X. Jin, H. Gao, and Z. Chen. “Stationary computed tomography with source and detector in linear symmetric geometry: Direct filtered backprojection reconstruction”. *Medical Physics* 47.5 (2020), pp. 2222–2236 (cit. on p. 43).
- [209] X. Zhang, J. Blaas, C. Botha, P. Reischig, A. Bravin, and J. Dik. “Process for the 3D virtual reconstruction of a microcultural heritage artifact obtained by synchrotron radiation CT technology using open source and free software”. *Journal of Cultural Heritage* 13.2 (2012), pp. 221–225 (cit. on p. 23).

- [210] J. Zhou, M. Maisl, H. Reiter, and W. Arnold. “Computed laminography for materials testing”. *Applied Physics Letters* 68.24 (1996), pp. 3500–3502 (cit. on p. 43).

# A

## Appendix A:

### Supplementary information

This appendix contains the supplementary information to chapter 4. In this appendix we extend upon the methods and implementation.

#### A.1 Supplementary methods

##### A.1.1 Model and optimisation

In this section we discuss the theory and model that underlies the implementation of our marker-based system parameter derivation. In less sophisticated X-ray imaging equipment, these parameters are often not available. By including small metal balls in the acquisition, we retrieve these parameters based on the radiographs. Each marker is visible as a circle on all (or most) projections, and we call its location the projected marker location (PML). For each marker we measure the PML on the X-ray images. Given a set of system parameters and marker positions, and for each marker at each rotation angle, we can draw a line from the source through the marker. The intersection of this line with the detector plane gives a predicted PML. The goal is to minimise the distance between the predicted PMLs and the measured PMLs. This will provide an estimated value for the system parameters, which we need for 3D reconstruction as described in section 4.3.

We aim to find parameters that can be used to produce a 3D reconstruction of the object. Our method does not aim to find the absolute physical distances. The only impact of this on the 3D reconstruction is the scale, which can if needed be obtained by including an object of known size in the scan or by measuring one distance on the object afterwards and scaling the reconstruction accordingly. In the next sections, we will first discuss the model used for the forward projection of marker positions and then the optimisation that is used for estimating the system parameters.

---

This is the appendix to chapter 4 and is published as Supplementary Information to F. G. Bossema, W. J. Palenstijn, A. Heginbotham, M. Corona, T. Van Leeuwen, R. Van Liere, J. Dorscheid, D. O’Flynn, J. Dyer, E. Hermens, and K. J. Batenburg. “Enabling 3D CT-scanning of cultural heritage objects using only in-house 2D X-ray equipment in museums”. *Nature Communications* (accepted, in press).

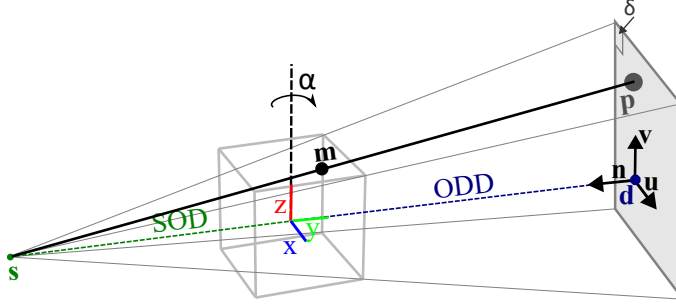


Figure A.1: Schematic indicating the variables and notation used in the forward model.

### The forward model

We assume that the setup consists of a cone-beam X-ray source, flat-panel detector and a rotation stage. A block of foam containing markers is mounted on the rotation stage next to the object. We assume that the components are stably mounted and do not drift during acquisition. For our calculations, we model the system as the source and detector rotating around the object, which is mathematically equivalent to a rotating object between a static source and detector.

We define a left handed coordinate system with the rotation axis being the  $z$ -axis. The  $y$ -axis is defined such that the source lies on it for the first projection. The first projection is defined as rotation angle  $0^\circ$ . The coordinate system and variables used to describe all the system components are shown in figure A.1.

A boldface small letter represents a vector with an  $x, y$  and  $z$  component, e.g.  $\mathbf{s} = (s_x, s_y, s_z)$ , which represents the location of the source. The detector plane is defined by a point  $\mathbf{d}$ , which is the center of the detector plane, the detector pixel size and the unit vectors  $\mathbf{u}$  and  $\mathbf{v}$  that span the detector plane. The normal vector to the detector plane is  $\mathbf{n} = \mathbf{v} \times \mathbf{u}$ . The out-of-plane rotations of the detector are given by angles  $\theta$  (around axis  $\mathbf{u}$ ) and  $\phi$  (around axis  $\mathbf{v}$ ). The parameter  $\eta$  defines the in-plane detector rotation (rotation around  $\mathbf{n}$ ). With a subscript  $i$ , e.g.  $\mathbf{s}_i$ , we denote the vector that is obtained when rotating the original vector around the  $z$ -axis by angle  $-\alpha_i$ . The marker position of marker  $j$  is denoted by  $\mathbf{m}_j = (m_{jx}, m_{jy}, m_{jz})$  for  $j \in \{1, \dots, N\}$ .

A line from the source through marker  $j$  for projection  $i$  is given as  $\mathbf{f}(t) = \mathbf{s}_i + t(\mathbf{m}_j - \mathbf{s}_i)$ . The vector defining the projected 3D location in space of the PML corresponding to marker  $j$  on projection  $i$ , is given by the intersection of this line with the detector plane defined by  $\mathbf{d}_i$  and  $\mathbf{n}_i$ :  $\mathbf{g} = \mathbf{s}_i + \frac{\mathbf{n}_i \cdot (\mathbf{d}_i - \mathbf{s}_i)}{\mathbf{n}_i \cdot (\mathbf{m}_j - \mathbf{s}_i)} (\mathbf{m}_j - \mathbf{s}_i)$ . This 3D location can be rewritten to the detector pixel on which the marker would fall. In other words, we obtain the PML  $\mathbf{p}_{i,j}^{pred}(\Theta, \mathbf{m}_j) = (a, b)$  (row, column) such that  $\mathbf{d}_i + a\mathbf{u}_i + b\mathbf{v}_i = \mathbf{g}$ .

Parameter	Notation
detector position	$\mathbf{d}$
detector tilt	$\theta, \phi$
detector in-plane rotation	$\eta$
projection angles	$\alpha_1, \dots, \alpha_{n-1}$
marker positions	$\mathbf{m}_1, \dots, \mathbf{m}_N$

**Table A.1:** Notation of the free system parameters and marker positions  $\mathbf{m}$  that are estimated in the optimisation scheme.

Parameter	Notation and fixed value
source position	$\mathbf{s}_0 = (0, SOD, 0)$
first projection angle	$\alpha_0 = 0$
detector pixel size	$\delta =$ detector pixel size

**Table A.2:** Fixed system parameters. The source to object distance (SOD) and detector pixel size are user input.

### The cost function

The measured PML  $\mathbf{p}_{ij}^{meas}$  of marker  $j$  on projection image  $i$ , is defined relative to  $\mathbf{d}_i$  and is given by  $(c, d)$  (row, column).

The set of free parameters, which we for convenience denote by  $\Theta$ , define the forward projections. The free parameters are given in Supplementary table A.1 and the fixed parameters in Supplementary table A.2. The source is fixed to the negative  $y$ -axis. We fix the detector pixel size, since this is often specified in the documentation of the manufacturer. We want to minimise the distance between the predicted PML  $\mathbf{p}_{ij}^{pred}(\Theta, \mathbf{m}_j)$  and the measured PML  $\mathbf{p}_{ij}^{meas}$  of marker  $j$  on projection image  $i$ . We therefore want to find the parameters  $\Theta$  and  $\mathbf{m}_j, j \in \{1, \dots, N\}$  that minimise the following:

$$\sum_i \sum_j |\mathbf{p}_{ij}^{meas} - \mathbf{p}_{ij}^{pred}(\Theta, \mathbf{m}_j)|^2. \quad (\text{A.1})$$

### A.1.2 Implementation

The proposed workflow consists of six steps (figure A.2), the first two are the practical data acquisition phase which takes place in the X-ray suite:

1. Object and marker holder preparation;
2. Data acquisition;

After data acquisition the computational workflow consist of the following steps:

1. Marker detection and labelling;
2. System parameter derivation;
3. Pre-processing and Inpainting;
4. 3D reconstruction.

In the following sections we expand on each of these steps.

#### Data acquisition in the X-ray suite

##### Object and marker holder preparation

First, a marker holder is made by inserting a number of markers into two or more pieces of foam. The size and shape can be arbitrary, the holder can be adjusted to the size and shape of the object. They should be distributed vertically to limit the overlap of the projected markers on the radiographs. The object is mounted on the rotation stage, the marker holder is placed next to it. Using the live radiographic inspection, the positions of the markers are checked and adjusted if needed.

Although a full discussion of the requirements of the positions of the markers within the foam is beyond the scope of this article, here we give some general guidelines. For an accurate parameter estimation, the markers should be distributed within the foam in three dimensions so that they span the detector field of view where the object is located. If the markers are on one vertical line for example, the depth information is not captured in their positions as well as when they are distributed. This is due to the fact that the trajectory of the markers on the detector forms an ellipse and therefore movement of the PML (and the corresponding geometric information gain) is less on the sides of the ellipse than in the center. The number of markers needs to be sufficient for the system of equations to be resolved. In practice, it is advisable to take more markers where possible, since the contrast with the object may not always be sufficient to find all markers in each radiograph or they rotate out of the field of view for a few radiographs. The overlap of markers on the radiographs should be avoided, because this hampers the correct labelling of the markers. Therefore, we distribute the markers vertically to limit overlap on radiographs. Since the rotation angles are part of the parameter set, in each radiograph markers should be present. For the scans in chapter 4, we have used a minimum distance between markers of 1cm. We have moreover used the live radiographic inspection to ensure as few projections as possible had overlapping markers. This facilitates the labelling and tracking of the markers. We used 10 markers for the wooden block and 17 markers for the case study.

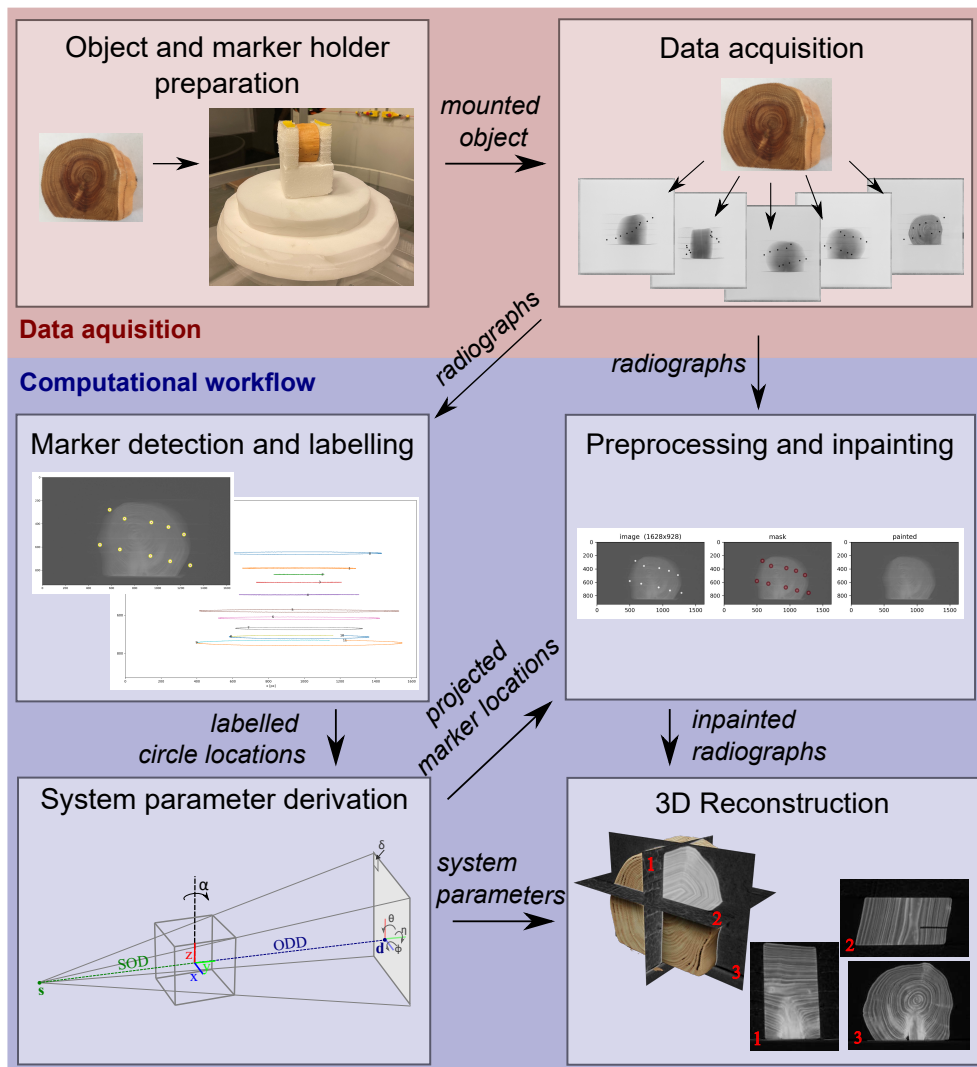


Figure A.2: Steps in the post-scan marker-based parameter derivation method for 3D reconstruction.

The following steps can be used to setup the markerholder:

1. Place the markers in two or more pieces of foam, keeping them at least 1cm apart and avoiding placing them on a straight line. The number of markers will depend on the size of the object and the magnification, since the main goal is to have no overlapping markers on the radiographs. See figure A.3a.
2. Place the pieces of foam on the rotation stage, next to the mounted object. If convenient, placing two at 90° gives a good spread of the markers on the detector view. See figure A.3b,c.
3. Turn on live radiographic inspection of the object and markers and determine the maximum magnification that ensures the object stays in the field of view during rotation. See figure A.3d.
4. Make sure that during rotation there is no radiograph on which no markers are visible. Markers can rotate out of the field of view, but in every radiograph markers need to be present.
5. If there are radiographs in which the markers overlap, try to increase the vertical space between markers until they do not overlap.



**Figure A.3: Preparing the markerholder.** a) Including markers in foam. b) Placing foam next to the wooden block. c) Placing the wooden block and markerholder on the rotation stage at the Rijksmuseum. d) Resulting radiograph in the Rijksmuseum facility.

## Data acquisition

Radiographs are collected over one or more revolutions of the rotation stage. A flatfield, an image with the source turned on without an object in view, and darkfield, an image with the source off, are collected for the pre-processing step [104].

## Computational workflow

### Marker detection and labelling

The computational workflow starts with measuring the PML on the projections, by first using the Canny Edge detector [171] and consequently an implementation of the Hough Transform to identify circles from the Scikit toolbox [172]. Making use of the Trackpy toolbox [194], we identify the same projected marker from projection to projection, forming the ellipse shaped trajectory followed by the projected marker (step 2 in figure A.2). Both locating and labelling may require user input, as the locating of projected marker on the image depends on the total brightness and contrast and wrongly labelled projected markers can make parameter estimation less reliable. During the locating step some dense features in the object may be identified as projected markers that do not correspond to markers. When the markers overlap with the

object or rotate out of the field of view, the corresponding projected markers may not be found in a number of projections. This causes errors in the labelling step. These errors are reduced by filtering out short trajectories, determining a maximum step size for the projected marker from projection to projection and a memory parameter that determines for how many projections a marker can be missing to still belong to the same label. These parameters can be influenced by the user based on visual inspection of the resulting trajectories. It is preferable to have a trajectory cut into multiple labels over mislabelling (e.g. crossover of labels between two markers). The number of found labels is  $N^*$ . Note that this can be a higher number than the actual number of markers  $N$ , due to features in the object being identified as projected markers or partially labelled trajectories, or a lower number due to non-identified projected markers in the locating step. During the optimisation in the next step this is taken into account.

### System parameter estimation

The System parameter estimation algorithm is given in Algorithm 1. It consist of two optimisation steps with a marker merging step in between. The required user input is the detector pixel size ( $\delta$ ) and an estimation of the source to object distance (SOD). This source position is used to fix the location of the source at distance SOD from the rotation axis on the negative  $y$ -axis (see section A.1.1). The resulting reconstruction will therefore be scaled relative to this given SOD.

To provide an educated initial guess on the system parameters, further input is requested from the user: estimated values for the ODD, the number of revolutions ( $n_{rounds}$ ) of the rotation stage and the approximate average distance  $r$  of the markers to the rotation center. These inputs are used to create the following initialisation: i) The detector is placed on the positive  $y$ -axis at distance ODD from the origin, ii) the detector tilts and skew are 0, iii) projection angles are equidistant over  $2\pi n_{rounds}$  (radians) and iv) the initial marker locations are placed randomly within a ball with radius  $r$ , their labels based on their vertical location. This initial guess and the residual function described by equation A.1 are input for the *scipy.optimize* package's *least\_squares* function [174]. Derivatives are calculated using an automated derivative package *autograd* [10], that is a wrapper for *numpy* [131].

For each iteration a reduced number of projected markers per projection image are used, to make the method robust against mislabelled markers. Projected markers are selected that have the lowest distance of the predicted PML to the measured PML. In other words, we use labels  $h_i(\Theta, N_k)$ , which are the  $N_k$  labels  $j$  with smallest  $|\mathbf{p}_{ij}^{meas} - \mathbf{p}_{ij}^{pred}(\Theta, \mathbf{m}_j)|$ . The number of projected markers that are used in the first and second optimisation step are given by  $N_1$  and  $N_2$  and are input by the user. The least squares optimisation terminates when the step size or cost function improvement are below a given threshold of  $10^{-6}$ . The user can give an upper limit  $n_{iter1}$  and  $n_{iter2}$  for the number of iterations of the least squares solver in the first and second optimisation step respectively. In the marker merging step a minimum distance between marker positions is used to decide whether or not to merge two labels. This distance can be chosen by the user.

**Algorithm 1** System parameter estimation.

- 1: **Initial Guess.** The initial guess is defined by a standard circular scan with equidistant angles and the user input values ODD,  $n_{rounds}$  and  $r$ .
- 2: **First optimisation.** Run least squares optimisation starting from the initial guess until thresholds are reached or until the number of iterations exceeds  $n_{iter1}$ , to find the parameters  $(\Theta^*$  and  $\mathbf{m}_1^* \dots, \mathbf{m}_N^*$ ) that minimise the following value

$$\sum_i \sum_{j \in h_i(\Theta^*, N_1)} |\mathbf{p}_{ij}^{meas} - \mathbf{p}_{ij}^{pred}(\Theta^*, \mathbf{m}_j^*)|^2.$$

- 3: **Merge markers.** If the distance between the positions of two markers  $|\mathbf{m}_j - \mathbf{m}_k|$  is smaller than a given threshold *and* do not overlap for more than a given number of frames, the labels  $j, k$  refer to the same projected marker and their trajectories are merged, or in other words  $k$  is relabelled  $j$  and removed.  $N^{**}$  denotes the number of labels after this merging step.
- 4: **Updated initial guess** Use  $\Theta^*$  and  $\mathbf{m}_j^*$ ,  $j \in \{1, \dots, N^{**}\}$  as updated initial guess for the second optimisation step.
- 5: **Second optimisation.** Run least squares optimisation starting from the initial guess until thresholds are reached or until the number of iterations exceeds  $n_{iter2}$ , to find the parameters  $(\Theta^{**}$  and  $\mathbf{m}_1^{**} \dots, \mathbf{m}_N^{**})$  that minimise the following value

$$\sum_i \sum_{j \in h_i(\Theta^{**}, N_2)} |\mathbf{p}_{ij}^{meas} - \mathbf{p}_{ij}^{pred}(\Theta^{**}, \mathbf{m}_j^{**})|^2.$$

- 6: **Calibrated parameters.** Return  $\Theta^{**}$ .

**Pre-processing and inpainting**

The recorded data is first flat- and darkfield corrected. Using the system parameters and marker positions found in the previous step, a forward projection is performed to obtain the predicted PML locations on all the projections. These are used to algorithmically remove the projections of the markers on the radiographs by the inpainting function of the scikit-image package [173], because high density material in a CT acquisition can cause image artefacts in the reconstruction [168]. It is possible to perform both a reconstruction with the original radiographs and the inpainted radiographs. Therefore the user can choose which reconstruction serves them best, since the effect of inpainting can differ per object and placement of the markers.

**3D reconstruction**

The inpainted projections, together with the system parameters resulting from the optimisation step are used to obtaining a 3D reconstruction. Because of the fixed source position, the solution that is obtained, is a scaled reconstruction. The estimated system parameters are transformed into a geometry description that is then used within the SIRT algorithm provided by the FleX-box toolbox [108] to make a 3D reconstruction of the object.

## A.2 Supplementary figures and tables

### A.2.1 Parameters

In Supplementary table A.3 the computed system parameters of the scans of the wooden block are given. In figure A.4 the found angles for each system are given. We see that the British Museum setup provides equidistant angles and the other two systems have less regular angular intervals.

<i>System parameters</i>	<b>BM system</b>	<b>BM markers</b>	<b>GM markers</b>	<b>RM markers</b>	<b>FleX-ray</b>
source location (mm)	(0,881,0)	(0,881,0)	(0, 881, 0)	(0,500,0)	(0,658.02,0)
detector location (mm)	(-31.46, 1362.0, 0)	(-31.32, 1471.44, -3.84)	(-32.97, 1351.04, -6.71)	(-2.63, 583.97, 2.78)	(0,430.98,0)
detector tilts (radians)	0, 0	0.027, 0.019	-0.004, 0.015	0.021, 0.001	0.0, 0.0
detector in-plane rotation	0.0	0.0	0.0	-0.002	-0.004

**Table A.3:** System parameters as reported by the system feedback (BM system) or the marker-based parameter retrieval (BM markers, GM markers, RM markers) for the scans of the wooden block (section 4.1.2). The source location is an estimate given by the user.

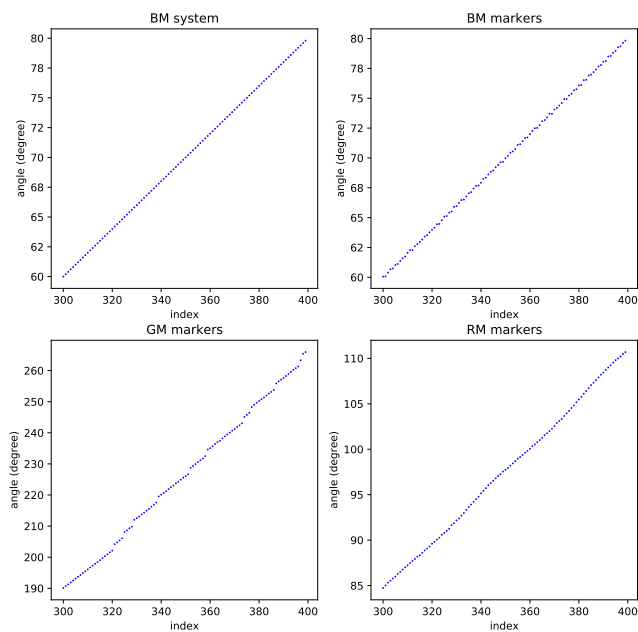


**Figure A.4:** Subset of the acquisition angles (index vs. angle (degrees)) of the test scans of the wooden block (main article section (section 4.1.2)), given by the British Museum system (BM system) and calculated by the marker-based parameter derivation at the British Museum (BM markers), The J. Paul Getty Museum (GM markers) and the Rijksmuseum (RM markers).

To investigate the accuracy and precision of the found marker positions, we performed simulation experiments. We simulated projected marker locations (PMLs) by forward projecting 3D marker locations. To simulate an incorrectly found center of the PML, we added gaussian noise with mean 0 and standard deviation from 0 up to 5 pixels to the PML. Next, we ran our parameter retrieval optimisation to obtain estimated 3D marker locations. Since our method does not assume the projection angles and other system parameters are known, the found 3D marker locations may have a slightly different orientation, vertical position, and scaling compared to the original marker positions. These variations do not affect the reconstruction quality, so to be able to measure the quality of the found marker locations, we compensate for them before comparing the found marker locations with the original marker locations used for the forward projection. For each choice of standard deviation, we ran this simulation with ten different random seeds, which influences the noise added to the PMLs, to obtain figure A.5 showing standard deviation (in pixels) versus the average error in the calculated marker positions (in mm). The average error is lower than the voxel size (0.13mm) except for a few outliers. In the practical datasets included in the manuscript, we found that the PML identification can be trusted to locate the centers within this error range.

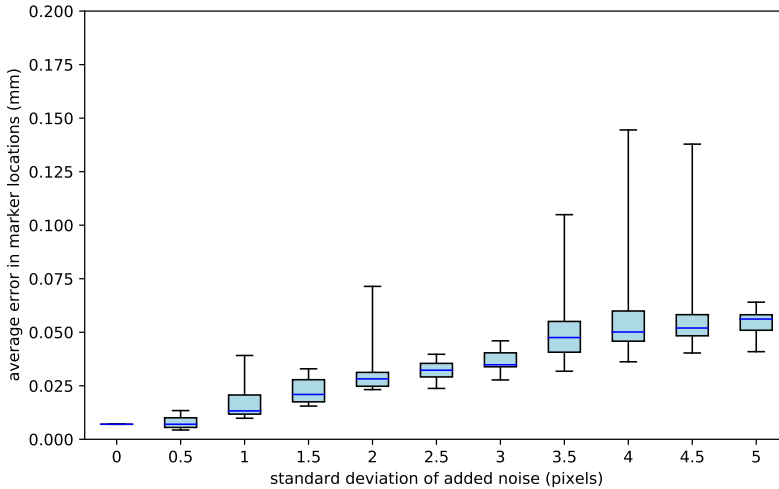


**Figure A.5: Results of the simulation experiment.** Boxplot showing average errors in the calculated marker positions (y-axis) when adding gaussian noise to the PML (standard deviation of noise on the x-axis). The boxplot shows the median (blue line), interquartile range (lightblue box), which shows where 50% of the data points around the median fall, and minima and maxima of the data (black horizontal bars).

## A.2.2 Comparison of the marker based approach and FDK

Here we show the type of image artefacts that can be encountered when an imperfect calibration is used for a CT reconstruction. In figure A.6 a slice from a reconstruction of the wooden block dataset recorded at the J. Paul Getty museum is shown using the approach outlined in the main text and using a straightforward FDK approach with the angles estimated to be equidistant. The irregularity of the angular interval produces wrongly back-projected radiographs in the second reconstruction, showing the need for estimating the individual angular intervals. In figure A.7 we show the effect of errors in the rotation speed. Here, these effects are shown on a dataset of the wooden block recorded at a micro-CT facility, the FleX-ray laboratory, located at the Center for Mathematics and Computer Science in Amsterdam. For figure A.7 we removed angles at the end of the full rotation to simulate a slower rotation speed.

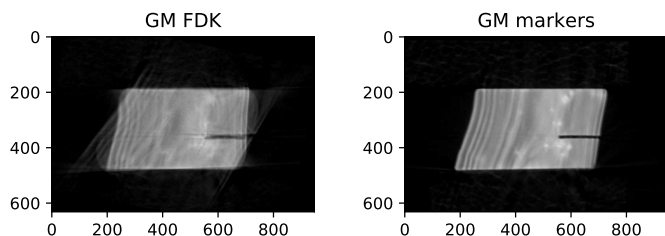


**Figure A.6: Comparing the marker-based parameter retrieval method with a straightforward FDK reconstruction.** A slice from the reconstruction of the dataset of the wooden block at the J. Paul Getty Museum with a) marker-based parameter retrieval and b) FDK with the angles estimated to be equidistant.

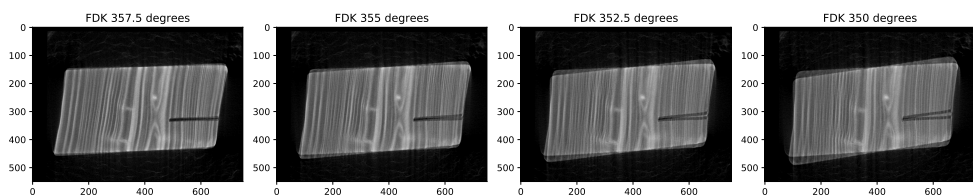


**Figure A.7: Effect of lower rotation speed on FDK reconstruction.** Here we show an FDK reconstruction where the rotation stage does not fully rotate to 360 degrees during one acquisition, reaching from left to right only 357.5, 355, 352.5 and 350 degrees, respectively, while the reconstruction incorrectly assumes that the rotation was over the full 360 degrees. The slower the rotation stage the larger the effect on the FDK reconstruction.

### A.2.3 Inpainting

In figure A.8 we show a radiograph from the dataset of the wooden block, recorded at the FleX-ray laboratory, the mask used for inpainting and the inpainted radiograph. In figure A.9 a slice from a reconstruction of the wooden block dataset recorded at the FleX-ray laboratory is shown using the original radiographs and the inpainted radiographs. The effect of the inpainting on the reconstruction of the wooden block is visible in a blurring on the left side of the wooden block. The effect of the inpainting is dependent on the magnification. Since this is a high resolution scan, the magnification is large and therefore the marker shades a larger portion of the object than when the magnification is smaller. In figure A.10 we show the effect of the inpainting on the dataset recorded at the J. Paul Getty museum. Here the effect is small. Thus, the effect of inpainting depends on the settings. Whether to use the original or inpainted radiographs can be decided by the user upon inspection of the reconstructions.

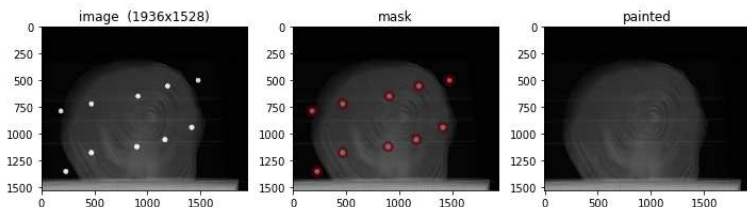


**Figure A.8: Inpainting of the radiographs.** A radiograph of the wooden block at the FleX-ray laboratory: original radiograph (left) and an overlay of the mask used for inpainting (in red) on the radiograph (middle) and resulting inpainted radiograph (right).

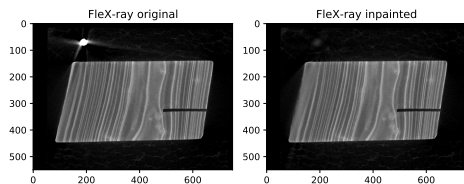


**Figure A.9: Comparing reconstructions with and without inpainting.** A slice from the reconstruction of the dataset of the wooden block at the FleX-ray laboratory with original radiographs (left) and inpainted radiographs (right).

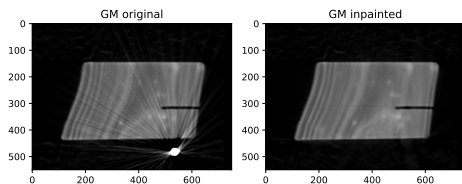


**Figure A.10: Comparing reconstructions with and without inpainting.** A slice from the reconstruction of the dataset of the wooden block at the J. Paul Getty museum, using the marker based approach with a) original radiographs and b) inpainted radiographs.

# B

## Appendix B:

### Intact user guidelines

This appendix to chapter 5 gives the user guidelines for the Intact plugin presented in that chapter.

## B.1 Installation

### B.1.1 Blender

#### Installation:

1. Go to <https://www.blender.org/download/> and pick the relevant version for your operating system and install.

#### Why Blender?

- Open source: Blender has a large community with plugins that could perhaps sustain future questions/demands of the INTACT tool.
- Old versions will stay available, so the plugin doesn't have to be updated for compatibility with future updates of Blender.
- Blender is based on Python. It is therefore easy to write and incorporate your own demands, and possible for any user to edit those based on their own needs.

---

This is the appendix to chapter 5 and has been published as Supplementary Material to F. G. Bossema, P. J. Van Laar, K. Meechan, D. O'Flynn, J. Dyer, T. Van Leeuwen, S. Meijer, E. Hermens, and K. J. Batenburg. "Inside out: Fusing 3D imaging modalities for the internal and external investigation of multi-material museum objects". *Digital Applications in Archaeology and Cultural Heritage* 31 (2023), e00296.

## B.1.2 Blender plugin – INTACT

### Installation:

1. Download the plugin here: [10.5281/zenodo.8041844](https://zenodo.org/record/8041844) or clone the github repository.
2. Open Blender
3. Go to “edit -> preferences” (figure B.1)
4. Go to “add-ons” and click "install" (figure B.2)
5. Navigate to the INTACT\_Windows\_main.zip file and select it. Blender will now automatically install the plugin. Make sure to activate it by checking the box next to the plugin name. (figure B.3)
6. The INTACT plugin is now installed within your Blender software. You can find it in the UI Side Panel. Open this panel by clicking the little arrow next to the orientation gimbal. (figure B.4) and then choose the INTACT panel (figure B.5).
7. When opening the INTACT panel, you’ll be prompted to click a button ‘Install Modules’. Do this. When it’s done close blender and restart.

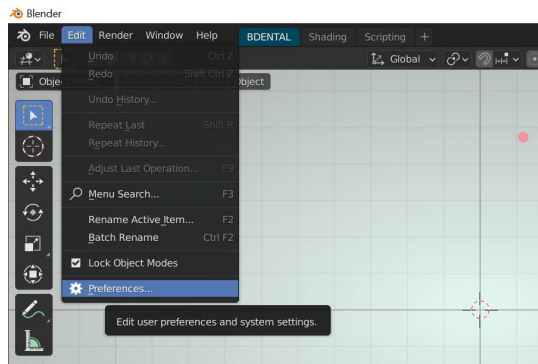


Figure B.1

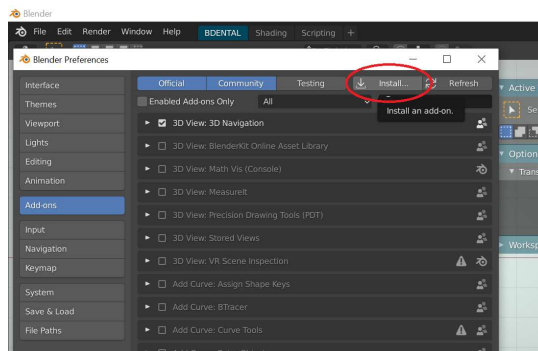


Figure B.2

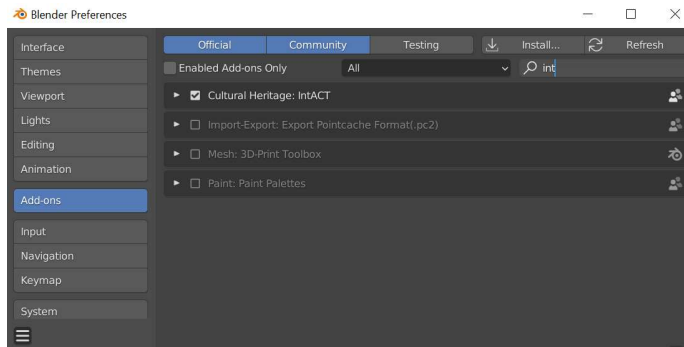


Figure B.3

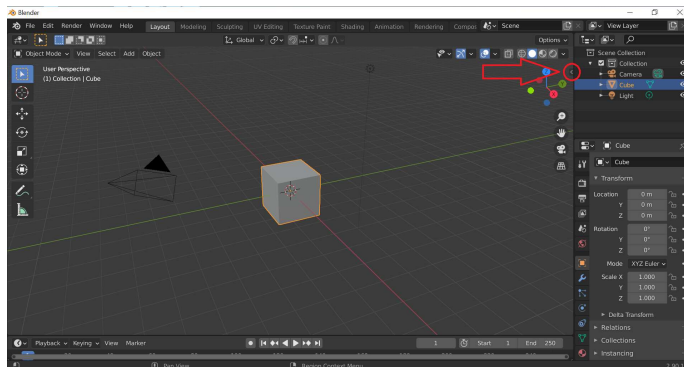


Figure B.4

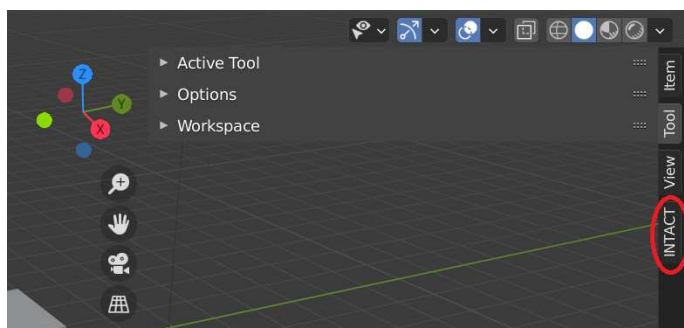


Figure B.5

## B.2 The INTACT plugin

The numbering of this section corresponds to the drop-down menu's in the plugin's User Interface (figure B.6).

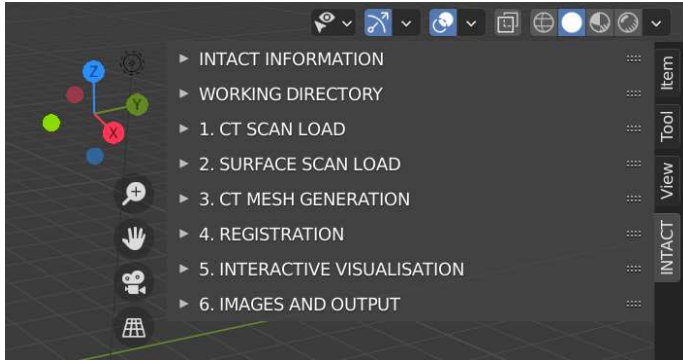


Figure B.6

### B.2.0 Setting up working directory

**Note:** An example dataset is made available to follow along with the guidelines. This includes a 3D-surface scan and a CT scan of a small wooden block. Download the example dataset here: [10.5281/zenodo.8041816](https://zenodo.org/record/8041816)

1. Open INTACT, make it bigger by dragging the side. In the 'Working Directory' tab choose a project directory by clicking on the folder next to the empty field. Make this an empty folder, this is where all the files generated by the plugin will be saved.

### B.2.1 Loading CT scan

1. Open the 'CT scan load' tab.
2. Choose a data type (default is Tiff).
3. Input the directory where your CT scan files are stored.
4. In case of Tiff, input the resolution (test dataset voxel size = 0.13mm).
5. Click "Load CT Scan", wait (may take a couple minutes)
6. You can move the view by holding the middle button while moving your mouse. Preferably don't move the CT scan. Don't worry if you do, its position can be reset in the 'CT Mesh Generation' tab.
7. For visualisation purposes you can change the threshold, and color + lighting. (figure B.7)

**Note:** If you do not have a surface scan of your object, you can skip to Visualisation (section B.2.5).

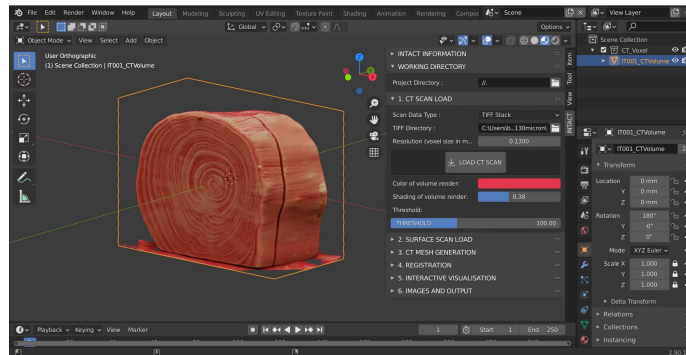


Figure B.7

## B.2.2 Surface scan load

1. In the 'Surface scan load' tab click on the icon of a folder.
2. In the resulting pop-up, navigate to the directory which holds your 3D model, select the .obj model and click accept. Then click the 'Load surface scan' button. (figure B.8).

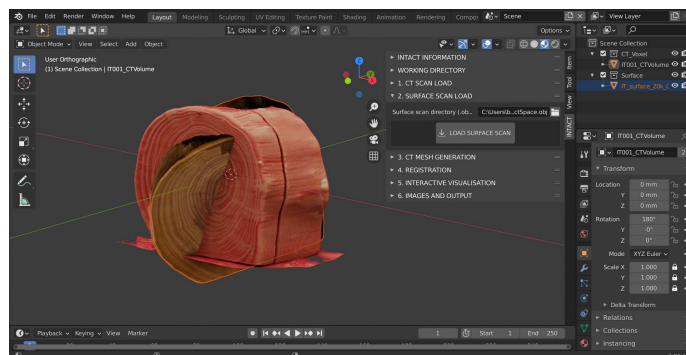


Figure B.8

**Tip:** Sometimes the surface scan is not shown as expected. This can have to do with how the 'normals' are defined. Try going into right hand lower menu, the red ball and change how the normals are calculated. See figure B.9.

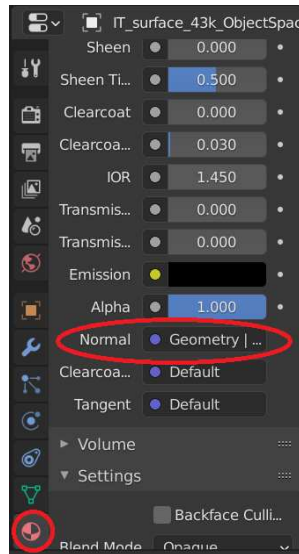


Figure B.9

### B.2.3 CT mesh generation

1. In the 'CT Mesh Generation' tab, play around with the threshold value to find a value that shows all of the object outline, but not much else. A little noise outside the object is fine.
2. When you're happy with the threshold, click Segmentation. You'll end up with a mesh of the CT scan (figure B.10). Wait, this may take a minute. For ease in the next section, it may be nice to turn off the CT volume view by clicking on the eye in the right hand panel, next to the IT001\_CTVolume.

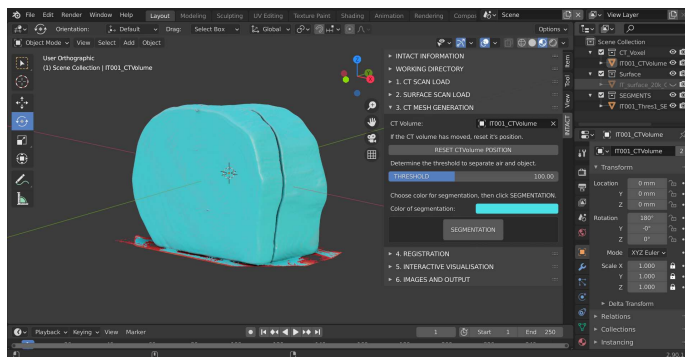


Figure B.10

## B.2.4 Registration

1. Select CT scan and if needed because the CT scan was moved, click ‘reset CT volume position’ in the ‘CT Mesh Generation’ tab. Double check that all values are zero (location, rotation) in the lower right panel, the orange square tab will give you these numbers. If not, change them to zero. Scale is 1.
2. Go to the Registration tab.
3. Manually align your 3D surface scan roughly to the produced CT segment, using the controls as described in section 3.3. This can be a rough alignment (figure B.11).
 

**Tip:** Use the pre-defined Front/Back – Left/Right – Top/Bottom views, the coloured axis in the top right corner. Switch between those to align your objects manually along each axis.
4. Check that the surface scan and CT segmentation have been identified correctly in the dropdown box and if not select the right objects by clicking the corresponding white eyedropper icon, then clicking the scan/segmentation in the 3D viewer or in the right hand side panel (segmentation is IT001\_Thres1\_SEGMENTATION). Check “Allow scaling” if you want the surface scan to be scaled if needed.
5. Press ‘Perform Registration’. Wait, this may take a while. You will see a live update of the surface scan mesh move towards the CT mesh (figure B.12).
6. Is the result satisfactory? If it isn’t aligned properly yet, run it again (click the ‘Perform Registration’ button).
  - (a) It won’t align properly? Perhaps your rough manual alignment can be improved. You can also increase the “Outlier %” to 10 or even higher and the iterations can be increased. Experiment a little bit.
  - (b) Look at some landmarks in your object.
  - (c) You should see bits of the CT mesh colour coming through the surface scan.
7. Select your surface scan to see the values for the transformation in the lower right hand panel, orange square tab.

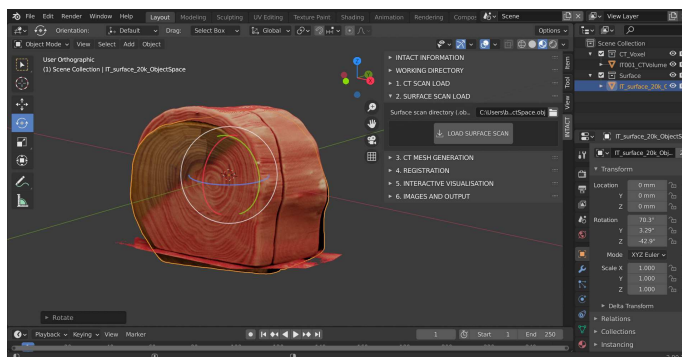


Figure B.11

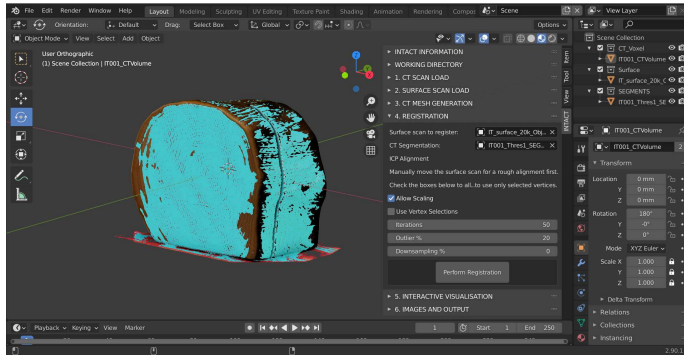


Figure B.12

## B.2.5 Interactive visualisation

1. It is usually convenient to hide the visibility of the Segmentation by clicking the eye symbol next to the Segmentation in the right hand upper menu.
2. If given, check the selected CT scan volume, segmentation and surface scan at the top of the 'Interactive visualisation' tab. If not, please select them from the dropdown menu, or with the white eyedropper icon as previously described.
3. Then click 'Slice volume', to create the CT slices (Figs. B.13 and B.14).
4. If required, adjust the contrast of the slices with the min and max sliders (figure B.15).
5. Click 'Create cropping cube'. This will create a cube, that when moved into the object will make everything within it transparent (figure B.16).
6. Check 'Track slices', to attach the slices to the sides of the cube and make them update when the cube is moved into the object.
7. Check 'Crop slices outside object' to show only the part of the CT Volume that is inside the object (and not the air around it) (figure B.16).
8. *Optional:* The 'Multi-view' button opens up a user interface that shows the X, Y, Z views plus the 3D view.
9. *Optional:* Surface scan roughness and slice thickness can be adjusted.

Now that everything is setup, it is possible to interactively manipulate the data, analyse and investigate. Use the visibilities in the upper right-hand menu and standard Blender controls to move (see section B.3).

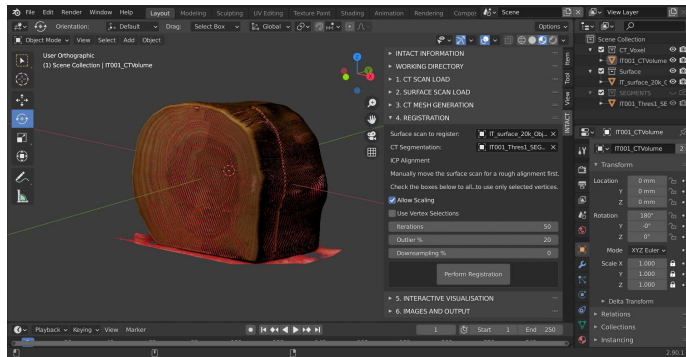


Figure B.13

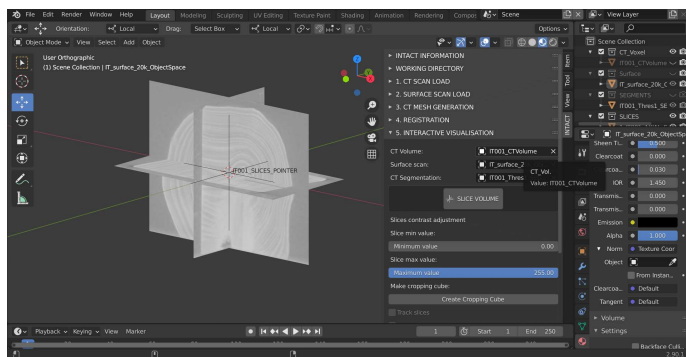


Figure B.14

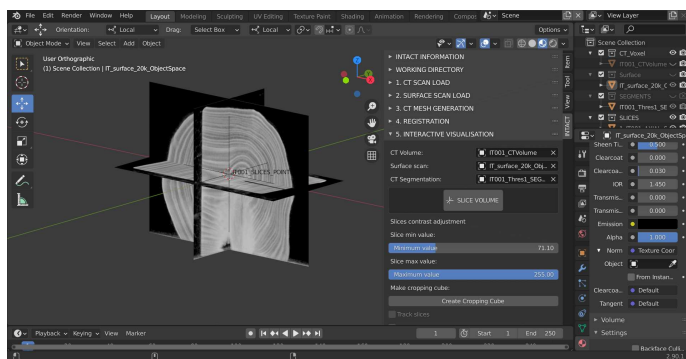


Figure B.15

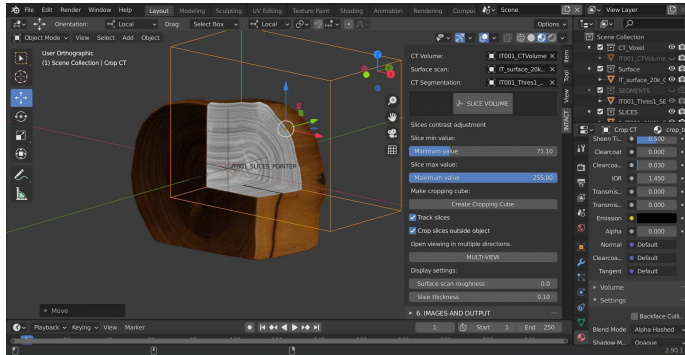


Figure B.16

## B.2.6 Images and output

### Screenshot:

1. To obtain a screenshot of the current view, including all lines and grids, click 'Take screenshot'.

### Rendering images:

1. Click 'Set camera position'. This opens up the camera view in a grey rectangle (figure B.17).
2. Change the view of the camera, by moving around using the normal blender controls.
3. Change the size of the camera by changing the resolution parameters.
4. When satisfied click 'confirm camera position'.
5. *Optional:* Adjust lighting and background colour for the image.
6. Click 'Render image'. When satisfied, click 'Image -> Save as...'

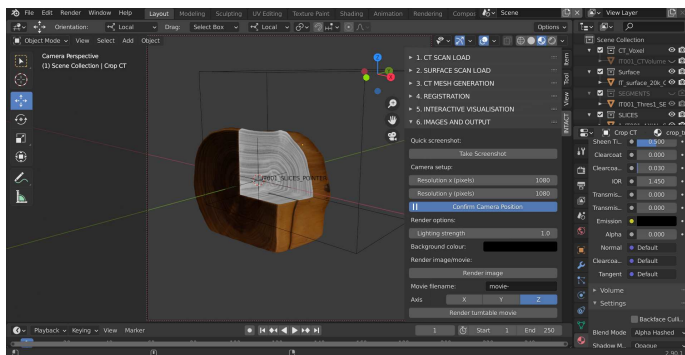


Figure B.17

**Rendering videos:**

1. The same camera position is used as for the image. If needed, adjust using step 1-4 of Rendering images above.
2. Choose an axis around which to rotate the object.
3. Name the movie - make sure to change this for every movie or the previous one will be overwritten.
4. Click 'Render turntable movie'. Each frame will be rendered separately and then saved in the working directory in a new folder called 'Movies'.

## B.3 Basic Blender controls

### B.3.1 Viewport shading options

The virtual space in which we place our 3D models and objects is called the viewport. There are 4 different shading options within Blender that we can choose from, each with a different appearance (Figs. B.18 and B.19).

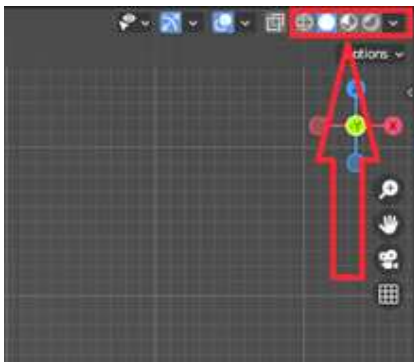


Figure B.18

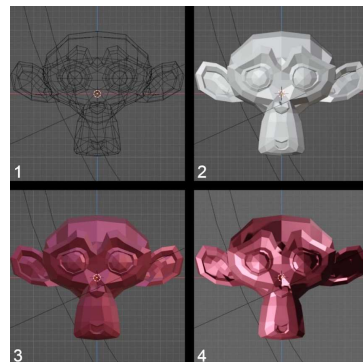


Figure B.19

1. **Wire edges**  
This mode is probably least interesting for our case, and displays the 3D-model as a wireframe.
2. **Solid mode**  
This is the standard mode upon opening blender, and displays the 3D-model as a solid object without its material properties. This mode is best when editing properties, aligning models, or setting up an animation as it's least computationally heavy.
3. **Material preview mode**  
In this mode the material properties are added to the object, as they would appear with relatively flat lighting (not the lights you can add yourself, but what is called 'world lighting').

#### 4. Render preview

In this mode the user's 'scene lights' are added. This makes it the most computationally heavy mode as the software has to calculate and render light, reflection, and shadow.

### B.3.2 Moving the view

#### 1. Translation

Move the view by holding shift and the middle mouse button, and moving your mouse.

#### 2. Rotation

Rotate the view by holding the middle mouse button, and moving your mouse.

#### 3. Zoom

Zoom in and out by scrolling (either using your trackpad or the middle mouse button).

#### 4. Front-Back-Top-Bottom-Left-Right view

Blender also has 6 built in views that are quickly accessible via the gimbal in the top right corner (figure B.20). You can click on each of the 6 dots (representing X, Y, Z in both positive and negative direction), which will bring you immediately to a view along that axis.

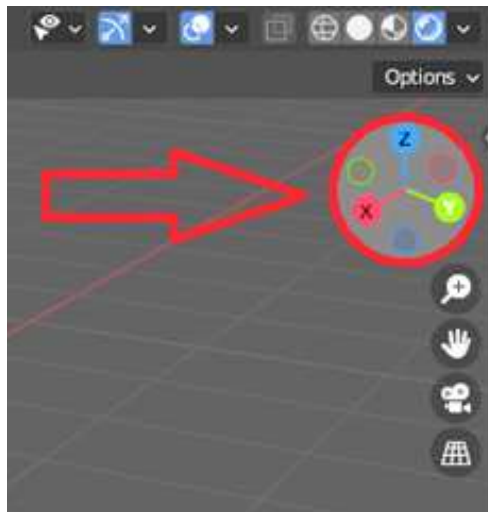


Figure B.20

### B.3.3 Object selection/translation/rotation/scaling

1. **Select an object**

Selecting an object can be done with your left mouse button. You'll see what object is selected in the top right of your screen, in what's called the "Scene collection" (figure B.21A).

2. **Translation/rotation/scaling**

There are two ways to move/rotate/scale your object:

- (a) Via the properties panel (figure B.21B) You can change the values in your object's properties panel. This is best for if you want some very subtle changes (e.g. 0.01°).
- (b) In the viewport Click your object, and on the left-hand side you can click "move" and "rotate" (figure B.22). In the centre of your object, handles will appear that allow you to perform these actions along a certain axis, or along all of them at once.

3. **Turn on/off visibility and rendering of objects**

You might want to enable/disable the visibility of certain objects in your viewport at a given point of time. You can do this by clicking the eye symbol beside the name of your object in the "Scene collection". Clicking the camera will turn on/off the visibility of that object in the rendered image (figure B.23).

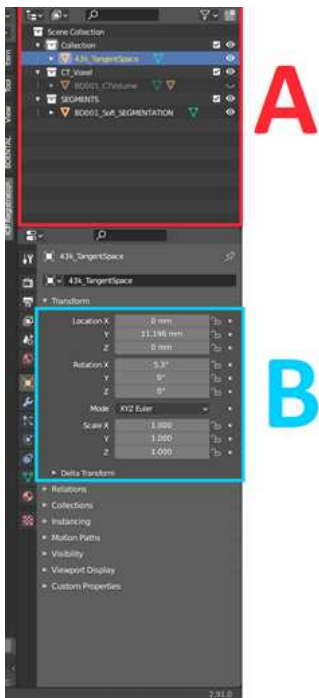


Figure B.21

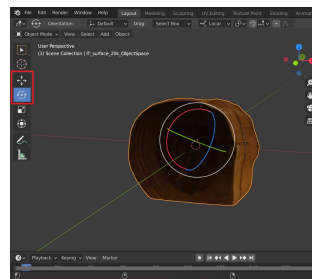


Figure B.22

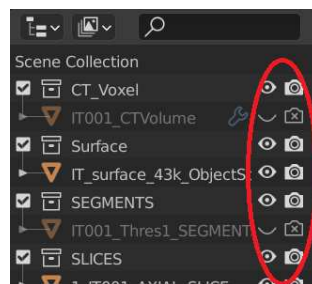


Figure B.23

## B.4 Using vertex selections for registration

### B.4.1 Enabling vertex selections

In cases where your X-ray CT or surface scan is incomplete, you may want to focus your registration on a sub-region for the best accuracy. This can be done by enabling the ‘Use Vertex Selections’ option in the Registration tab of the plugin (B.24). You will need to manually select which vertices to include from both your surface scan and CT segmentation mesh. Only choose areas that appear in both for the best accuracy.

### B.4.2 How to select vertices

1. To select vertices, you have to enter Blender’s ‘Edit mode’. First select the mesh you want to use, then change the dropdown menu in the top left of the viewport to edit mode (figure B.25). Alternatively, you can select the mesh, and press the tab key on your keyboard. To go back to the normal blender mode, change the menu to ‘Object Mode’, or press tab again.
2. Once in edit mode, you can select vertices by clicking and dragging across the parts of the mesh you want to include (figure B.26). Selected vertices will appear in bright orange. To add to your selection, hold down the shift key while you do this.
3. To select through your mesh (i.e. not just vertices on the face closest to you), you can enable Blender’s X-ray mode. Click the symbol with two overlapping squares in the top right of the viewport (figure B.27) or press alt + Z on your keyboard.

### B.4.3 Tips for selecting vertices

- In some meshes, you may have multiple regions that aren’t directly connected to each other. To select all vertices in one piece, you can click one vertex, then press ctrl + L to select everything connected to it.
- It can also be useful to hide parts of the mesh you don’t want to select. This can be done by selecting the vertices (in the usual way), and pressing H to hide them. Any hidden vertices can be shown again by pressing alt + H.
- A line of vertices can be selected by clicking a vertex at one end, then ctrl + click a vertex at the other end. Blender will select all vertices on the shortest path between the two.
- Combining these methods can make selecting sub-regions much faster. For example, you could select a line of vertices that separate your region of interest from the rest of the mesh. Hiding this will disconnect your region of interest, and allow it to be selected in one go with ctrl + L.

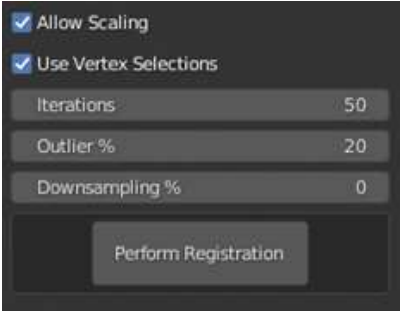


Figure B.24



Figure B.26

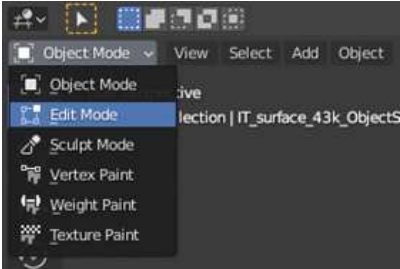


Figure B.25

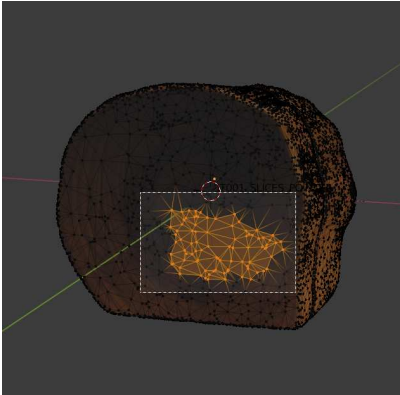


Figure B.27



# List of publications

Publications that are part of this thesis:

1. F. G. Bossema, W. J. Palenstijn, A. Heginbotham, M. Corona, T. Van Leeuwen, R. Van Liere, J. Dorscheid, D. O’Flynn, J. Dyer, E. Hermens, and K. J. Batenburg. “Enabling 3D CT-scanning of cultural heritage objects using only in-house 2D X-ray equipment in museums”. *Nature Communications* (accepted, in press).
2. F. G. Bossema, P. J. Van Laar, K. Meechan, D. O’Flynn, J. Dyer, T. Van Leeuwen, S. Meijer, E. Hermens, and K. J. Batenburg. “Inside out: Fusing 3D imaging modalities for the internal and external investigation of multi-material museum objects”. *Digital Applications in Archaeology and Cultural Heritage* 31 (2023), e00296.
3. F. G. Bossema, M. Domínguez-Delmás, W. J. Palenstijn, A. Kostenko, J. Dorscheid, S. B. Coban, E. Hermens, and K. J. Batenburg. “A novel method for dendrochronology of large historical wooden objects using line trajectory X-ray tomography”. *Scientific Reports* 11, 11024 (2021).
4. F. G. Bossema, S. B. Coban, A. Kostenko, P. van Duin, J. Dorscheid, I. Garachon, E. Hermens, R. van Liere, and K. J. Batenburg. “Integrating expert feedback on the spot in a time-efficient explorative CT scanning workflow for cultural heritage objects”. *Journal of Cultural Heritage* 49 (2021), pp. 38–47.

Publications that are not part of this thesis:

1. M. Domínguez-Delmás, P. Van Duin, J. Dorscheid, F. G. Bossema, K. J. Batenburg, and R. Van Langh. “Unravelling a 17th-century prison escape: The quest to identify the original Hugo Grotius bookchest”. In: *Working Towards a Sustainable Past*. ICOM-CC 20th Triennial Conference Preprints, Valencia, 18–22 September 2023, J. Bridgland. Paris: International Council of Museums, 2023
2. F. Bossema, C. Zwetsloot, and I. Smeets. “Math in the City: Designing a Math Trail for High School Students”. In: *World Scientific Series on Science Communication*. Vol. 03. WORLD SCIENTIFIC, 2023, pp. 53–72.
3. M. Kiss, F. G. Bossema, P. J. Van Laar, S. Meijer, F. Lucka, T. Van Leeuwen, and K. J. Batenburg. “Beam filtration for object-tailored X-ray CT of multi-material cultural heritage objects”. *Heritage Science* 11, 130 (2023).
4. J. Dorscheid, F. G. Bossema, P. van Duin, S. B. Coban, R. van Liere, K. J. Batenburg, and G. P. Di Stefano. “Looking under the skin: multi-scale CT scanning of a peculiarly constructed cornett in the Rijksmuseum”. *Heritage Science* 10, 161.1 (2022).

5. M. Domínguez-Delmás, F. G. Bossema, J. Dorscheid, M. Hall-Acquitania, S. B. Coban, K. J. Batenburg, and E. Hermens. “X-ray computed tomography for non-invasive dendrochronology reveals concealed double paneling on a painting from Rubens’ studio”. *PLOS ONE* (2021).
6. M. Domínguez-Delmás, F. G. Bossema, B. van der Mark, A. Kostenko, S. B. Coban, S. van Daalen, P. van Duin, and K. J. Batenburg. “Dating and provenancing the Woman with lantern sculpture – A contribution towards attribution of Netherlandish art”. *Journal of Cultural Heritage* 50 (2021), pp. 179–187.
7. F. G. Bossema, P. Burger, L. Bratton, A. Challenger, R. C. Adams, P. Sumner, J. Schat, M. E. Numans, and I. Smeets. “Expert quotes and exaggeration in health news: a retrospective quantitative content analysis”. *Wellcome Open Research* 4 (2019), p. 56.
8. J. Schat, F. Bossema, M. E. Numans, I. Smeets, and P. Burger. “Overdreven gezondheidsnieuws: Relatie tussen overdrijving in academische persberichten en in nieuwsmedia”. *Nederlands Tijdschrift voor Geneeskunde* (2018).
9. F. Bossema, J. Retrê, S. Pereira, and P. Russo. “Your night out under the stars: Reaching beyond native audiences”. *Communicating Astronomy with the Public* (2018).

Published datasets and code related to this thesis:

1. F. Bossema. *Radiographic data of a wooden block with metal markers at the FleX-ray laboratory (high resolution)*. 2024. URL: <https://zenodo.org/records/10557034> (visited on Mar. 19, 2024)
2. F. Bossema, A. Heginbotham, and M. Corona. *Radiographic data of 'Python killing a Gnu' by Antoine-Louis Barye, The J. Paul Getty Museum collection*. 2024. URL: <https://zenodo.org/records/8379913> (visited on Mar. 19, 2024)
3. F. Bossema and D. O’Flynn. *Radiographic data of a wooden block with metal markers at the British Museum X-ray facility*. 2024. URL: <https://zenodo.org/records/8379910> (visited on Mar. 19, 2024)
4. F. Bossema and A. Heginbotham. *Radiographic data of a wooden block with metal markers at the J. Paul Getty Museum X-ray facility*. 2024. URL: <https://zenodo.org/records/8379880> (visited on Mar. 19, 2024)
5. F. Bossema. *Radiographic data of a wooden block with metal markers at the Rijksmuseum X-ray facility*. 2024. URL: <https://zenodo.org/records/8379870> (visited on Mar. 19, 2024)
6. F. Bossema. *Code for 3D tomography using only basic X-ray equipment and metal markers*. 2024. URL: <https://zenodo.org/records/8379920> (visited on Mar. 19, 2024)

7. F. Bossema and P. Van Laar. *CT reconstruction and structured light scan of a small wooden block*. 2023. URL: <https://zenodo.org/records/8041816> (visited on Nov. 9, 2023)
8. F. Bossema, P. Van Laar, and K. Meechan. *IntACT plugin for Blender*. 2023. URL: <https://zenodo.org/records/8041844> (visited on Nov. 9, 2023)
9. F. G. Bossema. *A CT dataset of a small wooden block*. 2021. URL: <https://zenodo.org/record/4533882> (visited on Nov. 9, 2023)
10. F. G. Bossema. *A line trajectory X-ray tomography dataset of a wooden plank*. 2021. URL: <https://zenodo.org/record/4533887> (visited on Nov. 9, 2023)
11. F. G. Bossema, J. Dorscheid, A. Kostenko, and S. B. Coban. *A line trajectory X-ray tomography dataset of the Hugo de Groot bookchest*. 2021. URL: <https://zenodo.org/record/4533923> (visited on Nov. 9, 2023)
12. F. G. Bossema. *Three line trajectory X-ray tomography datasets of a small wooden block*. 2021. URL: <https://zenodo.org/record/4541555> (visited on Nov. 9, 2023)
13. F. G. Bossema and S. B. Coban. *Three tomographic CT datasets of a woven fabric*. 2020. URL: <https://zenodo.org/records/3741311> (visited on Nov. 9, 2023)
14. F. G. Bossema, A. Kostenko, and S. B. Coban. *A five-tile tomographic micro-CT dataset of the oak sculpture "Holy woman with lantern" - part 1 of 2*. 2020. URL: <https://zenodo.org/record/3747192> (visited on Nov. 9, 2023)
15. F. G. Bossema, A. Kostenko, and S. B. Coban. *A five-tile tomographic micro-CT dataset of the oak sculpture "Holy woman with lantern" - part 2 of 2*. 2020. URL: <https://zenodo.org/record/3747327> (visited on Nov. 9, 2023)



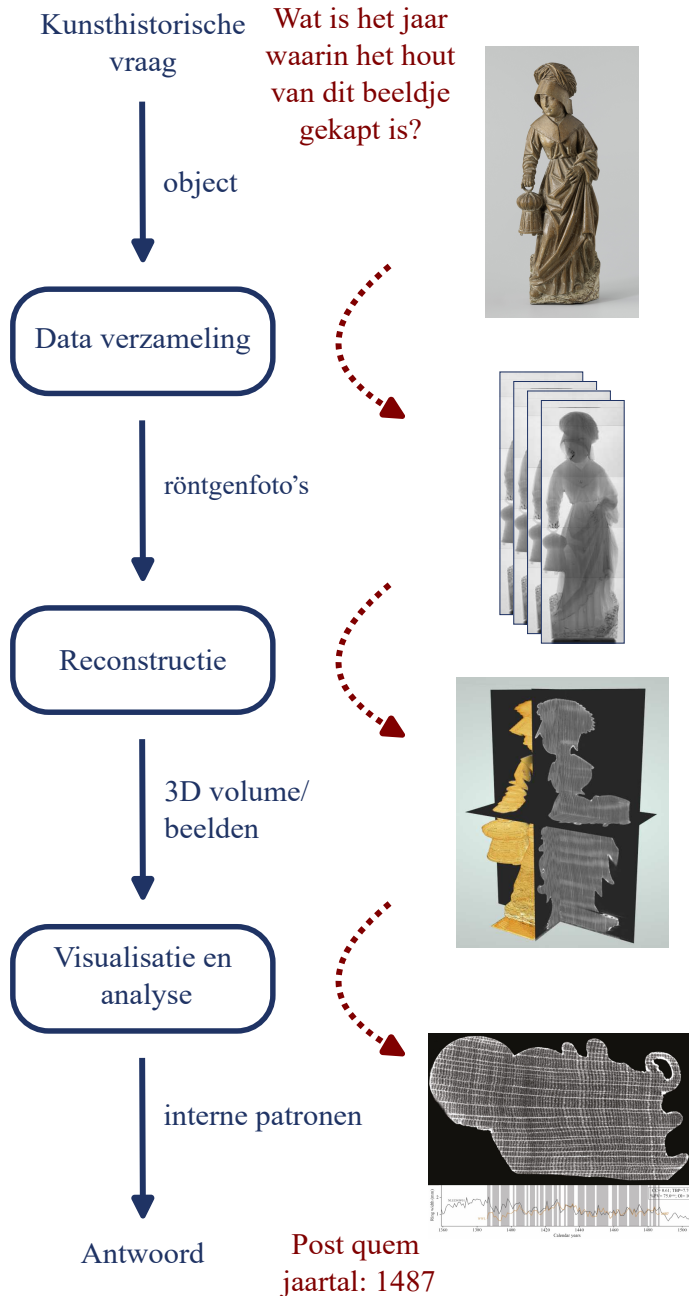
# Samenvatting

## Röntgentomografische technieken ontwikkelen voor onderzoek naar cultureel erfgoed

### Introductie

Het visualiseren van de binnenkant van kunstobjecten is een cruciale stap in het verwerven van kennis over de herkomst, huidige staat en samenstelling van cultureel erfgoed. Een van de meest krachtige technieken voor het zichtbaar maken van de binnenkant van museumobjecten is computer tomografie (CT). CT is een techniek die vooral bekend is uit de medische wereld. Met behulp van honderden röntgenfoto's uit verschillende hoeken wordt er een driedimensionaal digitaal beeld van het object opgebouwd, dat in verschillende richtingen kan worden doorsneden om de interne patronen van het object te bekijken. Het gebrek aan betaalbare en flexibele CT-setups in musea, gecombineerd met de uitdagingen die gepaard gaan met het vervoeren van waardevolle objecten uit de collectie, zorgt ervoor dat deze techniek op dit moment onbereikbaar is voor de meeste toepassingen binnen de kunstwereld. In dit proefschrift onderzoeken we hoe CT-scannen verder kan worden geïntegreerd voor toepassingen binnen de kunstwereld door 1) de experts actief bij het scanproces te betrekken, 2) de methoden waarop data wordt verzameld aan te passen aan de objecten om specifieke informatie te vergaren, 3) een betaalbare methode te ontwikkelen om de röntgenfaciliteiten die aanwezig zijn in musea te kunnen gebruiken voor CT-scans en 4) software te ontwikkelen om het interactief visualiseren en inspecteren van de CT-data te vergemakkelijken.

In figuur S1 is in blauw de workflow weergegeven voor het CT-scannen van kunstobjecten. Een voorbeeld van het toepassen van deze workflow is ernaast weergegeven in het rood. Het onderzoek wordt gedreven vanuit een kunsthistorische vraag. In het voorbeeld is dat: 'Wat is het jaar waarin het hout van dit beeldje gekapt is?'. Als de verwachting is dat die vraag beantwoord kan worden met behulp van CT-scans wordt er data opgenomen. De data bestaat uit een reeks van honderden röntgenfoto's uit verschillende hoeken. Vervolgens wordt die data met behulp van reconstructiealgoritmen verwerkt tot een driedimensionaal digitaal beeld van het object. Tot slot wordt deze reconstructie gevisualiseerd en geanalyseerd om tot een antwoord op de vraag te komen.



**Figuur S1:** Het CT-onderzoeksproces van vraag tot antwoord (in blauw), geïllustreerd met als voorbeeld de scans van de *Heilige vrouw met lantaarn* (in rood). Een *post quem jaartal* is het vroegste jaar waarin de boom gekapt kan zijn, zodat het object gemaakt moet zijn na dat jaar.

## CT-scans voor het onderzoeken van kunstobjecten

Een CT-scanner bestaat uit een röntgenbron en een detector met daartussen een draaitafel waarop het te scannen object wordt neergezet. De detector meet de intensiteit van de röntgenstraling, nadat deze door het object is heengegaan. Het beeld op de detector is afhankelijk van de dichtheid van het materiaal van het object en de dikte van het object. Daarnaast wordt het beeld beïnvloed door de oriëntatie van het object en de onderlinge afstand tussen de onderdelen.

Voor de dataverzameling worden honderden röntgenfoto's opgenomen, uit verschillende hoeken. Die worden vervolgens met behulp van reconstructiealgoritmen gecombineerd tot een driedimensionaal digitaal beeld van het object. Dit kan digitaal worden doorgesneden om de binnenkant van het object te bekijken. Dit is nuttig voor het onderzoeken van kunstobjecten, omdat de binnenkant vaak veel informatie bevat die van de buitenkant niet te zien is. CT-scans kunnen bijvoorbeeld informatie opleveren over de kunstenaar, hoe het object gemaakt is, hoe oud het is en of het in goede staat verkeert. Hierbij kijken we naar interne patronen zoals jaarringen, lijnlijnen of stukken van ander materiaal wat kan wijzen op een restauratie.

## Probleemstelling en samenvatting van de hoofdstukken

Het CT-scannen van kunstobjecten is een uitdaging vanwege de grote verscheidenheid aan materialen, vormen en maten van kunstobjecten. Daarnaast zijn CT-faciliteiten niet makkelijk toegankelijk voor het scannen van kunstobjecten. Ten eerste vanwege het feit dat er vaak transport van waardevolle objecten naar de CT-scanner nodig is en ten tweede vanwege de mogelijke kosten die transport en scans met zich meebrengen. Tot slot is het een uitdaging om tweedimensionale doorsnedes van driedimensionale objecten te interpreteren, met name voor de object experts die getraind zijn om objecten met het blote oog te bestuderen. In de hoofdstukken in dit proefschrift hebben we oplossingen aangedragen voor deze uitdagingen door algoritmes en software te ontwikkelen in samenwerking met object experts. In elk hoofdstuk worden de voorgestelde methoden toegepast op kunstobjecten uit museumcollecties.

In **Hoofdstuk 2** bespreken we het belang van het actief betrekken van de object experts bij het scanproces. Hun kennis kan de dataverzameling sturen, zodat precies die informatie verzameld wordt die de vragen kan beantwoorden. Ook kunnen zij tussentijdse resultaten analyseren die nieuwe vragen oproepen en wellicht leiden tot extra of aangepaste scans. In hoofdstuk 2 is dit toegepast op een houten muziekinstrument uit de Rijksmuseum-collectie: een cornetto.

In **Hoofdstuk 3** bekijken we het probleem dat veel grote objecten niet in de CT-scanner passen. De vraag om de jaarringen in beeld te brengen om de Hugo de Grootkist (Rijksmuseum-collectie) te kunnen dateren leidde tot een nieuwe vorm van dataverzameling, namelijk door het object alleen van links naar rechts te bewegen en zo vanuit een steeds net andere hoek de jaarringen te bekijken. Hierdoor was er steeds een deel van de jaarringen scherp te zien op de röntgenfoto's en was het mogelijk om een scherp beeld van de jaarringen te maken. In dit hoofdstuk werd de data-opname dus op maat gemaakt voor het beantwoorden van een specifieke vraag. Deze techniek

kan nu ook worden ingezet voor het dateren van andere grote houten voorwerpen.

In **Hoofdstuk 4** ontwikkelen we een methode om de röntgenopstellingen die vaak aanwezig zijn in grotere musea voor live-inspectie van een object, te gebruiken voor CT-reconstructies. Dit was voorheen niet mogelijk, omdat die opstellingen geen informatie geven over de locatie van alle onderdelen van de setup: waar de bron staat, waar de detector staat, waar het object staat en hoeveel de rotatietafel gedraaid is tussen twee opnames. We voegden kleine metalen balletjes toe aan een stuk foam, dat met het object werd meegescand. We ontwikkelden algoritmes die op basis van de locatie van die balletjes op de röntgenfoto's alle benodigde informatie terugrekenen. Zo maakten we CT-reconstructies met opstellingen waarmee dat tot nu toe niet kon. Deze methode maakt het makkelijker om CT-onderzoek toe te passen op kunstobjecten, omdat die niet naar een CT-scanner hoeven te worden gebracht, maar in het museum zelf kunnen worden gescand. Onze methode kost bovendien geen extra geld, terwijl een gespecialiseerde CT-scanner vaak niet binnen de financiële mogelijkheden van een museum ligt. Deze methode hebben we getest in het British Museum (London), waar wel een CT-scanner staat en we dus het resultaat van onze methode konden vergelijken met hun standaard protocollen. Daarna hebben we het toegepast in het J. Paul Getty Museum (Los Angeles) en het Rijksmuseum (Amsterdam), waar voorheen geen CT-scans konden worden gemaakt in de huidige röntgenopstelling. De toegevoegde waarde van onze aanpak voor het onderzoeken van kunstobjecten hebben we vervolgens geïllustreerd met een scan van een object van het J. Paul Getty Museum: *Python Killing a Gnu* van Antoine Barye. Uit de scan kwam duidelijk naar voren hoe het object uit verschillende lagen was opgebouwd en dat het object oorspronkelijk een andere vorm had en later opnieuw is vormgegeven.

In **Hoofdstuk 5** stellen we vast we dat het interpreteren van CT-scans voor kunstprofessionals een uitdaging kan zijn. Dit komt ten eerste doordat CT-data meestal wordt geanalyseerd in tweedimensionale doorsnedes, maar het object zelf natuurlijk driedimensionaal is. Het is daardoor lastig om wat er met het blote oog aan de buitenkant te zien is te relateren aan de CT-scan die informatie geeft over de binnenkant. Een tweede uitdaging is dat de CT-scan een zwart/wit beeld geeft, gebaseerd op de dichtheden van de materialen in het object. Het object zelf is vaak van buiten kleurrijk en heeft bepaalde structuren. Als oplossing hebben we software gebouwd om een driedimensionale oppervlakte scan (die de kleuren en texturen aan de buitenkant meet) te combineren met de CT-scan (die de informatie over de binnenkant bevat). Vervolgens kunnen beide scans op een interactieve manier bekeken worden. Dit draagt bij aan de kennisvergarig op basis van CT-scans en maakt het makkelijker voor conservatoren, restauratoren en kunsthistorici om de data te interpreteren.

# Curriculum Vitae



Francien Bossema was born in 1994 in Amsterdam, The Netherlands. She completed her secondary education in 2011 at the Vossius Gymnasium, Amsterdam, The Netherlands. She obtained two bachelors degrees in Mathematics and Physics & Astronomy from the Vrije Universiteit Amsterdam in 2015. During her bachelor studies she took a minor in Humanities at Greenwich University, London, United Kingdom. She obtained her master's degree (cum laude) in Mathematics focussing on Applied Mathematics, with an additional specialisation in Science Communication & Society in 2018 from Leiden University, The Netherlands. During her master degree she took internships at De Volkskrant (Amsterdam, The Netherlands) and Instituto de Astrofísica y Ciências do Espaço (Lisbon, Portugal).

From 2018-2023 she took a Ph.D. degree under supervision of prof. dr. K. J. Batenburg and prof. dr. E. Hermens at Centrum Wiskunde & Informatica, the national research institute for mathematics and computer science in Amsterdam, The Netherlands, in collaboration with the Rijksmuseum, Amsterdam. In 2022, she performed part of her research at the British Museum (London, United Kingdom) during an eight-month research placement. She is currently engaged as postdoctoral Migelien Gerritzen Fellow at the Rijksmuseum, Amsterdam, as Fellow at the eScience Center, Amsterdam and as postdoctoral researcher at the Centrum Wiskunde & Informatica. More information, such as presentations, blogs and videos, can be found on her website: [fgbossema.github.io](https://fgbossema.github.io).

Photograph by Heleen Klop Fotografen.  
Cover design by Joske Piepers.  
Printing by Ridderprint.

